ZINC AND ALUMINUM COMPLEXES BEARING MONOANIONIC BIDENTATE CYCLIC GUANIDINE-ETHENOLATE OR AMIDINE-ETHENOLATE LIGANDS FOR THE RING OPENING POLYMERIZATION OF LACTIDE.

LYA EVELYN CAMPOS RIVERA

A THESIS SUBMITTED TO THE FACULTY OF GRADUATE STUDIES IN PARTIAL FULFILMENT OF THE REQUIREMENTS FOR THE DEGREE OF MASTER OF SCIENCE

GRADUATE PROGRAM IN CHEMISTRY

YORK UNIVERSITY

TORONTO, ONTARIO

AUGUST 2024

Abstract

Aluminum and zinc complexes bearing bidentate guanidine-ethenolate ligands are reported and used in the solvent-free polymerization of *rac*-lactide at 130 °C. Solid-state structures of the zinc complexes showed a distorted tetrahedral geometry. Solid-state structures of the bischelated aluminum complex showed dynamic trigonal pyramidal and square-based pyramidal geometries. Polymerization using zinc complexes produced polylactic acid (PLA) with a heterotactic bias (P_r = 0.52–0.65) with molecular weights comparable to those obtained in the $SnOct_2$ control experiment. The most active zinc catalyst reported herein, Zn(**L1**)$_2$ is only about three times less active than $SnOct_2$, for the ROP of *rac*-LA at 130 °C. For the polymerization of *L*-LA under industrial conditions, at 150 °C, Zn(**L1**)$_2$ is only about 14.4 times slower compared to $Sn(Oct)_2$, and about only 2.5 times slower compared to Herres-Pawlis *et al*. zinc(II) Schiff base complex. Interestingly, the addition of benzyl alcohol as a co-initiator for the polymerization using Zn(**L1**)Et readily produced Zn(**L1**)$_2$ and $Zn(OBn)_2$, with both complexes giving comparable activities. Polymerization studies showed that $Zn(OBn)_2$ is only 2.5 times less active than $Sn(Oct)_2$ but with twice as large molecular weights. The Zn(**L5**)Et complex, in the presence of BnOH, resulted in a reaction rate three times faster than the monochelated guanidine-ethenolate Zn(**L1**)Et complex, due to the enhanced Lewis acidity of the metal center caused by the presence of the CAAI fragment. MALDI-TOF MS was used to determine the end groups of the polymer chain. The spectra provide evidence of hydroxy and **L1**H end group for PLA generated from Zn(**L1**)$_2$ with and without BnOH, as well as from Zn(**L1**)Et with BnOH. These terminated PLA chains result from water contaminants present in LA. However, it remains challenging to determine whether AMM or CIM is the dominant mechanism. In contrast, $Zn(OBn)_2$, both with and without BnOH, generated polymers with hydroxy, OBn, and macrocycles sodium adducted cationized open chain

polymers. The presence of OBn end groups indicates that the polymerization proceeded through CIM. All spectra indicated transesterification side reactions present due to peak separations of m/z 72 g/mol. The π-accepting properties of the guanidine moiety in the Zn(**L*x***)$_2$ complexes, as estimated by the ^{31}P NMR chemical shift of the corresponding N-heterocyclic carbene–phosphinidene adduct, resulted in a negative correlation in the rate for the ROP of LA.

Acknowledgments

First, I would like to thank Professor Gino G. Lavoie for his valuable mentorship, support, and patience in guiding my development as a chemist and for taking the time to write a letter of recommendation for my Advanced Masters's applications. I am also grateful to my Supervisory Committee members, Professor Christopher Caputo and Professor Thomas Baumgartner, for their support, advice, and patience. I would also like to thank the Chemistry Graduate Programme Director, Professor Ryan Hilli for his support and guidance. I am grateful to Professor Howard Hunter for his extensive knowledge and assistance with NMR experiments. Thank you to current member Nicholas L. Miceli for his engagement in insightful chemistry discussions, his constant availability to resolve any issues, and for his friendship. I would like to acknowledge former group member Brandon S. Khan for his valuable contributions to the development of zinc catalysts for the polymerization of LA. His work has significantly shaped our group's focus on polymerizing biodegradable polymers. I am very grateful for his support and friendship. I would also like to acknowledge Jesse LeBlanc for his mentorship in developing the required chemistry skills to understand his established synthesis pathway for the ligands **L1**H-**L4**H used in this work. I am grateful for his friendship and unending encouragement. Victor Flores Romero has my heartfelt gratitude for welcoming me into the lab and mentoring me to have a clearer understanding of the chemistry conducted. His consistent willingness to help and friendship have been invaluable. Finally, I would like to thank all the friends I've made at York: Casey, Taylor, Charley, Avik, Dusty, and Amaar. Their listening, help, and encouragement have made my time here enjoyable and memorable.

Dedication

Esta investigacion esta dedicada a los pilares de mi vida: mi mamá y mi papá. Agradezco profundamente todos sus sacrificios, su apoyo, y su amor constante. Han sido una fuente inagotable de inspiracion y fortaleza, ayudandome a mantener mis cualidades de honestidad, dedicacion y resiliencia.

Para mis queridos hermanos: Andrea, Nastia, Emilio y Milan. Gracias por compartir conmigo los momentos de desafio al igual que los de alegria. Su apoyo constante ha sido fundamental para alcanzar mis metas.

Table of Contents

List of Abbreviations

AMM	Activated Monomer Mechanism
BDI	β-diiminate
DCM	Dichloromethane
CAAC	Cyclic Alkyl Amino Carbene
CAAI	Cyclic Alkyl Amino Iminato
CIM	Coordination Insertion Mechanism
equiv.	Equivalent
Intens.	Intensity
LA	Lactide
L	Ligand
meso	mesomeric
M_n	Number-average molecular weight
M_w	Weight-average molecular weight
NaHMDS	Sodium bis(trimethylsilyl)amide
NHC	*N*-Heterocyclic Carbenes
NHI	*N*-Heterocyclic Imines
NMR	Nuclear Magnetic Resonance
PCL	Polycaprolactone
Đ	Polydispersity index
PDLA	Poly(D-lactic acid)
PE	Polyethylene
PET	Polyethylene terephthalate
PLA	Polylactic acid
PLLA	Poly(L-lactic acid)
PP	Polypropylene
PS	Polystyrene
rac	Racemic
Res.	Resolution
ROP	Ring opening polymerization
S/N	signal to noise ratio

T_m	Melting point
Tol	Toluene
THF	Tetrahydrofuran

List of Figures

List of Tables

List of Figures from Appendix

List of Figures from Appendix

CHAPTER 1: Introduction

1.1 Polylactic acid

Polymers play a major role in our daily lives, with a wide range of applications for medical devices, house insulations, impact-resistant textiles, films, and packaging, to name a few.[1] Polyolefins such as polyethylene (PE), polypropylene (PP), and polystyrene (PS) (Figure 1), belong to the largest class of plastics produced due to their low toxicity, low cost, mechanical and chemical versatility,[2] resulting in the annual production of over 150 million metric tons of polyolefins worldwide.[3] However, their chemical stability results in their persistence in the environment for hundreds of years after disposal.[4]

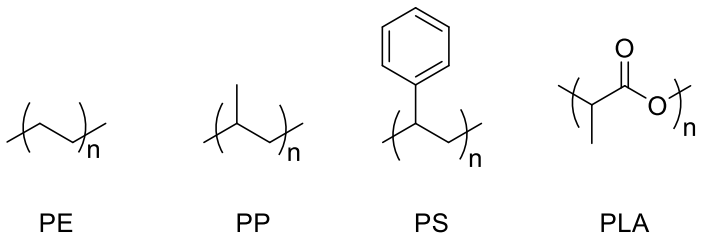

Figure 1. Polymers: polyethylene (PE), polypropylene (PP), polystyrene (PS) and polylactic acid (PLA)

To address the environmental impact that polyolefins cause, especially when used in single-use products, polyolefins may be replaced with more readily biodegradable polyesters. Polyesters have garnered attention due to their degradation by hydrolysis of the ester bond.[5] Poly(ethylene terephthalate) (PET), the most common polyester, is used extensively in many single-use applications, such as water and carbonated soft drink bottles, and is the most recycled polymer.[6] However, the building blocks for this polymer still, for the most part, come from fossil fuels.[7] Polylactic acid (PLA) (Figure 1) is, in contrast, derived entirely from renewable resources made

from fermented plant starch, such as corn, sugarcane, and sugar beet pulp.[8–10] PLA has garnered attention not only for its similar mechanical properties such as breaking stress,tensile strength and modulus to fossil fuel-based polymers such as PS and PET,[11–13] but also due to its non-toxicity, ease of processability, and synthesis from renewable resources.[14] Additionally, PLA films have demonstrated higher tensile strength compared to PS, though lower tensile strength than PET, making it suitable for applications requiring moderate strength.[15] PLA also has a lower melting point (T_m) compared to both PS and PET, enhancing its effectiveness in heat-sealing processes. Furthermore, PLA exhibits reduced permeability to CO_2 and O_2 compared to PS and has barrier properties similar to PET, which helps extend the shelf life of packaged items by limiting exposure.[15] These properties, combined with its biodegradability and renewable sourcing, make PLA suitable for applications in the production of single-use plastics that help reduce environmental pollution from conventional, fossil fuel-based plastics.[16]

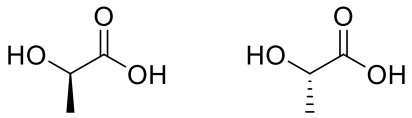

L-lactic acid *D*-lactic acid

Figure 2. Isomer of lactic acid: *L*-lactic acid and *D*-lactic acid.

Lactic acid, which can undergo polycondensation into PLA, is a chiral molecule, with two possible enantiomers: *L*- and *D*-lactic acid (Figure 2).[17] Lactic acid is produced industrially through the microbial fermentation of carbohydrates, converting starches into *L*-lactic acid.[17–19] However, PLA is more favorably synthesized from its corresponding cyclic dimer, lactide (LA), through ring-opening polymerization (ROP). LA has two stereogenic centers present, generating three isomers: *D-, L-* and *meso*-LA (Figure 3). *L*-LA has garnered interest over *D*-LA due to the

biocompatible characteristics of *L*-lactide, which mammals can metabolize.[20,21] Furthermore, PLA produced by ROP of LA leads to lower dispersity (*Đ*), which describes the uniformity of polymer length in a given polymer mixture, and higher molecular weights when compared to PLA produced by polycondensation.[22]

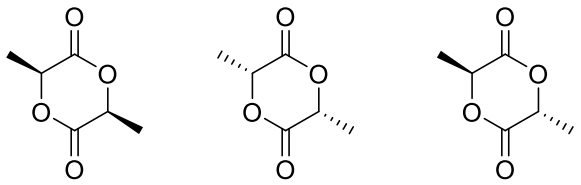

Figure 3. Isomers of lactide: *L*-LA, *D*-LA, and *meso*-LA.

LA synthesis begins with the oligomerization of two lactic acid molecules through a condensation reaction, where the carboxyl and hydroxyl groups form ester bonds, releasing water and forming a low molecular weight oligomer.[20] These oligomers are then depolymerized under heat and reduced pressure, breaking ester bonds forming LA.[20] The resulting LA can subsequently be polymerized to high quality PLA by ROP (Figure 4). Although PLA is considered a biodegradable plastic, it is not a polymer that can decompose naturally.[23] The rate at which PLA can degrade is significantly impacted by its environment.[23] Complete degradation of PLA can be ensured under industrial composting conditions; compared to soil degradation at 30°C, at least a year is required for full decomposition.[23] Once PLA has served its purpose, simple hydrolysis of the ester bond can break down the PLA into its lactic acid building block.[23,24]

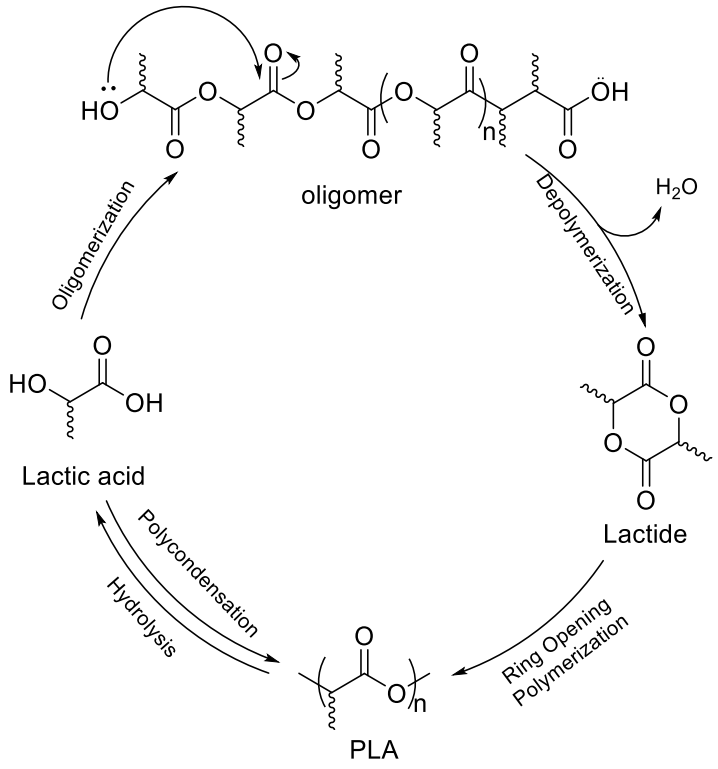

Figure 4. Relationship between lactic acid, lactide, and PLA. Reproduced from literature.[20]

Racemic LA (*rac*-LA), which is the equal mixture of *D*, and *L*-LA, has increased interest for the development of catalysts that can control tacticity in PLA. As a result, the PLA mainchain can have different microstructures, such as atactic, heterotactic, stereoblock, syndiotactic, and isotactic (Figure 5). Tacticity describes the arrangement of consecutive substituents in a polymer's stereogenic centers (*R* or *S*) which significantly influences the polymer's characteristics and properties.[25] The tacticity of the polymers, which varies from atactic to isotactic or heterotactic (to mention a few), affects thermal properties and characteristics like crystallinity.[25] Isotactic PLA consist entirely of substituents with the same relative configuration (e.g. *RRRRRR* or *SSSSSS*) and resulting in a crystalline PLA with T_m of 180 °C.[26] The crystallinity in isotactic PLA enhances its mechanical strength and rigidity, making it suitable for applications that require structural

durability.[26] Atactic polymers can be generated from *rac*-lactide or *meso*-lactide, resulting in random stereocenter configurations;[27] which in turn produce an amorphous polymer not suitable for industrial use like other polymers of different microstructures.[22] Heterotactic PLA can also be generated from *rac*-lactide or *meso*-lactide but gives an alternating sequence of *D*-LA and *L*-LA repeating units (e.g. *SSRRSSRRSS*).[26,28] Despite the regular alternating sequence, heterotactic PLA forms an amorphous polymer due random distribution of *D*-LA and *L*-LA units introducing steric hindrance, which disrupts the uniform alignment of polymer chains and prevents the formation of a highly ordered crystalline lattice.[26,28,29] Syndiotactic PLA can be generated from *meso*-lactide, and featuring sequential stereocenters with alternating relative configuration of adjacent stereogenic centers (e.g. *SRSRSRSRSR*), which results in high crystallinity polymer with a melting temperature of 152 °C.[26,30] Stereoblock PLA contain distinct blocks of PLLA and PDLA obtained by the ROP of *rac*- or *meso*-LA (e.g *RRRRRRSSSSS*) with a stereoselective catalyst (Figure 5).[22,30,31] Additionally, stereoblock PLA can lead to the formation of stereocomplex-type PLA with T_m of 235 °C, resulting in enhanced mechanical and thermal properties.[32–34] This allows stereocomplex-type PLA to compete with fossil-fuel-derived plastics in applications where material durability and high performance are important.[33]

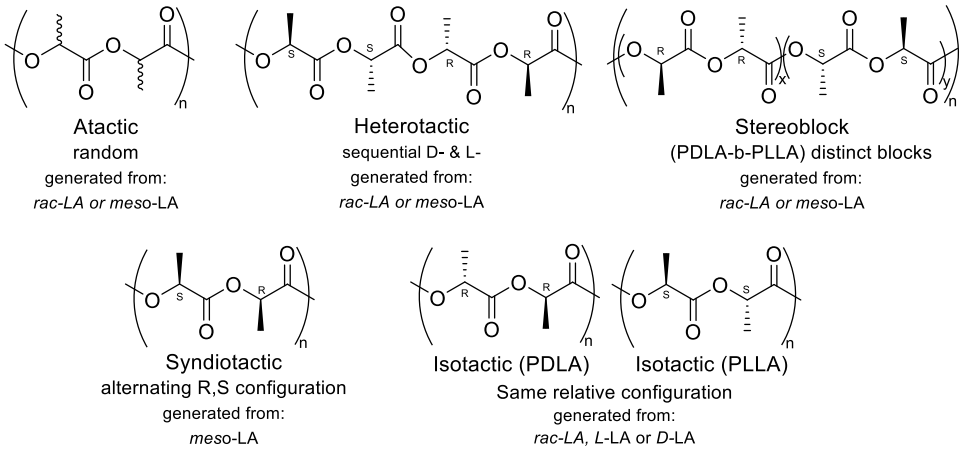

Figure 5. Microstructures of PLA. Reproduced from literature.[22]

Tacticity can be further described by the probability of *racemic* or *mesomeric* enchainment, P_r, and P_m, respectively.[22] P_r is the probability of forming two neighboring stereocenters with the opposite chirality or a new *racemic* diad, whereas P_m is the probability of forming two neighboring stereocenters with the same chirality.[19,22,30,35] These values, P_r and P_m, are calculated using homonuclear decoupled $^1H\{^1H\}$ NMR spectroscopy experiments on a concentrated polymer sample.[19,27,36,37] This technique removes scalar coupling between methyl groups, resulting in five distinct resonances from tetrads that correspond to the possible configurations of the four stereocenters present in PLA.[36,37] P_r values are determined by integrating the methine region in the ^1H NMR and calculated using the formula $P_r = 2\ I_1/(\ I_1 + I_2)$ where I_1 is the integration from 5.20 to 5.25 ppm and I_2 from 5.13 to 5.20 ppm.[37,38] Similarly, P_m is calculated using the formula to $P_m = 1 - 2\ I_1/(\ I_1 + I_2)$ with I_1 ranging from 5.07 to 5.14 ppm and I_2 from 4.94 to 5.07 ppm a.[39] For the ROP of *rac*-LA, $P_r = 1.00$ ($P_m = 0.00$) and $P_m = 1.00$ $P_r = 0.00$) describe perfect heterotactic and isotactic polymers, respectively.[22,35]

1.2 Polymerization Mechanisms for PLA

Step-growth polymerization is a polymerization mechanism characterized by a slow increment in molecular weight. Polymer growth can occur between monomers, oligomers, or polymers of any length.[40] To obtain longer polymer chains, high reaction rates are required where the polymerization exceeds 98-99% conversion.[24,41] Therefore, due to the requirement of pure conditions to avoid side reactions that can lead to incomplete polymerization, PLA synthesis through polycondensation fails to achieve conversions exceeding 98-99% resulting in a low-molecular-weight polymer, which in turn restricts its applications.[24,41] High molecular weight PLA can be synthesized using azeotropic polycondensation where water is effectively extracted using

suitable azeotropic solvents, shifting the equilibrium between the monomer and the polymer in the solvent.[42] However, this method is limited by the equilibrium of the polycondensation reaction, as the hydrolysis of the ester bonds can interfere with the polymerization process.[42] Additionally, polycondensation results in PLA with a high dispersity (*Đ*) value of 2.0, further becoming an unfavorable method as polymers are not uniform.[43,44]

An alternative to step-growth polymerization is chain growth polymerization. Unlike step-growth polymerization, which produces polymers with high molecular weight only after the reaction has progressed significantly, chain-growth polymerization can afford high molecular weight polymers produced early in the polymerization process.[45] In chain-growth polymerization, monomers are added continuously to the active site of a growing polymer chain, which rapidly increases the size of the polymer.[45] As each monomer is added, the active site is regenerated, allowing the polymer chain to grow fast and efficiently.[45] Chain growth polymerization results in defined molecular weights and overall lower *Đ* when conducted under living polymerization conditions. Living polymerization is characterized by the absence of termination and transfer reactions, allowing for continuous growth of polymer chains without losing the reactivity of the end groups.[46] This process ensures that the polymer end groups, such as carboxyl and hydroxy groups, are stable, enabling the precise control over the molecular weight and resulting in a narrower molecular weight distribution.[47] The focus herein is on three chain-growth polymerization mechanisms to produce PLA: Coordination-insertion mechanism (CIM), activated monomer mechanism (AMM), and hydrogen bonding mechanism.

CIM is the established mechanism of a system based on an organometallic catalyst of the type LM-OR, where L represents n spectator ligands coordinated to the metal center, and OR is a nucleophilic alkoxide that can ring open the LA.[48] Metal alkoxide-catalyzed ROP of lactide has

been studied using a wide range of metals such as Li, Mg, Zn, Ca, Sn, Al, and. Sc.[49,50] The first step of the CIM involves the coordination of LA to the Lewis-acidic metal center through the carbonyl oxygen.[19] This coordination causes the electrophilic activation of the carbonyl carbon in LA leading to the formation of a tetrahedral intermediate.[50] This tetrahedral intermediate undergoes ring opening while maintaining its original stereochemical configuration.[19,50] Consequently, this newly opened ring becomes the new R group to continue the cycle until the metal alkoxide bond is cleaved, as shown in Figure 6.[19,50,51] Moreover, when using alcohol with a non-alkoxide pre-catalyst, the alkoxide complex (LM-OR) can be generated *in situ*, through the reaction of the alcohol with the catalyst, facilitating the ROP of LA.[19,48]

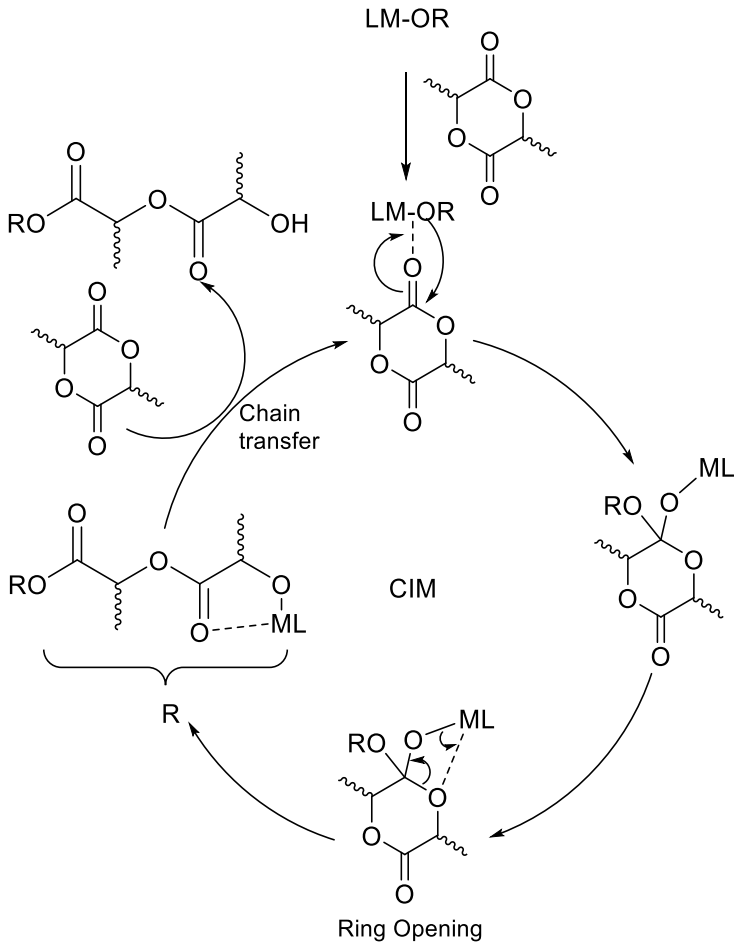

Figure 6. Coordination-insertion mechanism of lactide, LM-OR is the catalyst, where L is a spectator ligand, M is a metal center, and OR refers either to the nucleophilic alkoxy group or to the growing polymer chain. Reproduced from literature.[51]

The extent of transesterification side reactions, which involve the cleavage of ester bonds, occurring during the ROP of LA, can also impact the efficiency of molecular weight control in the process.[51] Transesterification can lead to the broadening of the *Đ*, occurring both intramolecularly by backbiting, leading to macrocyclic structures and shorter chains, as well as

intermolecularly leading to chain redistributions.[51] The degree to which these undesirable transesterification reactions occur is dependent on the organometallic catalyst used.[51]

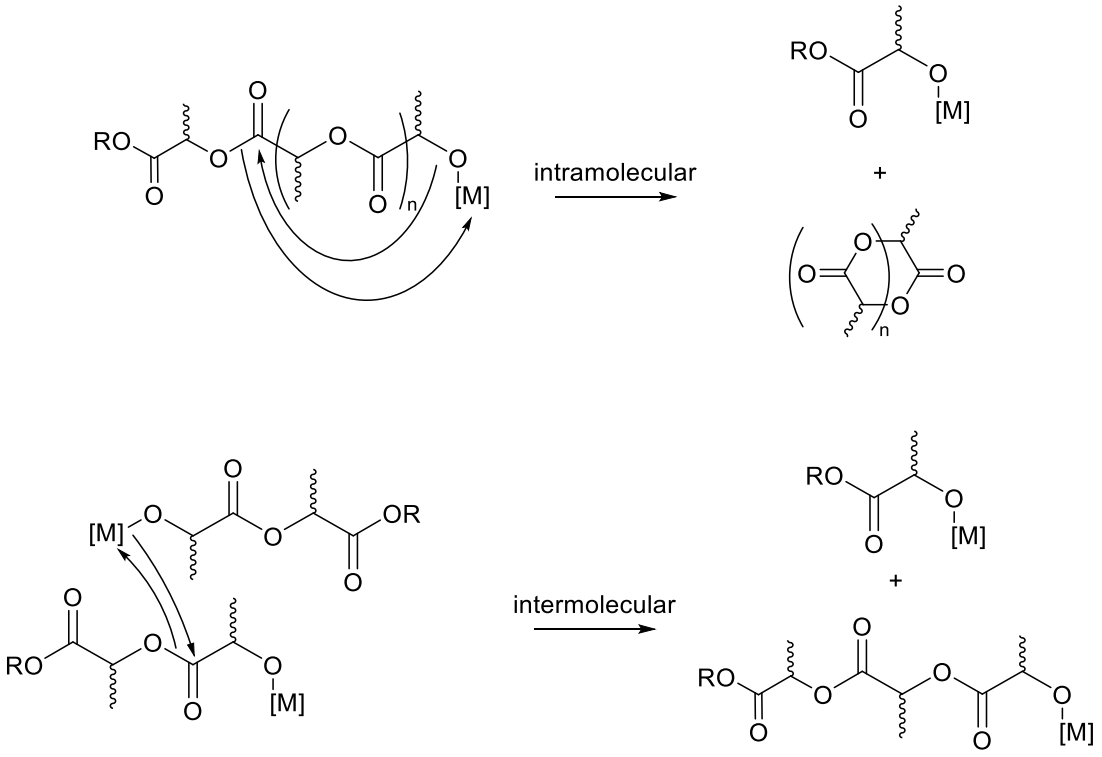

Figure 7. Representation for the intramolecular and intermolecular transesterification side reactions. Reproduced from literature.[51]

Alternatively, Lewis acidic metal salt catalysts and organometallic catalysts without an alkoxide ligand can induce ROP lactide by an activated monomer mechanism (AMM).[51,52] In CIM, the nucleophile is coordinated to the Lewis acidic metal center, while in AMM, the unavailability of this coordinated nucleophile requires a nucleophilic additive, such as an alcohol as shown in Figure 8.[19,48,53] Like in CIM, the first step in AMM consists of LA coordination to the Lewis acidic metal center through the carbonyl oxygen.[19,53] Following this, the external nucleophile initiates the polymerization process by attacking the electrophilic carbonyl carbon.[19]

This is followed by proton transfer to the endocyclic oxygen of LA, resulting in the formation of a tetrahedral intermediate at the carbonyl carbon. [19,50,53] This intermediate then undergoes ring opening, continuing the polymerization process.[48,50,53] In the unavailability of an external alcohol additive, polar contaminants found in LA such as water, ethanol or lactic acid can act as an external nucleophile.[19,48,54] During the process, the ring opened hydroxy end capped LA undergoes a chain transfer and exhibits similar reactivity towards the activated LA, acting as the external nucleophile to ring open an additional LA.[19,48]

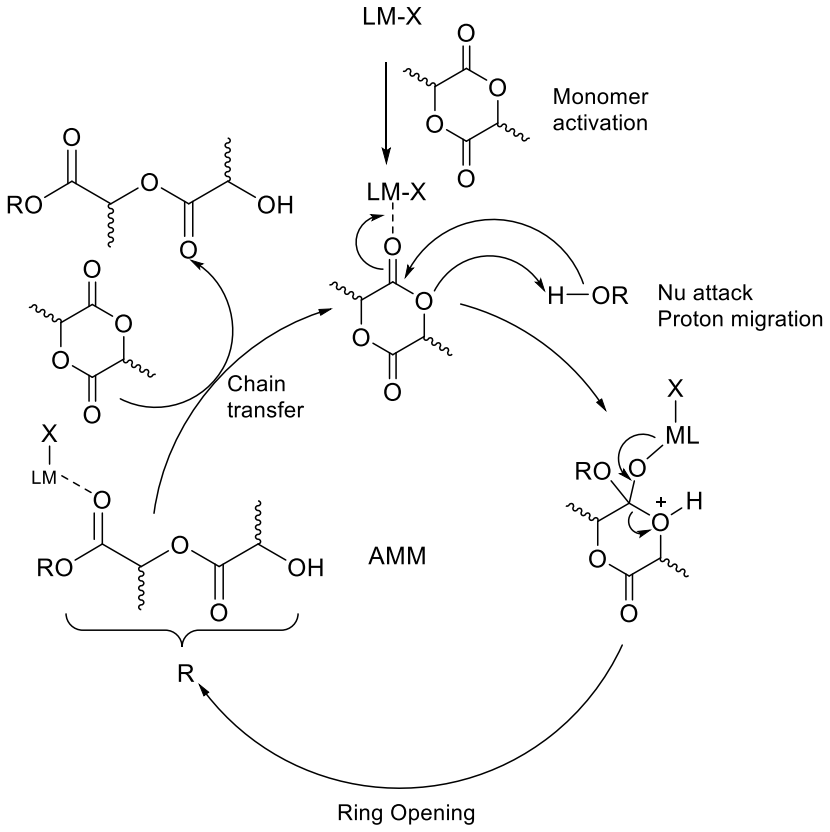

Figure 8. Activated monomer mechanism of lactide. LM-X is the Lewis acidic metal salt or organometallic catalyst. Nu is the external nucleophile such as an alcohol (H-OR). Reproduced from literature.[53]

Metal-free ROP of lactide has been proven successful by N-heterocyclic imines (NHI), which will be discussed in more detail below. Recently, the bicyclic guanidine-based catalyst triazabicyclodecene (TBD) has shown controlled high activity for solution phase ROP of cyclic esters.[55,56] In the initial step of the mechanism, the nitrogen bound hydrogen of TBD activates the carbonyl group of the *L*-lactide through hydrogen bonding.[55] Simultaneously, the imine nitrogen activates the alcohol by attracting the hydrogen from its hydroxyl group via lone pair interaction as shown in Figure 9. The catalyst (TBD) then facilitates the ring opening by maintaining a hydrogen bond to the oxygen of the carbonyl group while transferring the hydrogen, originally from the alcohol, to the ring oxygen adjacent to the carbonyl group.[55]

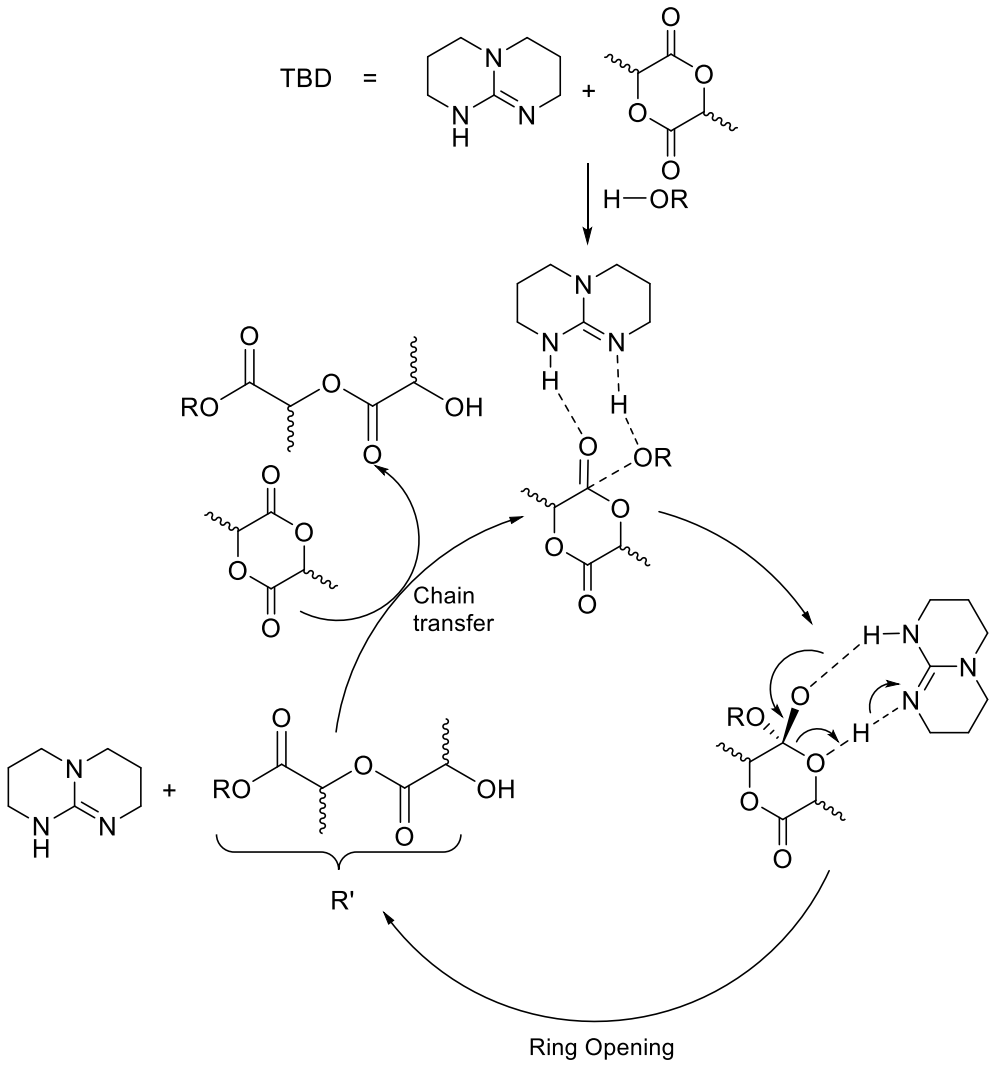

Figure 9. Hydrogen bonding mechanism of lactide by TBD. Reproduced from literature.[55]

1.3 Catalysts for Lactide ROP

1.3.1 Tin Octoate for Lactide ROP

Many metal-based catalysts can polymerize LA by ROP. The industrial standards include zinc(II) lactate, aluminium(III) isopropoxide and tin(II) octoate ($Sn(Oct)_2$, shown in Figure 10) alongside alcohol co-initiators such as benzyl alcohol or isopropyl alcohol, to polymerize through ROP neat at 130 °C or in solution.[14,19] While $Sn(Oct)_2$ is the preferred catalyst due to its high

activity, low cost, and effectiveness in generating high molecular weight polymers, it also promotes transesterification, causing a decrease in molecular weight and an increase in dispersity.[57,58]

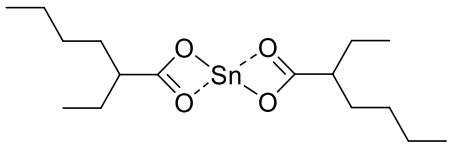

Figure 10. Structure of $Sn(Oct)_2$ catalyst.

$Sn(Oct)_2$ also lacks stereoselectivity for the production of PLA if *rac*-LA is used; however, if *L*-LA is used, $Sn(Oct)_2$ results in PLLA that is 90% isotactic.[59] It is commonly accepted that the ROP of *L*-LA in the presence of $Sn(Oct)_2$ goes through CIM. Accordingly, $Sn(Oct)_2$ reacts with hydroxyl bearing molecules such as octanoic acid, contaminant found in commercial $Sn(Oct)_2$, to form an alkoxide, which is considered the actual active species in the polymerization process (Figure 11).[60] Beyond their role in forming the mentioned alkoxide species, hydroxyl groups can also function as chain transfer agents. Therefore, it is important to regulate their concentration as they can affect the rate of polymerization and molecular weight of PLA.[60] Furthermore, the contamination of the polymer with residual tin limits the implementation of PLA in biomedical and food contact applications, as complete removal of the cytotoxic metal from the polymer is challenging and costly.[61]

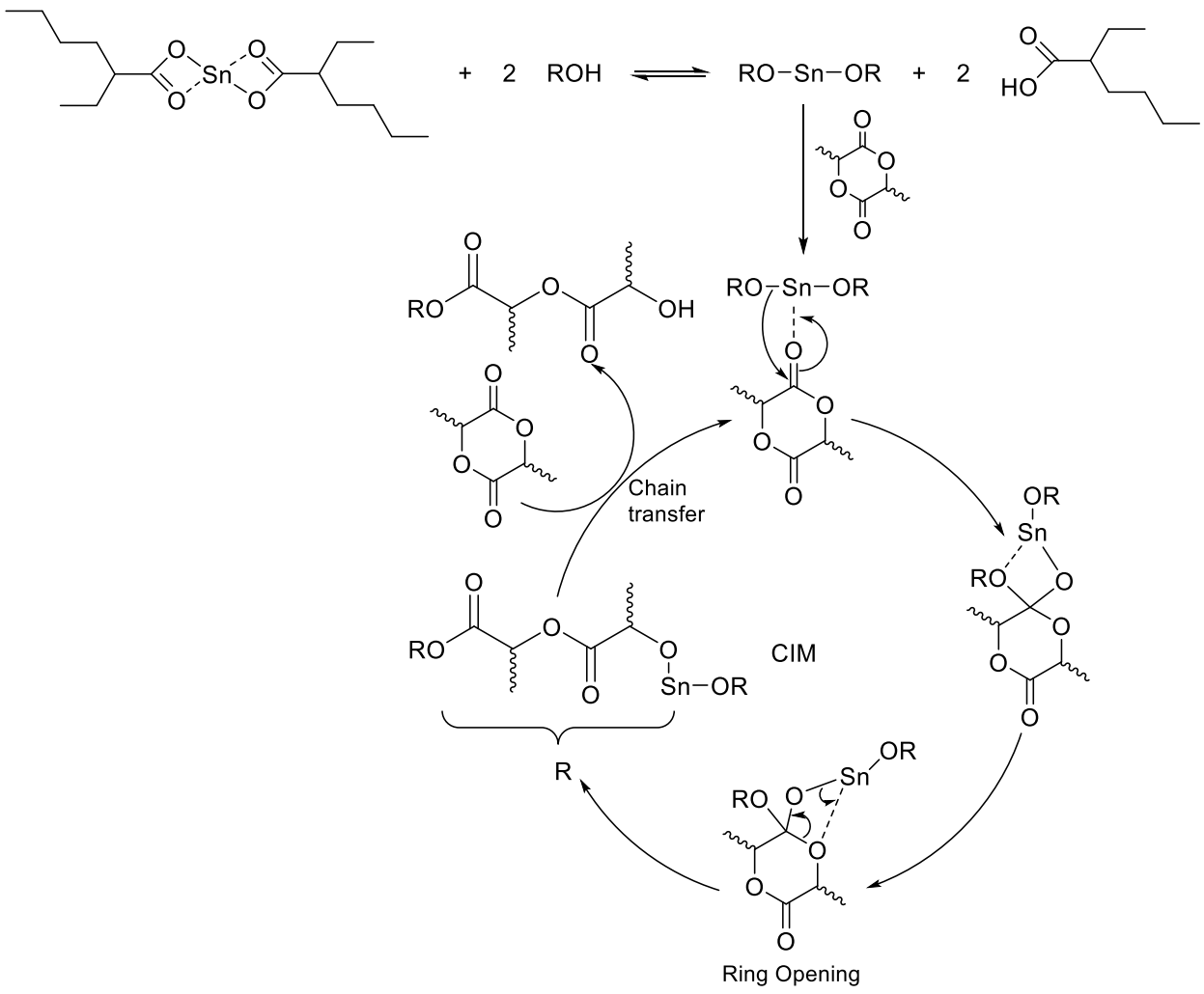

Figure 11. Formation of tin alkoxide initiator, and CIM of LA by $Sn(OR)_2$. Reproduced from literature.[46]

1.3.2 Zinc Complexes for Lactide ROP

Recently, bio-metal containing complexes such as zinc(II) have gathered attention due to their innocuous nature, ready availability[62], and efficacy in polymerizing LA via ROP. These zinc catalytic systems exhibit high activity, low toxicity, low cost, require low catalyst concentrations, and are highly tolerant to polar contaminants found in LA, becoming an alternative to the cytotoxic industrial $Sn(Oct)_2$.[63] Zinc catalysts are composed of ligands bearing nitrogen atoms,

such as β-diiminate (BDI), amine-phenolate, and phenoxy-imine (FI) type ligands (Figure 12) have garnered attention because of their good donor properties, straightforward synthesis, capacity to stabilize low-coordinate metal alkoxides, and high activity.[64,65] Coates *et al*. developed the BDI zinc isopropoxide complex that polymerized *rac*-LA with high activities for the production of heterotactic PLA (Figure 12, left).[65] The group determined that because zinc isopropoxide complex has an alkoxide moiety that closely mimics the putative propagating groups of the presumed active species, it produces PLA with predictable number-average molecular weight (M_n) and low dispersity, *Đ* (M_w/M_n) of 1.10 within 30 minutes, at room temperature in DCM (97% conversion).[65] Furthermore, the microstructural analysis of the polymers showed that ligands influenced tacticity of polymer chains.[65] Tolman *et al.* reported a zinc-based catalyst bearing a tridentate diamino-phenolate ligand (Figure 12, middle) that successfully polymerized *rac*-LA with high activity to yield atactic PLA with a relatively low Đ of 1.40 at room temperature in DCM.[66] More recently, Herres-Pawlis *et al.* reported a robust zinc catalyst bearing a phenoxy-imine ligand (Figure 12, right) which resulted in effective *L*-LA polymerization under industrial conditions (150 °C, solvent-free, using a stoichiometric ratio of 1:1000 catalyst-to-lactide) with a low *Đ* of 1.30.[67]

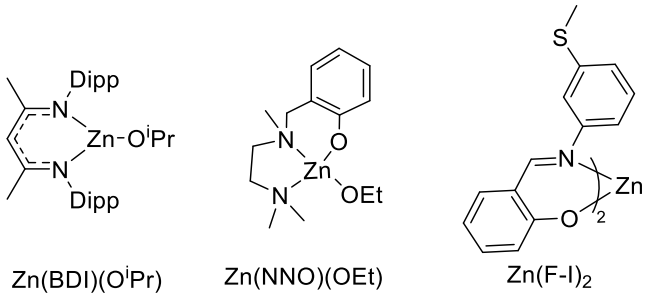

Zn(BDI)(O^{i}Pr) Zn(NNO)(OEt) Zn(F-I)$_2$

Figure 12. Catalysts for LA polymerization: β-diiminate (left), amine-phenolate (middle) and phenoxy-imine (right) zinc catalysts.

1.3.3 Aluminum Complexes for Lactide ROP

High Lewis acidity and low toxicity aluminum complexes such as aluminium triisopropoxide, $Al(O^iPr)_3$ have garnered attention for the ROP of lactide, but its activity is low as bulk polymerization must achieve near complete conversion within less than 10 minutes.[68,69] $Al(O^iPr)_3$, can polymerize *rac*- or *meso*-LA through CIM, where the polymerization remains living until a molecular weight of 90,000 Da is reached, resulting in an amorphous atactic polymer.[65,70] Unfortunately, $Al(O^iPr)_3$ is much less active than the industrial standard $Sn(Oct)_2$.[69,69,70] Salen-type ligands coordinated to aluminum based complexes polymerized *rac*-LA to yield an isoselective PLA.[22] It has been observed that electron withdrawing phenoxy substituents in Salen ligand containing complexes increased the rate of polymerization of *rac*-LA, likely due to their ability to stabilize the growing polymer.[22] In contrast, sterically hindering groups at the *ortho*-position tended to slow the polymerization rate, but increased stereoselectivity.[22,65] Spassky *et al*. developed a Salen-aluminium complex (Figure 13, left) for the ROP of *rac*-lactide to form highly isotactic and crystalline PLA.[22,71,72] In 1999, Coates *et al*. evaluated this BINAP-derived Salen-aluminium complex for the ROP of *meso*-LA, where they were able to determine the successful production of syndiotactic PLA.[22,73] On the other hand, aluminum derivatives of bidentate phenoxy-imine ligands (Figure 13, right) were also shown to be effective in the ROP of other cyclic esters, but did not offer stereocontrol when applied to *rac*-lactide. [74]

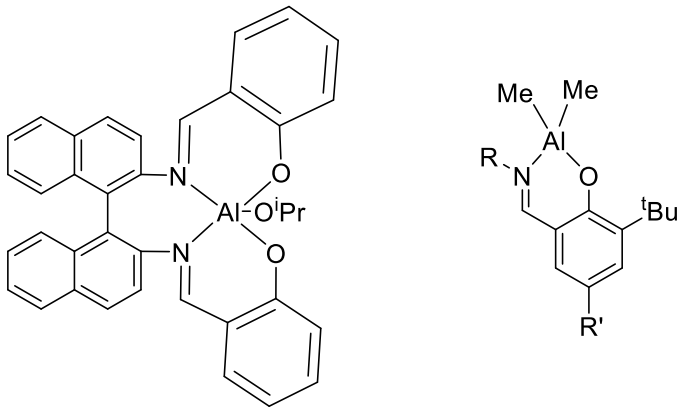

Figure 13. Catalysts for LA polymerization: Salen (right) and bidentate phenoxy-imine (right) aluminum catalysts.

1.4 Cyclic Iminates

1.4.1 *N*-Heterocyclic Imine/Iminates

In 1991, Arduengo *et al.* isolated the first *N*-Heterocyclic Carbene (NHC), demonstrating that free carbenes can be kinetically stabilized by bulky substituents on the nitrogen atoms (Figure 14, left). The lone pairs at the planar nitrogen atoms stabilize these carbenes through π-donation to the empty p-orbital on the central carbon.[75] Arduengo *et al.*'s work resulted in their ample use as ancillary ligands for transition metal catalysts due to their strong σ-donating ability, leading to strong carbene–metal bonds and enhancing the thermal stability of complexes.[76,77] Later in the 2000s, the explored reactivity of NHCs toward azides inspired the development of a new class of imidazol-2-iminato ligands: *N*-Heterocyclic Iminates (NHI).[78–81] These cyclic guanidinates are represented by two mesomeric forms that show their donor character through their ability to delocalize electron density across the imidazolium ring (Figure 14, right).[82] The guanidinates are highly modular, and therefore, the electronic and steric properties can be varied as the electron-donating capacity of the exocyclic nitrogen can be modulated by the substituents in the imidazole ring. This can be leveraged in the development of novel ligand systems.[83]

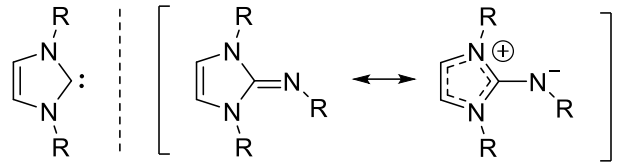

Figure 14.left. NHC; right. Mesomeric structure of NHIs

Titanium complexes bearing an imidazoline-2-iminato scaffold synthesized by Tamm *et al*. showed moderate activities in the polymerization of ethylene (Figure 15, left).[84] Herres-Pawlis *et al*. synthesized zinc complexes bearing imidazoline-2-iminato ligands that were highly active for ROP of lactide (Figure 15, left-middle).[85] The Lavoie group has reported a new family of cyclic guanidine–ethenolate ligands that coordinate to group 4 metals in a bidentate fashion through the formally neutral exocyclic guanidine nitrogen and the anionic ethenol (Figure 15, right-middle), causing the Lewis acidic metal centre to possibly become more tolerant towards σ-coordination of polar monomers present in olefin polymerization.[86] Titanium complexes bearing guanidine enolate ligands proved active towards olefin polymerization.[86] More recently, the Lavoie group reported a series of zinc complexes containing a neutral bidentate ligand with an acylated cyclic guanidine donor varying the second fragment donor that proved to be active toward the ROP of LA (Figure 15, right).[87]

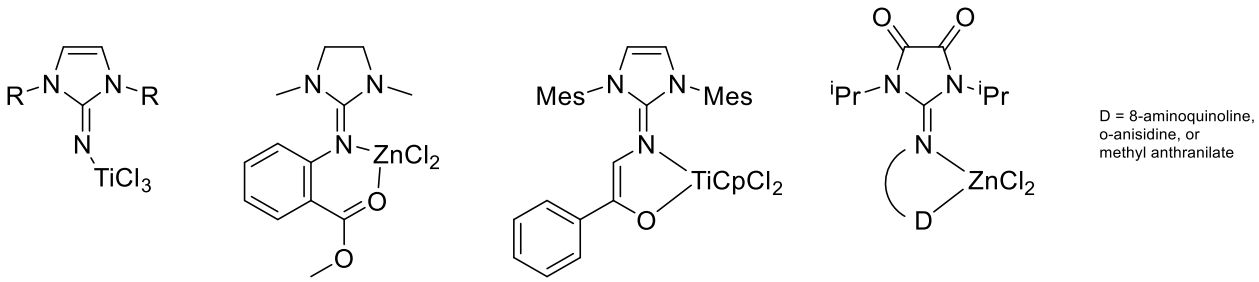

Figure 15. imidazoline-2-iminato titanium complexes (left); imidazoline-2-imine zinc complex (left-middle); guanidine-enolate titanium complexes (right-middle); acylated cyclic guanidine zinc complexes (right).

1.4.2 Cyclic Alkylamino Iminates

Cyclic alkylamino carbenes (CAAC) are another class of stable cyclic carbenes in which one of the electronegative and π-donor amino substituents of NHC is replaced by a σ-donating but not π-donating alkyl group.[88] Therefore, CAACs are more nucleophilic (σ-donating) and more electrophilic (π-accepting) than NHCs. Cyclic alkyl amino iminates (CAAI) shown in Figure 16 are ligands that have only one endocyclic nitrogen atom. This endocyclic nitrogen enhances the ligand's ability to donate electron density to metal centers, making CAAI a stronger σ donor than NHIs. In contrast, NHIs have two endocyclic nitrogens, leading to a greater electron delocalization within the ring, which reduces their σ donation ability compared to CAAI ligands.[82]

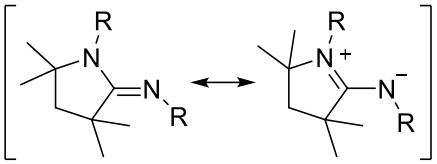

Figure 16. Cyclic alkyl amino iminate (CAAIs).

1.4.3 Carbene–Phosphinidene Adducts as Indicators of the π-Accepting Properties of Carbenes

Initially, it was first considered that the high catalytic activity of transition metals bearing NHCs was due to their strong σ-donating ability, however, it has been shown that non-negligible π-backdonation occurs between the NHC and the transition metal bond. A method based on ^{31}P NMR chemical shifts of the corresponding easily synthesized phenylphospinidene-carbene adducts was developed by Bertrand *et al*., allowing the evaluation of the π -accepting ability of carbenes (Figure 17). An increase in the π-accepting property of the carbene enhances lone pair backdonation from the phosphorus atom to the carbene's vacant p orbital.[89] Therefore, the ^{31}P NMR chemical shift of carbene–phosphinidene adducts provides a method to evaluate the π-

accepting property of the carbene, as the more π-accepting the carbene is, the further downfield the chemical shift of the phosphorus nucleus will be.[89]

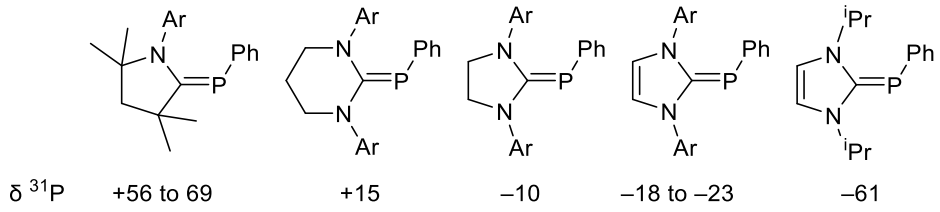

Figure 17. ^{31}P NMR chemical shift of phenylphosphinidene-carbene adducts.

1.5 Scope of thesis.

The proposed research focuses on the development of various Zn(II) complexes and an Al(III) complex bearing monoanionic bidentate guanidine-ethenolate ligands, with the synthesis pathway for the ligands, **L1**H–**L4**H, established by Jesse LeBlanc. The modular nature of guanidines allows for the control of steric and electronic properties, allowing for a systematic study of their impact on the catalytic activity of the complexes. This investigation involves varying R groups and the backbone of the imidazole, which serves as the cyclic guanidine precursor. The R groups used are isopropyl and methyl groups analogous to the phenylphospinidene-carbene adducts used in the Bertrand *et al*. study where the π-accepting characteristics were analyzed by ^{31}P NMR spectroscopy. This thesis aims to assess if there is any correlation between these π-accepting characteristics of the NHC moiety and the ROP of *rac*-LA. Additionally, a zinc complex bearing an amidine-ethenolate ligand is also explored to see the effect of replacing a σ-donating but not π-donating alkyl group on the catalytic activity for the ROP of *rac*-LA.[88] Furthermore, the synthesized guanidine-ethenolate Zn(II) complexes will be compared to previous group 4 metal complexes bearing guanidine-ethenolate ligands for their ability to ROP *rac*-LA. All synthesized complexes and ligands have been characterized using ^{1}H and ^{13}C NMR spectrometry, elemental analysis, and further used for the ROP studies of *rac*-LA.

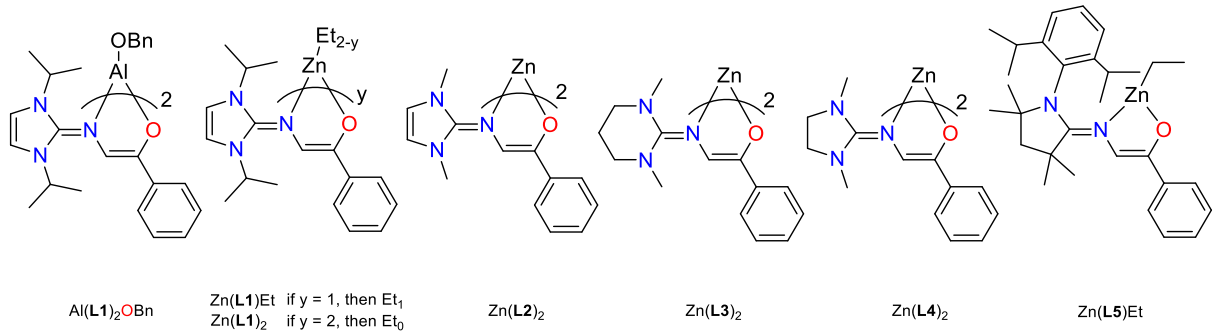

Figure 18. Complexes synthesized.

CHAPTER 2: Results and Discussion

Scheme 1. Synthesis of zinc metal complexes of **L1**–**L5**.

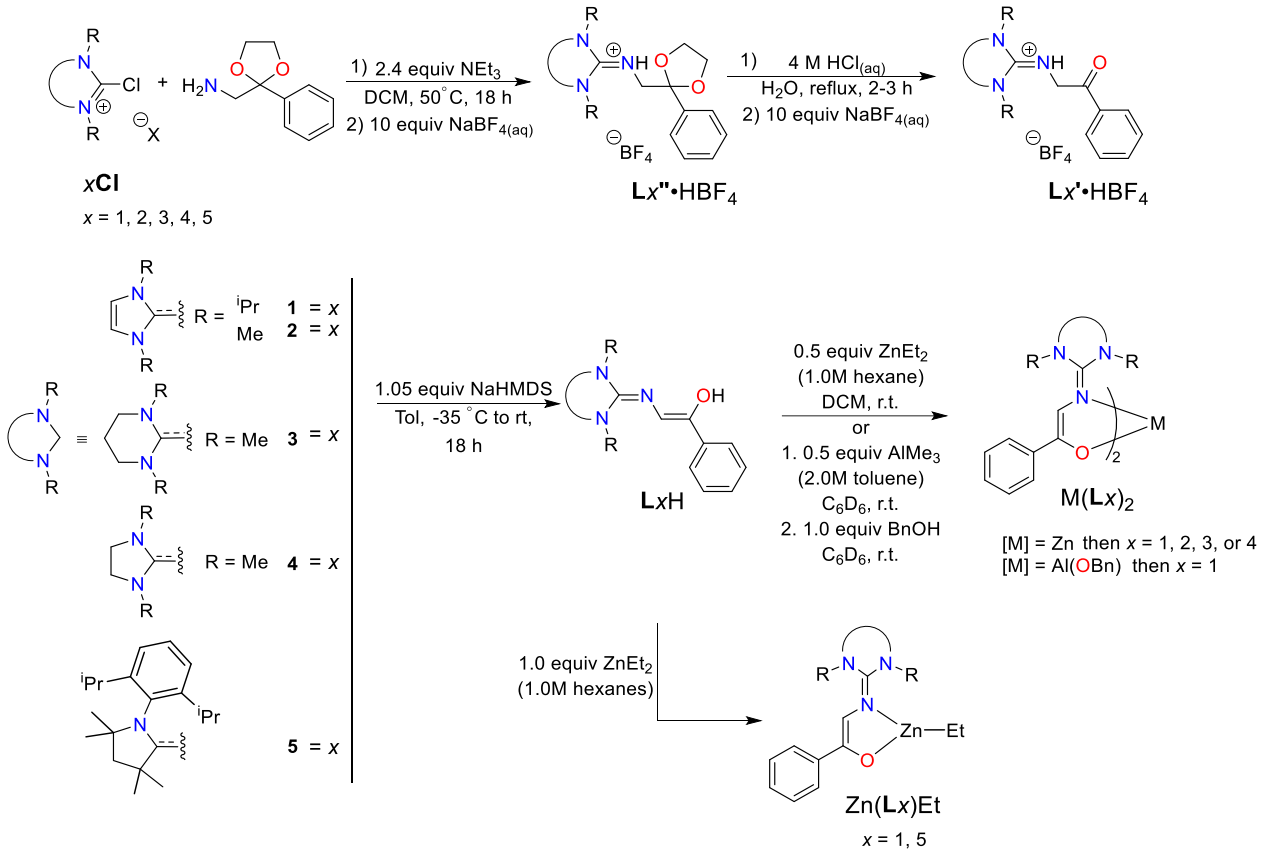

2.1 Synthesis of **L1**H–**L5**H.

Ligand synthesis pathway to **L1**H–**L4**H was established by Jesse LeBlanc and used to optimize the ligand synthesis pathway for **L5**H. The dioxolane tetrafluoroborate salt **L*x*"**•HBF_4 was prepared by reacting the chloro halide salt ***x*Cl** with 1-(2-phenyl-1,3-dioxolan-2-yl)methanamine in the presence of triethylamine, followed by an ion exchange using $NaBF_{4(aq)}$ and subsequent deprotection to give the guanidinium derivative **L*x*'**•HBF_4 (Scheme **1**). Deprotonation with sodium hexamethyldisilazide (NaHMDS) gave the neutral guanidine–ethenol **L*x*H** (with the corresponding minor keto tautomer) in a combined 78–99 % isolated yield.

Single crystals of all four guanidine–ethenol (**L1**H–**L4**H) suitable for X-ray diffraction analysis were obtained by Jesse LeBlanc by slow evaporation of a saturated ether solution for each respective ligand (Figure 19). The solid-state structures showed the selective crystallization of the major tautomer observed in solution by ^{1}H NMR spectroscopy. The syn arrangement of N1 and O1 allows for H-bonding between enol H and N. The enol hydrogen, located from the difference Fourier electron density map, is 1.88–2.03 Å from N1, well within the range for intermolecular interactions. The extended π-electron density delocalization is evidenced by the N1–C[*x*]–C[*y*]–O1 dihedral angle ranging from 0.9(4) to 7.4(5)° (Table 1), indicating that the arrangement of these atoms is nearly planar, and suggests effective conjugation. The C1–N1 bond lengths range from 1.292(4)–1.312(5) Å, and the N1–C[*x*] bond lengths range from 1.382(5)–1.401(4) Å, intermediate between that of a C–N single bond (1.46 Å) and a double bond (1.27 Å), further evidence of extended π-electron density delocalization.[90] Additionally, the C[*x*]–C[*y*] bond lengths range from 1.339(3)–1.358(5) Å, closer to typical C=C double bonds than to C–C single bonds.[90]

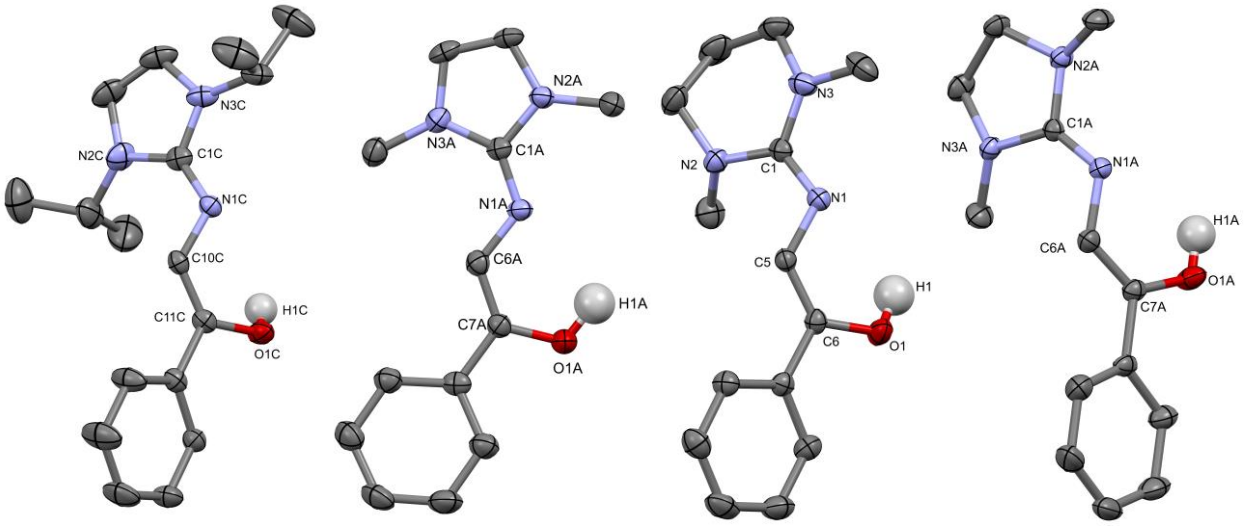

L1H **L2**H **L3**H **L4**H

Figure 19. Solid-state structure of **L1**H–**L4**H. All hydrogen atoms but H1 are omitted for clarity. ORTEP drawn at 50% probability.

Table 1. Select bond lengths (Å), dihedral angle (°), and tautomeric ratio of ligands **L1**H–**L4**H.

	L1H	**L2**H	**L3**H	**L4**H
C1–N1	1.312(5)	1.310(3)	1.310(4)	1.292(4)
C[*y*]–O1	1.374(4)	1.377(3)	1.367(1)	1.365(4)
N1–O1	2.914	2.828	2.878	2.869
N1–C[*x*]	1.382(5)	1.388(3)	1.400(15)	1.401(4)
C[*x*]–C[*y*]	1.358(5)	1.339(3)	1.341(17)	1.353(4)
N1–C[*x*]–C[*y*]–O1	4.9(6)	0.9(4)	6.74(19)	7.4(5)

Averages of all unique molecules in the unit cell are reported for **L1**H, **L2**H, and **L4**H.

2.2 Synthesis of zinc guanidine–ethenolate complexes.

The bischelated zinc complexes Zn(**L1-L4**)$_2$ were prepared in good yields (>75%) by a simple addition of two equivalents of **L*x***H to $ZnEt_2$ in 1.0 M hexane (Scheme 1). The ^{1}H NMR spectra of all zinc complexes are consistent with the structure proposed. Repeated attempts to cleanly prepare and isolate Zn(**L5**)$_2$ were unsuccessful by the addition of 1.0 equivalent of $ZnEt_2$ in 1.0 M hexane to 2.5 equivalents of **L5**H in DCM, following attempted purification methods. The presence of two septet resonances for two chemically inequivalent methine protons at 3.23 and 3.08 ppm in the ^{1}H NMR spectrum, indicates the formation of two species. Furthermore, a broad resonance at 0.39 ppm indicates the presence of a –$(CH)_2$– fragment integrating in a 1:1 ratio with the septet resonance at 3.08 ppm, indicating the presence of Zn(**L5**)Et. The septet resonance at 3.23 ppm integrates at a 4 : 28 ratio with the aromatic region, indicating the presence of more than one species, indicating the presence of Zn(**L5**)Et and residual **L5**H. Moreover, the presence of two singlet resonances for two chemically inequivalent =N-CH= protons at 6.46 ppm integrating to 2.50 and 6.40 ppm integrating to 1.35 also suggests the presence of residual **L5**H and the formation of Zn(**L5**)Et. Subsequent addition of **L5**H did not result in the full formation of Zn(**L5**)$_2$, unaltering the ^{1}H NMR spectrum. To confirm this, a 2D ^{1}H-^{1}H COSY NMR spectrum was obtained (Figure 20). The septet resonance at 3.23 ppm integrated to 4.00 correlates to two different doublet resonances at 1.25 and 1.35 ppm integrating to 19 and 9, respectively, totaling to 28 protons, which could be the isopropyl methyl protons. The septet resonance at 3.08 ppm integrates to a 2 : 12 ratio coupling to a doublet resonance at 1.10 ppm, which are the isopropyl methyl protons. The presence of these additional resonances suggests the formation of Zn(**L5**)Et with residual **L5**H due to the stoichiometric ratio used, rather than the exclusive formation of Zn(**L5**)$_2$. This unsuccessful attempt to synthesize Zn(**L5**)$_2$ could be due to the steric hindrance of the bulky diisopropylphenyl group present in **L5**H.

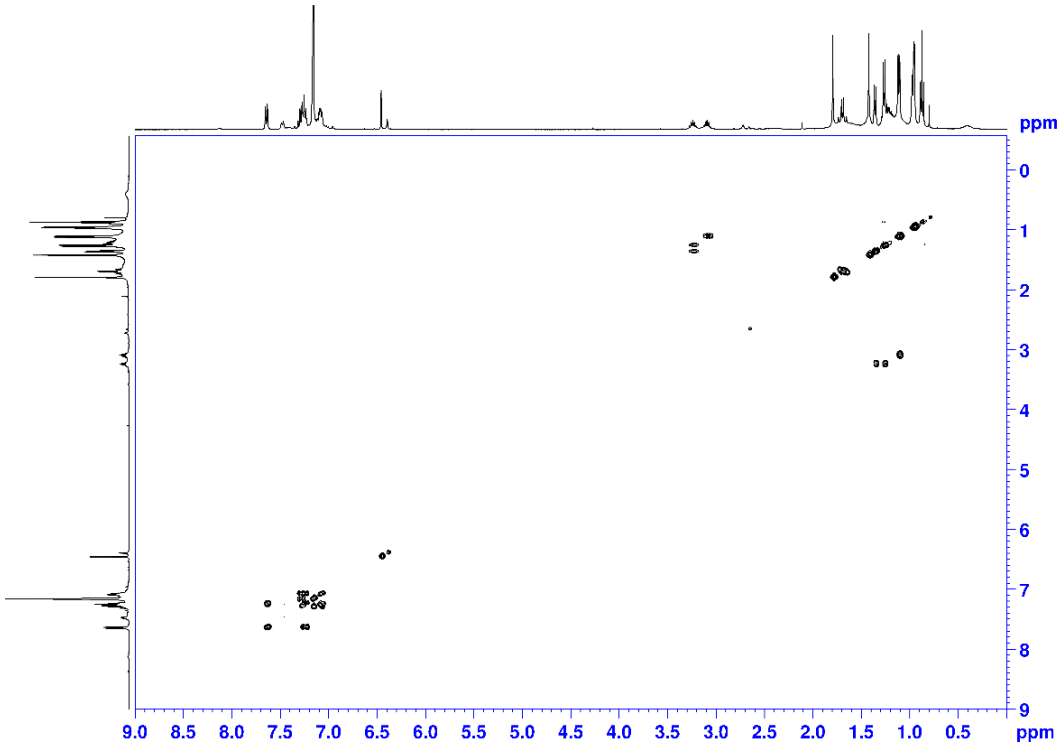

Figure 20. 2D ^{1}H-^{1}H COSY NMR spectrum (400 MHz, C_6D_6) of two species Zn(**L5**)Et and **L5**H

The monochelated Zn(**L1**)Et and Zn(**L5**)Et were also prepared in high yields (>97%) by the addition of 1.0 equivalent of **L1**H or **L5**H, respectively, to $ZnEt_2$ in 1.0 M hexane. **L1** and **L5** represent the extreme poles of π–accepting properties in the NHC fragment reported herein,[89] leading to a different coordination environment for the study polymerization of lactide. In contrast to the corresponding bischelated Zn(**L*x***)$_2$ complexes, the monochelated Zn(**L*x***)Et complexes showed broad resonances in the ^{1}H NMR spectrum, possibly a result of a dynamic equilibrium between monomeric and dimeric species (Figure 21).[91]

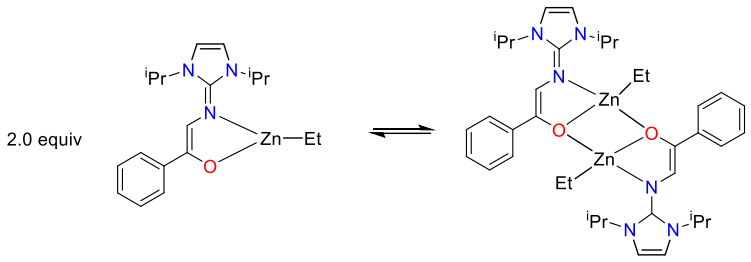

Figure 21. Dimerization equilibrium of Zn(**L1**)Et to [Zn(**L1**)Et]$_2$

Single crystals of Zn(**L1**)$_2$, Zn(**L3**)$_2$, and Zn(**L4**)$_2$ complexes suitable for X-ray diffraction were obtained by vapour diffusion of ether or toluene into a saturated solution of the corresponding complex (Figure 23) in DCM at room temperature. The guanidine-ethenolate ligands bind to the metal in a bidentate fashion resulting in a five membered metallocycle with a bite angle of N1–Zn1–O1 of 86.07(14), 86.58(16), and 86.16(5)° for Zn(**L1**)$_2$, Zn(**L3**)$_2$, and Zn(**L4**)$_2$ respectively, with the complexes adopting a distorted tetrahedral geometry as supported with τ_4 values of 0.77–0.82 (Table 3).[92] Zn(**L*x***)$_2$ complexes have ρ values of 0.99–0.98, indicating extensive delocalization within the guanidine moiety (Figure 22).[93] This extensive electron delocalization can explain the consistent bond length of the C1–N1 bonds for Zn(**L1**)$_2$, Zn(**L3**)$_2$, and Zn(**L4**)$_2$ (1.327(6), 1.314(7), and 1.307(2)Å, respectively) and **L1**H, **L3**H, and **L4**H (1.312(5), 1.310(4) and 1.292(4)Å, respectively), causing overall stabilization without causing significant bond length elongation or contraction.

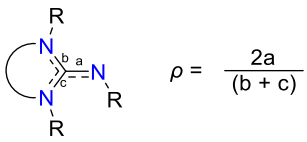

Figure 22. Calculation of the structural parameter ρ of guanidines.

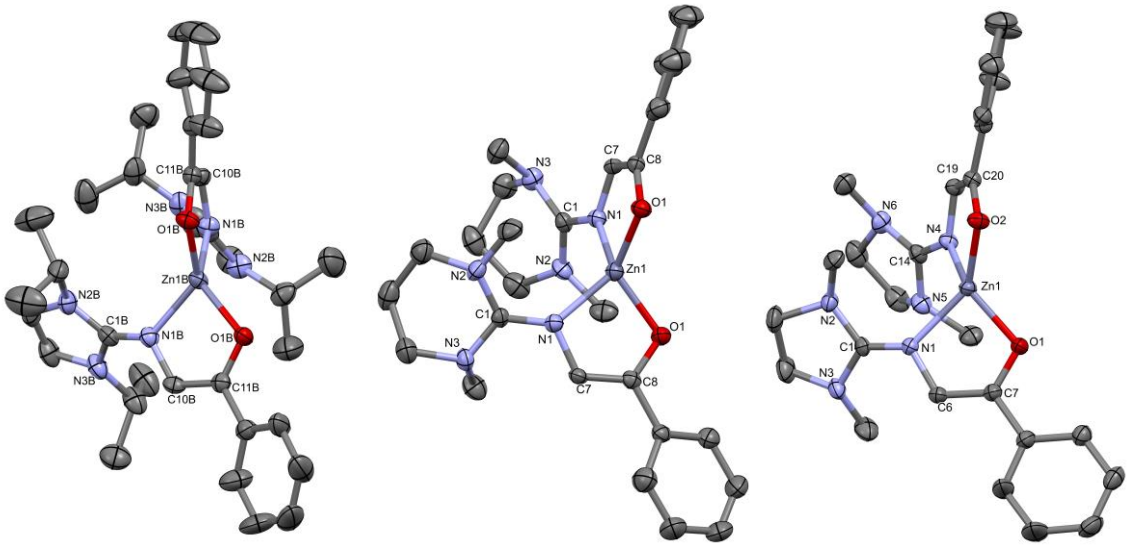

Zn(**L1**)$_2$ Zn(**L3**)$_2$ Zn(**L4**)$_2$

Figure 23. Solid-state structure of complexes Zn(**L*x***)$_2$. Hydrogen atoms and solvent molecules in unit cells have been omitted for clarity. ORTEP drawn at 50% probability.

Table 2. Select bond lengths (Å) and bond angles (°) for complexes Zn(**L*x***)$_2$.[a]

	Zn(**L1**)$_2$	Zn(**L3**)$_2$	Zn(**L4**)$_2$
N1–C1	1.327(6)	1.314(7)	1.307(2)
N2/3–C1	1.360(6)	1.372(7)	1.370(2)
Zn–N1	2.016(4)	2.025(4)	2.033(13)
Zn–O1	1.950(3)	1.936(3)	1.937(12)
N1–Zn–O1	86.07(14)	86.58(16)	86.16(5)
ρ[b]	0.97	0.96	0.95
τ_4[b]	0.79	0.82	0.77

[a]Average bond lengths and angles of all molecules in the unit cell are reported. [b]ρ and τ_4 were calculated as reported elsewhere. [92,93]

2.3 Synthesis of aluminum guanidine–ethenolate alkoxide complex.

The synthesis of the aluminum complex was attempted by the addition of two equivalents of **L1**H to trimethylaluminium in benzene-d_6 at room temperature, which was then reacted with benzyl alcohol in toluene at room temperature to give Al(**L1**)$_2$OBn shown in Scheme 1. Benzyl-alkoxy substituents were aimed over methyl substituents because they provide stronger nucleophilic character, which can promote ROP. In addition, it has been shown that group 13 metal-bearing alkoxy substituents and phenoxy-imine ligands produce high molecular weight PLA with certain stereocontrol.[94] Single crystals of complex Al(**L1**)$_2$OBn suitable for X-ray diffraction were obtained by cooling a benzene-d_6 solution of the corresponding complex (Figure 24). Unfortunately, a good model could not be defined (R_1 value of 12.81). As a result, bond lengths and angles cannot be determined reliably. Regardless, atom connectivity indicates bis-chelated connectivity and bidentate coordination of the guanidine-ethenolate ligand, **L1**, to the metal resulting in a five-membered metallocycle with a bite angle of N-Al-O of 85.7(3) or 83.2(3)° for either a trigonal pyramidal or square-based pyramid geometry as supported by τ_5 values of 0.71 and 0.41 respectively (Table 3).[92] Studies of five-coordinate bimetallic aluminum Salen complexes have shown to possess dynamic structures, converting between square-based pyramidal and trigonal bipyramidal geometries.[95] It was concluded that an intramolecular rearrangement of the non-Salen moiety of the aluminium Salen complex shifts from one face of a square-based pyramidal structure to the other face, forming trigonal bipyramidal geometries as well.[95] The Al(**L1**)$_2$OBn complex has a ρ value of 0.98, indicating extensive delocalization within the guanidine moiety.[93]

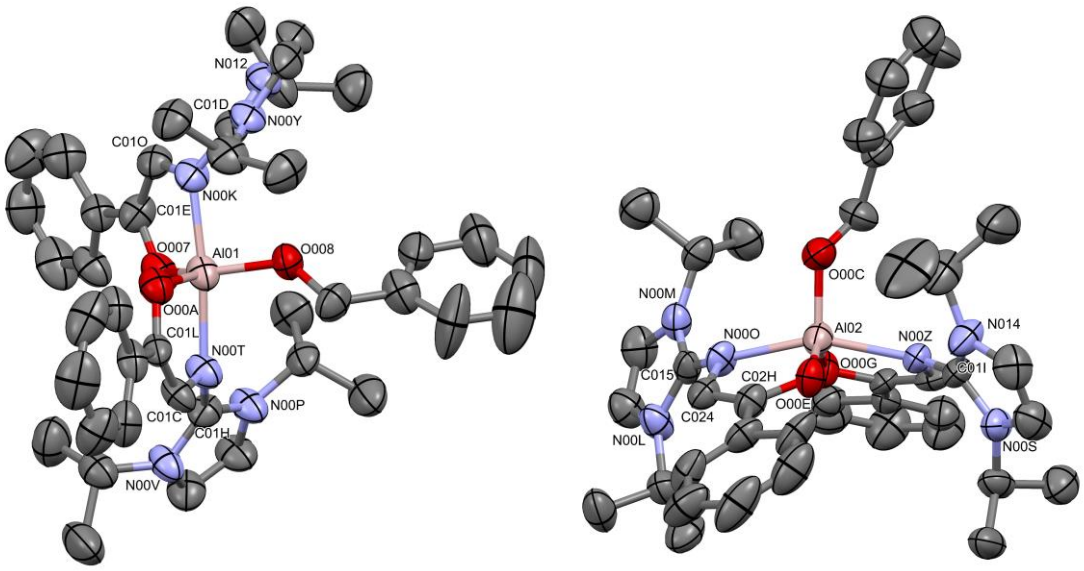

Figure 24. Dynamic solid-state structures of Al(**L1**)$_2$OBn, interconverting between trigonal bipyramidal and square-based pyramidal geometries. Most hydrogen atoms have been omitted for clarity.

Table 3. Select bond angles (°) for complex Al(**L1**)$_2$OBn.[a]

	Trigonal bipyramidal	Square-based pyramidal
N-Al-O	85.7	83.2
N–Al-N	171.2	157.2
O–Al-O	128.5	132.7
ρ^b	0.98	0.98
$\tau_5{}^b$	0.71	0.41

[a]Average bond lengths and angles of all molecules in the unit cell are reported . [b]ρ *and* τ_5 were calculated as reported elsewhere. [92,93]

2.3 Ring-opening polymerization of *rac*-lactide with Zn and Al complexes.

All zinc complexes were tested in the ROP of technical grade, unpurified *rac*-lactide, with either a 100:1 or 500:1 stoichiometric ratio of lactide to catalyst, at 130 °C in the absence of any solvent (Table 4). The additional 100:1 stoichiometric ratio of lactide to group 12 catalysts were performed to increase the polymerization rate, which was observed to be on average six times more active due to a higher concentration of catalyst as opposed to the 500:1 stoichiometric ratio. The rate of a catalyst can be quantified by the rate of propagation (R_p) (equation 1).[19] Where [LA] represents the concentration of the monomer LA, k_p is the propagation rate constant, and [I] represents the concentration of the catalyst used. Since k_p and [I] are constants, they can be rewritten as a single constant (equation 2).[19]

$$R_p = -\frac{d[LA]}{dt} = k_p[I][LA] \qquad 1$$

$$R_p = -\frac{d[LA]}{dt} = k_{obs}[LA] \qquad 2$$

k_{obs} is calculated by observing the consumption of LA into PLA during the ROP over time by ^{1}H NMR spectroscopy. k_{obs} is determined from the slope of the $\ln(([LA]_0/[LA]_t)$ versus time (t) plot (which is based on the differential rate equations 3 and 4).[19]

$$\ln[LA]_t = ln[LA]_0 - k_{obs}t \qquad 3$$

$$\ln\left(\frac{[LA]_0}{[LA]_t}\right) = k_{obs}t \qquad 4$$

All polymerizations of LA using zinc complexes at a 1:100 catalyst to LA ratio reached full conversion within 120 min, with k_{obs} values of 27.8–67.0×10^{-5} s^{-1}. M_n of the generated PLA

were determined by both ^{1}H NMR end group analysis and GPC, with values of 1,100–2,500 Da and 1,100–4,200 Da, respectively, while M_w DOSY and GPC, with values of 1,700–4,200 Da, and 1,700–6,300 Da, respectively.[96,97] The isolated PLAs showed a heterotactic bias (P_r = 0.52–0.61) similar to that observed with $Sn(Oct)_2$ under identical conditions.[27,36,37]

Zn(**L1**)$_2$ is the most active catalyst, with full conversion within 90 min and a k_{obs} value of 67.0×10^{-5} s $^{-1}$, approximately a third of the value measured for $Sn(Oct)_2$ under identical conditions (Table 4, entry 19). The decrease in steric bulk from an isopropyl group in Zn(**L1**)$_2$ (entries 1 and 2) to a methyl group in Zn(**L2**)$_2$ (Table 4, entries 6 and 7) increases the π–accepting properties of the NHC fragment, leading to the decrease in catalytic activity.[89] Zn(**L3**)$_2$ and Zn(**L4**)$_2$ (Table 4, entries 12, 13, 9, and 10) are, on average, 1.6 times slower than Zn(**L2**)$_2$ (Table 4, entries 6 and 7) this can be due to the decrease of electron conjugation of the NHC moieties in **L4** and **L3,** which increases the π–accepting properties of the NHC in comparison to **L2,** leading to a decrease in catalytic activity (Figure 26).[89]

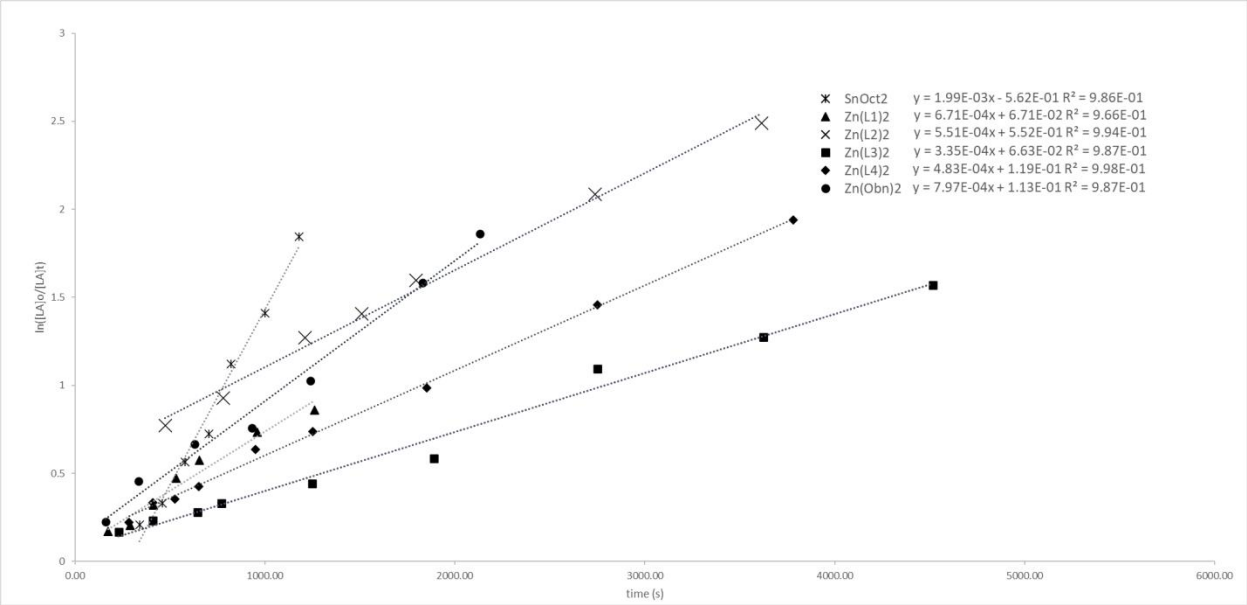

Figure 25. Kinetic plot for the polymerization of rac-lactide by $Sn(Oct)_2$, Zn(**L1**)$_2$, Zn(**L2**)$_2$, Zn(**L3**)$_2$, Zn(**L4**)$_2$, and $Zn(OBn)_2$ at 130°C in a 100:1 stoichiometric ratio of lactide to catalyst.

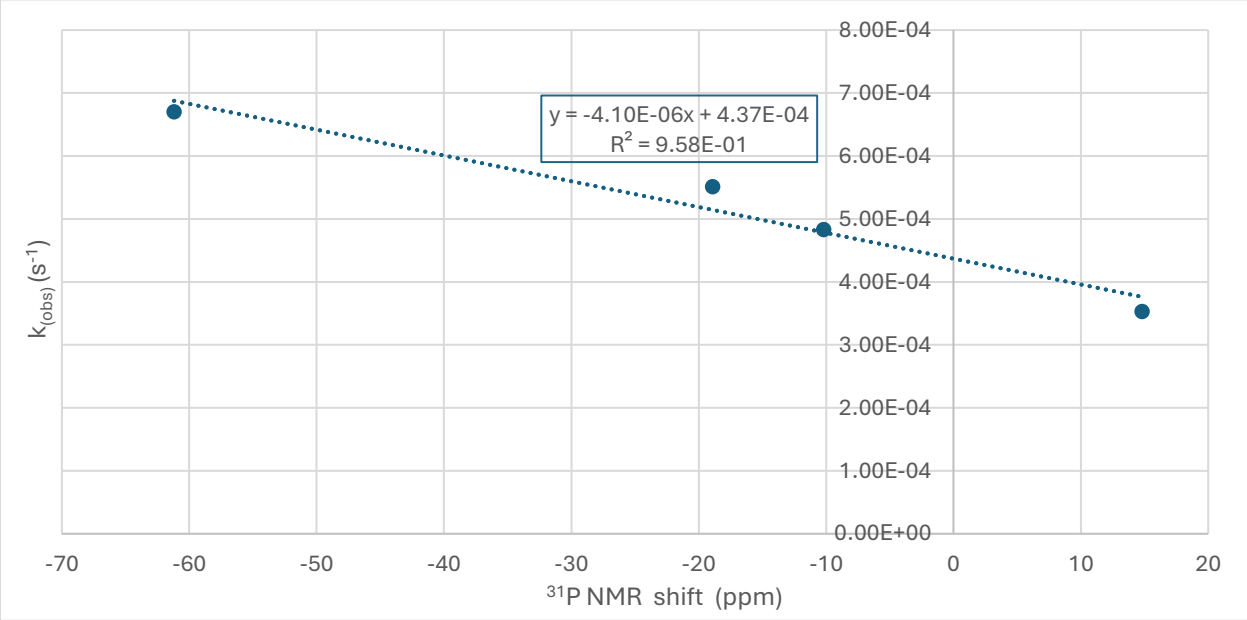

Figure 26. ^{31}P NMR shift of corresponding phenylphosphinidene-carbene adducts vs k_{obs} of Zn(**L1-L4**)$_2$ complexes at 130°C in a 100:1 stoichiometric ratio of lactide to catalyst.

Bischelated Zn(**L*x***)$_2$ complexes (Table 4, entries 3, 8, 11, and 14) and the monochelated Zn(**L1**)Et complex (Table 4, entry 5, Figure 28) were tested for the ROP of LA in the presence of 1.0 equivalent of benzyl alcohol for two separate roles. For the ROP of *rac*-LA by Zn(**L1**)Et, BnOH can act as a co-initiator to promote the generation of an alkoxide active species rather than relying on trace amounts of water present in the unpurified monomer. While for the ROP of *rac*-LA by Zn(**L1**)$_2$, BnOH can act as a nucleophile. Surprisingly, the addition of BnOH for both Zn(**L*x***)$_2$ and Sn(Oct)$_2$ resulted in a 25% decrease in activity and an increase in the dispersity, possibly due to BnOH poisoning the catalyst which is confirmed by the lack of incorporation of BnOH to the polymer as observed by MALDI-TOF MS spectra discussed in detail below.[98] In contrast, Zn(**L1**)Et in the presence of 1.0 equivalent of BnOH resulted in a 50% rate increase over that observed in the absence of BnOH (Table 4, entry 4). However, it remains 70% less active than the Zn(**L1**)$_2$ under identical conditions (Table 4, entry 3), which is possibly a result of disproportionation, previously reported in Schiff-based systems in the absence of bulky groups (Figure 27).[99] The addition of one equivalent of benzyl alcohol to Zn(**L1**)Et in pentane at room temperature rapidly gave Zn(**L1**)$_2$ and Zn(OBn)$_2$ through disproportionation of the putative Zn(**L1**)(OBn) intermediate and confirmed through ^{1}H NMR spectroscopy. The *in situ* formation of Zn(**L1**)(OBn) thereby effectively increases the concentration of the active catalyst Zn(**L1**)$_2$ explaining the 50% rate increase over that observed in the absence of BnOH (Table 4, entry 4).

Given the formation of Zn(OBn)$_2$ (Table 4, entry 16) upon addition of BnOH to Zn(**L1**)Et, its activity in the polymerization of lactide was also explored. Zn(OBn)$_2$ was synthesized upon the addition of 2.0 equivalents of BnOH to Zn(Et)$_2$ in 1.0 M of Hexane, using DCM as the solvent. The mixture was stirred for 30 minutes to allow for sufficient reaction time. Following this, mixture was placed in vacuo to remove volatiles. The resulting solids were purified sequentially

using diethyl ether and pentane yielding a white solid. Characterization of the product using ^{13}C NMR spectroscopy in $CDCl_3$, shows three resonances in the aromatic region. One of these resonances is weak, close to the baseline, which is notable since four resonances were expected, including the quaternary carbon that might be lost in the baseline noise due to solubility issues in $CDCl_3$. Additionally, elemental analysis confirmed the presence of the desired product.

The catalytic activity of $Zn(OBn)_2$ for the polymerization of LA (Table **4**, entry 16) is 5.0 times more active than Zn(**L1**)Et in the presence of BnOH (Table 4, entry 5). This observation indicates that both Zn(**L1**)$_2$ and $Zn(OBn)_2$ are active species generated *in situ* upon the addition of BnOH to Zn(**L1**)Et (see above). The 5-fold reduction in activity for Zn(**L1**)Et + BnOH compared to the expected value of 73.0 10^{-5} s^{-1} (based on the average of activities of Zn(**L1**)$_2$ and $Zn(OBn)_2$), may result from inefficient *in situ* formation of the active species, Zn(**L1**)$_2$ and $Zn(OBn)_2$. However, this 5-fold reduction in activity cannot be fully explained by current data, therefore, further investigation is required to confirm this. Moreover, $Zn(OBn)_2$ is 1.2 times more active than the most active catalysts synthesized herein, Zn(**L1**)$_2$ (Table 4, entry 2), and $Zn(OBn)_2$ is only 2.5 times less active than $Sn(Oct)_2$ (Table 4, entry 19) but generates twice as large molecular weight polymer. Polymerization with $Zn(OBn)_2$ in the presence of 1.0 equivalent of BnOH (Table 4, entry 17) resulted in 2.4 times less activity than without the presence of BnOH. As postulated above, this activity decrease might be due to the BnOH enhancing transesterification and/or chain transfer confirmed by the incorporation of BnOH to the polymer as observed by MALDI-TOF MS spectra discussed in detail below.[98]

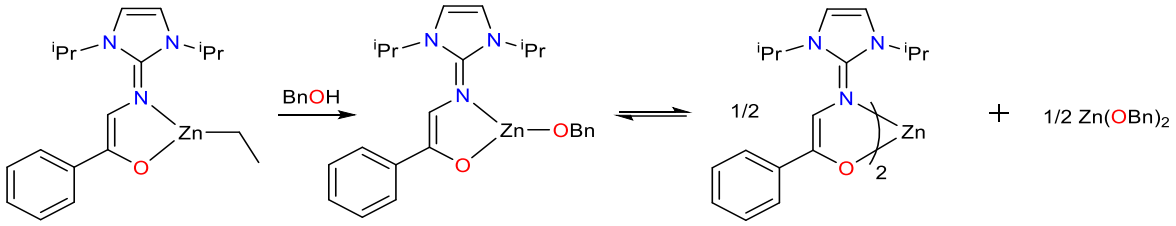

Figure 27. Protonolysis of Zn(**L1**)Et by BnOH

Zn(**L5**)Et in the presence of BnOH as co-initiator (Table 4, entry 15) resulted in a three-fold increase in rate compared to that of Zn(**L1**)Et (Table 4, entry 5, Figure 28). This could be due to the bulkier substituent (diisopropylphenyl group) in comparison to Zn(**L1**)Et, which could prevent disproportionation as mentioned previously, resulting in a higher rate.[99] Additionally, the increased rate could be due to the presence of the CAAI fragment in Zn(**L5**)Et. Although the CAAI fragment is a stronger σ donor compared to the NHI, it contains only one endocyclic nitrogen which, limits its ability to engage in π-donation, and so reduces the Lewis acidity of the metal center. Moreover, to fully understand the enhanced activity observed in the Zn(**L5**)Et + BnOH, further investigation into the mechanism is required. Furthermore, Zn(**L5**)Et in the presence of BnOH is only 8.5% slower than Zn(**L1**)$_2$ (Table 4, entry 3) under the same conditions. This result requires the synthesis of Zn(**L5**)$_2$ to determine if it shows a similar trend in reaction rate and correlates to the observed rate increase for the ROP of *rac*-LA when using Zn(**L1**)$_2$ instead of Zn(**L1**)Et. In contrast, it should also be confirmed if its activity correlates with the activity of the Zn(**L1-L4**)$_2$ complexes and the π-accepting properties of the N-heterocyclic carbene building block, therefore, due to **L5** CAAI's strong π-accepting properties, there could be a decrease in catalytic rate. Further studies are required.

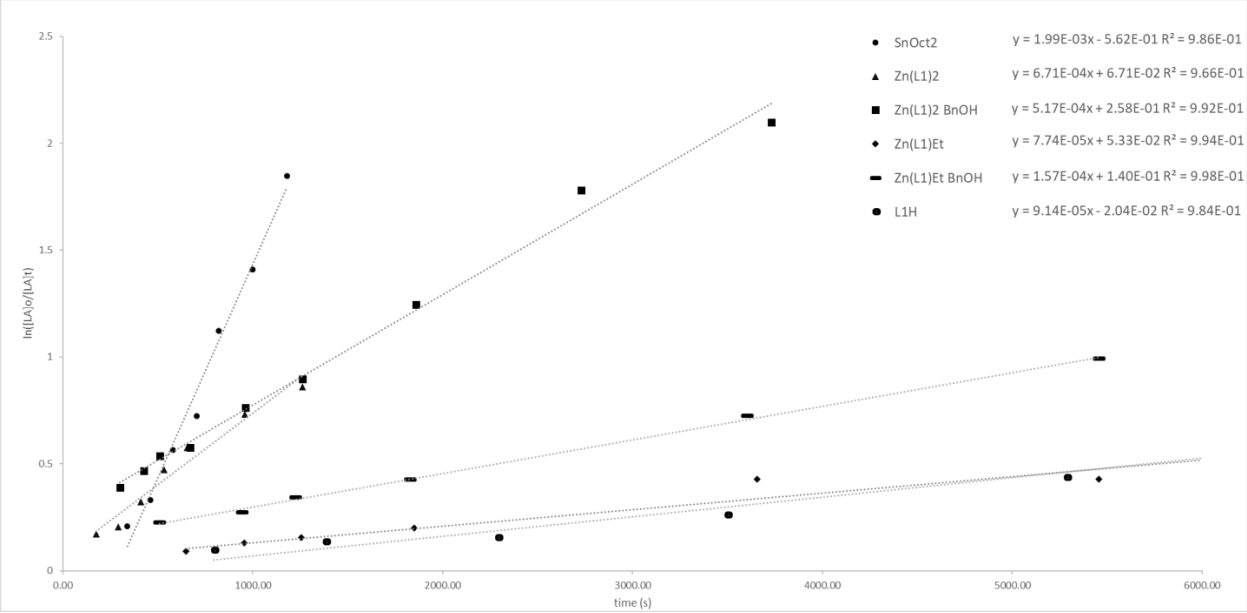

Figure 28. Kinetic plot for the polymerization of rac-lactide by $Sn(Oct)_2$, Zn(**L1**)$_2$, Zn(**L1**)$_2$ with BnOH as a co-initiator, Zn(**L1**)Et, Zn(**L1**)Et with BnOH as a co-initiator, and **L1**H at 130°C in a 100:1 stoichiometric ratio of lactide to catalyst.

As mentioned previously, guanidines are good initiators for the ROP of LA through hydrogen bonding mechanism, resulting in activities comparable to metal-based catalytic systems.[55,56] Therefore, polymerization studies of **L1**H free ligand was performed under identical conditions as the zinc complexes. Polymerization with **L1**H as an organic catalyst (Table 4, entry 19) gave polylactic acid at a rate and with molecular weights comparable to those observed using Zn(**L1**)Et (Table 4, entry 4) under identical conditions, indicating that the protonated ligand itself, possibly released during the reaction, might in fact play an important role. Moreover, Zn(**L1**)$_2$ (Table 4, entry 2) is 6.4 times more active than Zn(**L1**)Et (Table 4, entry 4), which could be due to an increase in **L1**H concentration per Zn atom available. However, this factor alone does not fully account for the observed increase, as there are only twice as many **L1**H molecules per Zn atom. A more likely explanation could be the reaction of Zn(**L1**)Et with alcohol

impurities present in LA, resulting in the inefficient formation of the active species *in situ.* This interference could reduce the overall catalytic activity of Zn(**L1**)Et compared to Zn(**L1**)$_2$. Finally, to directly compare the group 4 catalysts to group 12 catalysts, kinetic studies were carried out with bischelated Zn(**L*x***)$_2$ complexes (Table 4, entries 1, 6, 9, and 12) in 500:1 LA:catalyst ratio, which resulted in 0.8 times less active on average compared to M(**L*x***)$_2$(O^iPr)$_2$. Al(**L1**)$_2$OBn (Table 4, entry 18) completed polymerization under 6 hours and produced a polymer with an M_n of 1300 g mol^{-1}, M_w of 2900 g mol^{-1} and k_{obs} of 8.3×10^{-4} s^{-1}. Comparing Al(**L1**)$_2$OBn and Zn(**L1**)$_2$ using benzyl alcohol as a co-initiator (Table 4, entry 3), the former is 6.2 times slower than the zinc complex, which could be due to aluminum metal center being a stronger Lewis acid, resulting in a stronger metal alkoxide bond. This stronger bond could lead to hindering the coordination of LA to the metal center in the CIM, therefore decreasing the overall rate of polymerization compared to the zinc metal complex.

Table 4. Solvent-free polymerization of *rac*-lactide using zinc catalysts.[a]

entry	Catalyst	LA:Cat:BnOH	k_{obs} (10^{-5} s^{-1})	Standard error (10^{-5} s^{-1})	M_n[b] (Da)	M_w[c] (Da)	Đ[d]	M_n[e] (Da)	M_w[e] (Da)	Đ[f]	P_r[g]
1	Zn(**L1**)$_2$	500:1:0	11.0	0.2	1200	1800	1.5	1800	2400	1.3	0.60
2	Zn(**L1**)$_2$	100:1:0	67.0	2.0	2200	3600	1.6	3200	4900	1.5	0.52
3	Zn(**L1**)$_2$	100:1:1	51.7	0.8	1400	3900	2.8	3400	5300	1.5	0.60
4	Zn(**L1**)Et	100:1:0	10.4	0.2	1300	1700	1.3	4200	6300	1.5	0.52
5	Zn(**L1**)Et	100:1:1	15.7	0.9	2400	4200	1.7	2700	5900	2.2	0.55
6	Zn(**L2**)$_2$	500:1:0	8.7	0.8	1400	2300	1.6	2600	3800	1.5	0.56
7	Zn(**L2**)$_2$	100:1:0	55.1	3.5	2500	4200	1.7	1800	3000	1.7	0.58
8	Zn(**L2**)$_2$	100:1:1	63.5	3.2	2000	3400	1.7	2600	4100	1.6	0.55
9	Zn(**L3**)$_2$	500:1:0	6.3	0.2	1000	1900	2.0	2200	3000	1.4	0.54
10	Zn(**L3**)$_2$	100:1:0	35.3	1.8	1700	3900	2.3	2800	4500	1.6	0.57
11	Zn(**L3**)$_2$	100:1:1	27.8	1.1	1400	2300	1.6	2700	4200	1.5	0.57
12	Zn(**L4**)$_2$	500:1:0	4.1	0.1	2800	3000	1.1	5100	7900	1.5	0.58
13	Zn(**L4**)$_2$	100:1:0	48.3	1.2	1800	3100	1.7	2800	4400	1.6	0.61
14	Zn(**L4**)$_2$	100:1:1	45.1	1.5	1500	2800	1.9	2100	2900	1.4	0.65
15	Zn(**L5**)Et	100:1:1	47.3	1.8	1500	2300	1.5	2800	3700	1.3	0.57
16	Zn(OBn)$_2$	100:1:0	79.7	4.7	6100	5300	0.9	8800	20600	2.3	0.57
17	Zn(OBn)$_2$	100:1:1	32.7	1.1	4500	1400	0.3	6500	12000	1.8	0.60
18	Al(**L1**)$_2$OBn	100:1:0	8.3	0.9	1300	2900	2.2	2100	3100	1.4	0.43
19	**L1**H	100:1:0	9.1	1.3	1100	1800	1.6	1600	2300	1.4	0.55
20	Sn(Oct)$_2$	100:1:0	199.0	0.1	4200	6200	1.5	4100	8000	1.9	0.62

21	$Sn(Oct)_2$	100:1:1	151.0	0.1	2900	3600	1.2	3300	5800	1.7	0.62

[a]All polymerizations were performed at 130 °C in the absence of solvent. [b]Determined by ^1H NMR end-group analysis. [c]Determined by DOSY NMR in C_6D_6. [d]$Đ = M_w \div M_n$ as determined by NMR spectroscopy. [e]Determined by GPC in THF. [f]$Đ = M_w \div M_n$ as determined by GPC. [g]P_r is the probability of racemic linkages between monomer units and is determined by homonuclear-decoupled $^1H\{^1H\}$ NMR spectroscopy.

To assess the performance of our catalysts based on conversion rate and selectivity within the research field, the catalytic activity of Zn(**L1**)$_2$ was also tested for the ROP of recrystallized *L*-LA under industrially relevant conditions at 150 °C in bulk without an additional co-initiator (Table 5). Recrystallized *L*–LA was used to ensure a consistent quality of the monomer and avoid side effects caused by residual water or acid in the used lactide.[67] It was determined that Zn(**L1**)$_2$ (Table 5, entry 1) catalyzed *L*-LA only 8 times slower compared to the Herres-Pawlis *et al*. zinc(II) Schiff base complex (Table 5, entry 2[d]). All entries showed isotactic bias as expected, with our complex exhibiting a Pr value of 0.36, indicating the presence of epimerization reactions. It is important to note that enhanced Lewis acidity at the zinc center results in higher activities in the ROP of lactide.[67] In fact, Herres-Pawlis *et al.* saw an increase of catalytic activity by 3.3 times when a thioester moiety in the ligand's backbone is replaced with a fluorine atom, resulting in the increase of the electron-withdrawing effect of the ligand and ability to stabilize the growing polymer.[67]

Table 5. Solvent-free polymerization of *L*-lactide[a]

entry	Catalyst	k_{obs} (10^{-5} s^{-1})	M_n[b] (Da)	P_r[c]
1	Zn(**L1**)$_2$	5.43	4200	0.36
2[d]	Zn(F-I)$_2$	44.3	7700	
3	Sn(Oct)$_2$	78.2	9100	0.18

[a]All polymerizations were performed at 150 °C solvent-free with a 1000:1: *L*-LA-to-catalyst ratio. Recrystallized *L*-LA was used. [b]Determined by ^{1}H NMR end-group analysis. [c]Pr is the probability of racemic linkages between monomer units and is determined by homonuclear-decoupled ^{1}H{^{1}H} NMR spectroscopy. [d]Entry 2 reported by Herres-Pawlis *et al*.[67]

2.4 Mass Spectrometry

Matrix-assisted laser desorption/ionization time-of-flight (MALDI-TOF) mass spectrometry was employed to understand the polymerization mechanism of *rac*-LA to PLA using the synthesized catalyst reported herein.[100] Mass-to-charge ratio of an ion can be determined by the time known for a particle to reach a detector and experimental parameters used.[100] Ions can be generated from neutral PLA when a proton or a metal cation like H^+, NH_4^+, Na^+, or K^+ is introduced by cationizing agents.[19,100] The quality of the MALDI-TOF spectra can be influenced by the choice of matrix and cation used, and the composition of the polymers being analyzed, which may explain why not all peaks are labelled in the spectra.[100]

In the ROP of LA absent of transesterification, which leads to the breaking of an ester bond, the polymerization cycle increases the polymer's molecular weight by 144 g/mol, which is the molar mass of LA.[19,57] Therefore, MALDI-TOF MS can be used to confirm the transesterification side reaction if present.[19,100] The MALDI-TOF mass spectra **L1**H, Zn(**L1**)$_2$, and Zn(**L1**)$_2$ with BnOH, indicated polymers with a peak separation of m/z 72 g/mol, suggesting transesterification side reactions are occurring, which accounts for the observed low molecular weight.[19,101] In addition, the spectra provide evidence of hydroxy sodium adducted terminated polymer chains for **L1**H, Zn(**L1**)$_2$, and Zn(**L1**)$_2$ with BnOH. These terminated polymer chains result from water contaminants present in LA, while no OBn capped polymers were detected. This suggests that BnOH acted as a poisoning agent rather than a co-initiator upon its addition in the polymerization, as mentioned previously and discussed in detail below. The peaks in Figure 29 represent sodium-adducted-cationized open-chain PLA, with each peak separated by 72 g/mol. Peaks that are not separated by 72 g/mol might be due to different polymer chain end adducts or variations in chain end cationization. For example, the peak at m/z 833.0 corresponds

to H-Pol-OH · Na^+, while the peak at m/z 854.7 corresponds to H-Pol-ONa · Na^+. Furthermore, these peaks can be expressed as m/z = 1+ 72n + 17 + 23, where m/z is the theoretical m/z value of the polymer, 1 represents the terminal H end group, 17 represents the molar mass of the hydroxy group capping the polymer, 72n accounts for the n repeating units in the open-chain polymer (Pol), and 23 corresponds to the molar mass of the sodium ion (Na^+).[102]

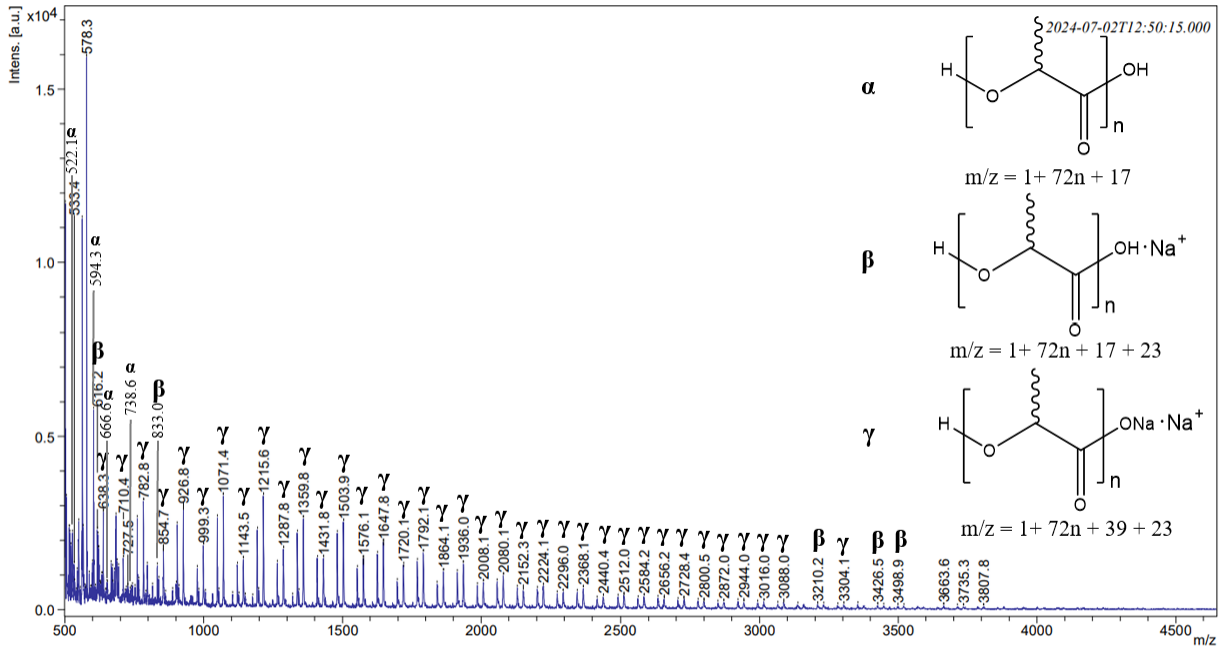

Figure 29. MALDI-TOF mass spectrum of PLA generated from **L1**H (Table 4, entry 19). All peaks can be found in Table A1.

Additionally, the free ligand does not show significant incorporation of the ligand into the polymer, suggesting that polymerization proceeded primarily through AMM. The absence of end groups corresponding to the ligand **L1**H (with expected m/z value of 285) supports this conclusion.[19] The predicted structure of PLA incorporating **L1**H is shown in Figure 30 and the corresponding equation to predict the m/z values for such polymer can be expressed as: m/z = 1 + 72n + 284 + 1, where 1 represents the molar mass of the H end group, 72n accounts for the n

repeating units of LA, 284 represents the molar mass of **L1** and 1 corresponds to the molar mass of the hydrogen ion (H^+).

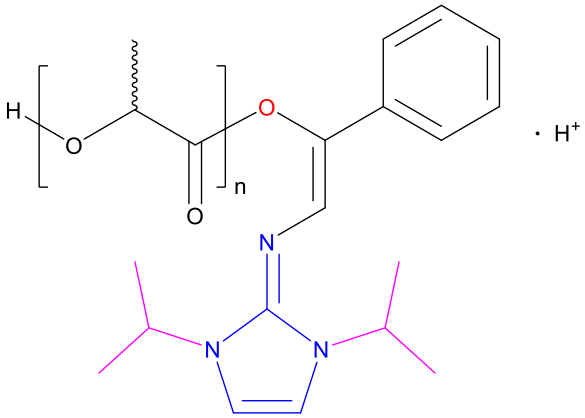

m/z = 1 + 72n + 284 + 1

Figure 30. Predicted structure of PLA incorporating **L1**H and the corresponding equation.

Upon closer analysis of Figure A50, Figure 31, and Figure A52 showing MALDI-TOF mass spectra of PLA generated from Zn(**L1**)$_2$, Zn(**L1**)$_2$ with BnOH, and Zn(**L1**)Et with BnOH, respectively, a peak is observed around m/z 1077. This peak is consistent with the previously mentioned equation of m/z = 1 + 72(11) + 285 = 1078 where n = 11, close to the observed m/z 1077 value. This suggests ligand incorporation in the polymer. The mass spectra of PLA generated from Zn(**L1**)$_2$ with BnOH (Figure A51) and Zn(**L1**)Et with BnOH (Figure A52) show that the most abundant polymers are H-Pol-OH · Na^+ and H-Pol-ONa · Na^+ followed by H-Pol-**L1** · H^+. The latter (also present in Figure A50) could result from the dissociation of the ligand **L1** from the metal center due to reaction conditions (as mentioned previously). This free ligand could then act as an external nucleophile, functioning through AMM, explaining the ligand's incorporation into the polymer. Additionally, the spectra do not show any trace of H-Pol-OBn polymer when BnOH is used as co-initiator, whichmay be due to the hydrolysis of the OBn-end

group by water contaminants, where H-Pol-OBn + H_2O → H-Pol-OH + BnOH generating the OH-terminated PLA polymer. Further analysis with purified LA would reduce the presence of water contaminants, potentially limiting hydrolysis and allowing the detection of the OBn-terminated PLA in the mass spectrum, offering clearer evidence of the polymerization mechanism. However, CIM is also a plausible mechanism, where the chain growth is initiated by the ligand in the zinc complex as discussed previously, leading to ligand incorporation, it remains challenging to determine whether AMM or CIM is the dominant mechanism.[67] Moreover, the mass spectrum of Zn(**L1**) $_2$ without BnOH (Figure A50), the pointed out poisoning agent, resulted in a much poorly resolved spectrum compared to the mass spectrum of PLA generated from Zn(**L1**)$_2$ with BnOH (Figure A51). In Figure A50, the observed polymer, H-Pol-**L1** · H^+, exhibits irregular mass separations of both 72 g/mol and 144 g/mol, while remaining peaks could not be correlated with any other identified polymer species in similar systems discussed previously. The difference in spectral resolution and peak distribution of Figure A50 compared to the mass spectrum of PLA generated from Zn(**L1**)$_2$ with BnOH (Figure A51) cannot not be readily explained with current data, indicating the need for further investigation.

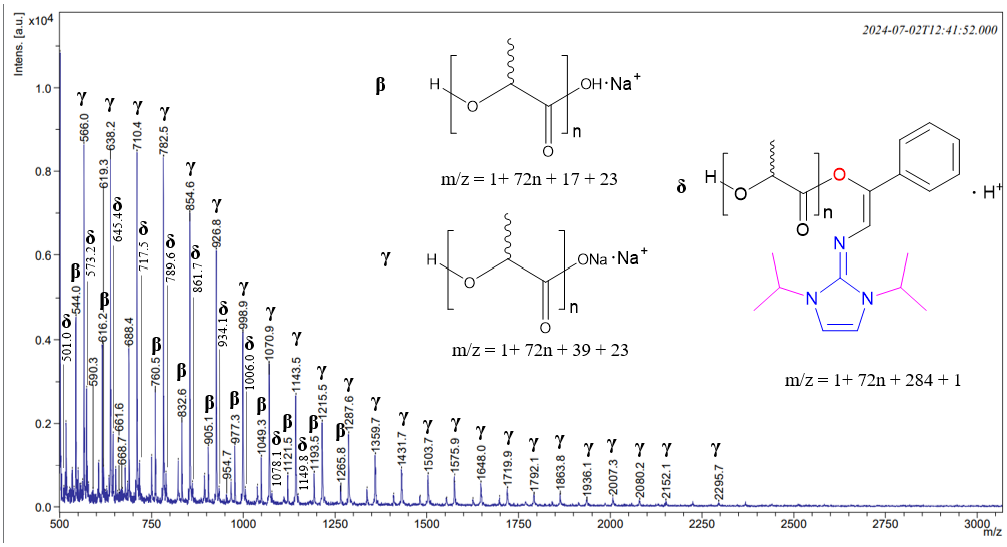

Figure 31. MALDI-TOF mass spectrum of PLA generated from Zn(**L1**)$_2$ in the presence of BnOH (Table 4, entry 3). All peaks can be found listed in Table A3.

In contrast, Zn(OBn)$_2$, both with and without BnOH, generated polymers with OH, OBn, and macrocycles sodium adducted cationized polymers. The presence of OBn-terminated PLA indicates that the polymerization proceeded through CIM. Further analysis of the MALDI-TOF mass spectra (Figure A53 and Figure A54) suggest that the most abundant polymer type in the sample is OH-terminated PLA followed by OBn-terminated PLA and macrocyclic polymers. The abundance of OH-terminated polymer is attributed to water contaminants in the LA, leading to the hydrolysis of the OBn-terminated polymers, where H-Pol-OBn + H_2O → H-Pol-OH + BnOH. Upon further analysis of the mass spectrum, the m/z peaks correspond to the sodium-adducted macrocycles determined using the equation m/z = 72n + 23, where 23 represents the mass of the sodium adduct (Na^+). For instance, the peak at m/z 526 (refer to Table A5 for all listed peaks) indicates a macrocycle containing 7 repeating units, while the peak at m/z 2544.3 indicates a macrocycle containing 35 repeating units. These macrocycle sizes are comparable

with literature reports of around 32 repeating units by Bonnet et *al*. and 43 repeating units by Mao et *al*.[103,104] Moreover, the most favoured macrocycle size, corresponding to the peak at m/z 670.2, represents a macrocycle with 9 repeating units. This observation aligns with reports in the literature, where macrocyclic PLA sizes range from 6 to 18 repeating units.[103,105]

CHAPTER 3: Conclusions

These first-generation aluminum and zinc complexes bearing monoanionic bidentate cyclic guanidine–ethenolate ligands show promising performance for the ROP of lactide. Solid-state structures of the bischelated zinc complexes showed a distorted tetrahedral geometry. Solid-state structure of the bischelate aluminum complex showed dynamic trigonal pyramidal and square-based pyramidal geometries.[95] All complexes were active in the polymerization of *rac*-lactide, giving polymers with a heterotactic bias. Zn(**L1**)$_2$, the most active zinc catalyst reported herein, is only about three times less active than the industrial standard, Sn(Oct)$_2$, in the polymerization of *rac*-LA at 130 °C. For the polymerization of *L*-LA at 150 °C, Zn(**L1**)$_2$ is only about 14.4 times slower compared to Sn(Oct)$_2$, and about only 2.5 times slower compared to Herres-Pawlis *et al*. zinc(II) Schiff base complex.[67] The addition of benzyl alcohol as a co-initiator for the polymerization using Zn(**L1**)Et readily gave Zn(**L1**)$_2$ and Zn(OBn)$_2$, with both complexes having comparable activities. The imine-ethenolate monochelated Zn(**L5**)Et complex, in the presence of BnOH, resulted in three times faster than the monochelated guanidine-ethenolate Zn(**L1**)Et complex. MALDI-TOF MS was used to determine the end groups of the polymer chain. The spectra provide evidence of hydroxy and ethoxy sodium adducted terminated polymer chains for **L1**H, Zn(**L1**)$_2$, and Zn(**L1**)$_2$ with BnOH, with no detectable OBn capped polymers suggesting that BnOH acted as a poisoning agent rather than a co-initiator upon its addition in the polymerization. MALDI-TOF indicated presence of transesterification reactions due to the presence of peak separations of m/z 72.[100] The activity of Zn(**L*x***)$_2$ correlated with the variation of the π-accepting properties of the N-heterocyclic carbene building block used in the synthesis of the ligand, thus offering the opportunity to further improve the performance of this

new class of catalysts.[89] The monochelated imine-ethenolate zinc complex, Zn(**L5**)Et, in the presence of BnOH, is only 8.5% slower than Zn(**L1**)$_2$ under the same conditions, which could be due to the enhanced the Lewis acidity of the metal center due to the presence of the CAAI fragment. Therefore, to further confirm the correlation between the activity of the bischelated guanidine-ethenolate zinc complexes and the π-accepting properties of the N-heterocyclic carbene building block, the exploration of bischelated zinc complexes bearing imine-ethenolate ligands for their catalytic studies in the ROP of *rac*-LA should be done. Furthermore, the exploration of incorporating withdrawing groups in the guanidine-ethenolate ligands could enhance our understanding of their catalytic behavior in the polymerization of lactide.

CHAPTER 4: Experimental methods.

4.1 General Remarks

Unless otherwise stated, all reactions and manipulations were performed under an inert atmosphere of dry argon, using standard Schlenk techniques or in a nitrogen filled glovebox. Sodium hydride was purchased from Sigma Aldrich as a 60% dispersion in mineral oil that was thoroughly washed with pentane prior to use. 2-[(2-phenyl-1,3-dioxolan-2-yl)methyl]-2,3-dihydro-1H-isoindole-1,3-dione, **1Cl**, **2Cl**, **3Cl**, **4Cl**, and **5Cl** were prepared according to reported literature procedures.[106–109] 1-(2-phenyl-1,3-dioxolan-2-yl)methanamine was prepared according to methodology established by Jesse LeBlanc. All other reagents were purchased from Sigma-Aldrich or Alfa Aesar and used as received. All protio solvents were dried over activated alumina columns, degassed with dry argon, and stored on molecular sieves prior to use. C_6D_6, $CDCl_3$ and CD_2Cl_2 were purchased from Sigma-Aldrich, degassed using three freeze-pump-thaw cycles, vacuum-distilled from sodium and benzophenone for C_6D_6 and from CaH_2 for $CDCl_3$ and CD_2Cl_2, and stored under argon. Unless otherwise stated, ^{1}H NMR spectra were referenced to the residual protio solvent resonance (δ 7.26 ppm for $CDCl_3$, 7.15 ppm for C_6D_6, 5.32 ppm for CD_2Cl_2, 1.94 ppm for CD_3CN, 4.67 ppm for D_2O and 2.04 ppm for acetone-d_6). All glassware was oven dried overnight in an oven prior to use. ^{1}H, ^{13}C and ^{19}F NMR spectra were recorded on a Bruker UltraShield 600, Bruker 400, or Bruker UltraShield 300 MHz NMR spectrometer at room temperature. NMR multiplicities are abbreviated as follows: s = singlet, d = doublet, t = triplet, q = quadruplet, m = multiplet, br = broad.

4.2 Crystal Structure Determinations

Diffraction data for complexes were collected on a Bruker APEX-II CCD diffractometer with a Mo *Kα* (λ = 0.71073 Å) radiation source. Crystals were selected under paratone oil and mounted under a steam of N_2 and kept at 173K during data collection. Structures were solved in Olex2 using direct methods and refined with ShelXL refinement package using least-squares minimization.

4.3 Ring-opening polymerization of *rac*-lactide with complexes.

Polymerizations were performed in the absence of solvent at 130 °C in a 500:1 or 100:1 stoichiometric ratio of lactide to catalyst, using unpurified monomer. All complexes gave full conversion within 6 h. The polymerization rate constants were obtained by monitoring the consumption of the monomer over time using ^{1}H NMR spectroscopy. The number- (M_n) and

weight-average (M_w) molecular weights of the unpurified polymer were determined by end-group analysis using ^{1}H NMR spectroscopy and by diffusion-ordered spectroscopy (DOSY), respectively, and by gel permeation chromatography (GPC).[96,97] The tacticity (P_r) of resulting polymers were determined by the homonuclear-decoupled ^{1}H{^{1}H} NMR spectroscopy.[27,36,37]

4.4 Size Exclusion Chromatography

Number- and weight-average molecular weights and dispersity (Đ; M_w/M_n) of samples (1 to 2 mg/mL in tetrahydrofuran) were also determined by gel permeation chromatography (GPC) using two PLgel miniMIX-B columns (4.6 mm x 250 mm) and two PLgel miniMIX-C columns (4.6 mm x 250 mm) from Agilent on elution with tetrahydrofuran (0.4 mL/min) at 30 °C equipped with an Agilent multi detector suite composed of an Agilent G7801A refractive index detector, an Agilent G7803A dual-angle light scattering detector and an Agilent G7802A viscometer, all of them at 30 °C. The three detectors were calibrated using a narrow polystyrene standard (PS) from Agilent (M_p = 27,060 g/mol). Columns were calibrated using eight PS standards with a conventional approach (data from refractive index detector only). Data were analyzed using the Agilent GPC software version A.02.01 software (Santa Clara, CA 95051, United States).

4.5 MALDI-TOF Mass spectrometry

Matrix-assisted laser desorption ionization time-of-flight mass spectrometer (MALDI-TOF) data was obtained at the AIMS laboratory of University of Toronto on a Bruker AutoFlex Speed MALDI-TOF instrument. Using a 2 kHz frequency with tripled Nd:YAG laser (λ = 355 nm). Samples were prepared in a dithranol THF matrix.

4.6 **L5"•**HBF_4. A 100-mL flask was charged with **5Cl** (200 mg, 0.561 mmol, 1.0 equiv.), 1-(2-phenyl-1,3-dioxolan-2-yl)methanamine (100 mg, 0.598 mmol, 1.1 equiv.) and approximately 50 mL of DCM. The mixture was stirred for 30 min and anhydrous triethylamine (235 µL, 1.70 mmol, 3.0 equiv.) was added. The mixture was refluxed and stirred for 12 h. The reaction mixture was cooled to room temperature, a 20 mL aqueous solution of $NaBF_4$ (635 mg, 5.80 mmol, 15.0 equiv.) was added. After 30 min, the organic layer was extracted, dried over $MgSO_4$, filtrated, and the volatiles removed in vacuo. The crude product was extracted by sonication with toluene (3 × 15 mL), dried in vacuo, which was followed by washes with diethyl ether (2 × 10 mL) to yield a pale orange solid. **L5"•**HBF_4**,** 185 mg, 0.332 mmol, 85%. ^{1}H NMR (400 MHz, $CDCl_3$) δ 7.62–7.58 (t, *J* = 8.0 Hz , 1H, *p*–Ph_{dipp}), 7.43–7.42 (d, *J* = 4.0 Hz, 2H, *m*–Ph_{dipp}), 7.34 (m, 5H, *m,p,o*–Ph), 5.74

(br s, H, —NHCH$_2$C–), 3.81 (s, 2H –NHCH$_2$C–), 3.67–3.66 (m, 2H, –OCH$_2$CH$_2$O–), 3.63-2.61 (m, 2H, –OCH$_2$CH$_2$O–), 2.81 (m, 2H, –CCH(CH$_3$)$_2$ Ph$_{dipp}$), 2.55 (s, 2H, –CCH$_2$C–), 1.71 (s, 6H, –NC(CH$_3$)$_2$–), 1.54 (s, 6H, –CH$_2$C(CH$_3$)$_2$C–), 1.35 (d, *J* = 8.0 Hz, 6H, –CCH(CH$_3$)$_2$ Ph$_{dipp}$), 1.17 (d, *J* = 8.0 Hz, 6H, –CCH(CH$_3$)$_2$ Ph$_{dipp}$). ^{13}C{^{1}H} NMR (100 MHz, CDCl$_3$) δ 173.2, 147.9, 137.1, 132.3, 129.9, 129.1, 126.7, 125.8, 124.9, 106.6, 71.2, 51.9, 49.2, 43.8, 29.1, 28.9, 26.8, 25.5, 23.7 ppm. ^{19}F{^{1}H} NMR (377 MHz, CDCl$_3$) δ –153.26, –153.31 ppm. Anal. Calcd for C$_{30}$H$_{43}$BF$_4$N$_2$O$_2$ (%): C, 65.46; H, 7.87; N, 5.09. Found (%): C, 65.52; H, 7.89; N, 4.89.

4.7 **L5'**•HBF$_4$. A 50 mL round-bottom flask was charged with **L5''**•HBF$_4$ (48 mg, 0.088 mmol, 1.0 equiv.) and 20 mL of H$_2$O and allowed to mix for 10 minutes, an aqueous solution of 4 M HCl (6 equiv.) was then added. The reaction vessel was then equipped with a reflux condenser and brought to 110 °C and allowed to stir for 6 h 40 min. The mixture was then slowly brought down to room temperature, 20 mL of DCM and a solution of NaBF$_{4(aq)}$ (104 mg, 0.947 mmol, 11.0 equiv.) were then added and allowed to vigorously stir for 10 minutes. The resulting mixture was then transferred into a separatory funnel, the organic layer was extracted, dried over MgSO$_4$, filtrated, and dried in vacuo to yield a yellow/white solid. The product was then recrystallized in warm EtOH and allowed to slowly evaporate to yield crystals suitable for XRD. **L5'**•HBF$_4$**,** 43 mg, 0.085 mmol, 96%. ^{1}H NMR (400 MHz, CDCl$_3$) δ 8.08 (d, *J* = 4.0 Hz , 2H, Ph$_{dipp}$), 7.66–7.63 (m, 2H, *m*–Ph), 7.55–7.51 (m, 2H, *m*–Ph), 7.47–7.45 (d, 2H, *m*–Ph), 7.36–7.32 (m, 1H, Ph$_{dipp}$), 7.20 (br s, 1H, —NHCHC–), 5.20 (d, *J* = 4.0 Hz, 2H, —NHCH$_2$C–), 3.81 (s, 2H –NHCH$_2$C–), 3.67–3.66 (m, 2H, –OCH$_2$CH$_2$O–), 3.63-2.61 (m, 2H, –OCH$_2$CH$_2$O–), 2.81 (m, 2H, –CCH(CH$_3$)$_2$ Ph$_{dipp}$), 2.55 (s, 2H, –CCH$_2$C–), 1.71 (s, 6H, –NC(CH$_3$)$_2$–), 1.54 (s, 6H, –CH$_2$C(CH$_3$)$_2$C–), 1.35 (d, *J* = 8.0 Hz, 6H, –CCH(CH$_3$)$_2$ Ph$_{dipp}$), 1.17 (d, *J* = 8.0 Hz, 6H, –CCH(CH$_3$)$_2$ Ph$_{dipp}$). ^{13}C{^{1}H} NMR (100 MHz, CDCl$_3$) δ 191.5, 173.2, 147.8, 135.4, 132.4, 129.4, 129.1, 126.6, 124.7, 70.6, 52.6, 48.4, 44.1, 29.3, 28.9, 26.6, 23.4 ppm. ^{19}F{^{1}H} NMR (377 MHz, CDCl$_3$) δ –151.9, –152.0 ppm. Anal. Calcd for C$_{28}$H$_{39}$BF$_4$N$_2$O (%): C, 66.41; H, 7.76; N, 5.53. Found (%): C, 66.34; H, 7.90; N, 5.44.

4.8 **L5**H**.** A 20 mL vial was charged with **L5'**•HBF$_4$ (181 mg, 0.357 mmol, 1.0 equiv.) and 5 mL of anhydrous diethyl ether then cooled to –40 °C. The cold suspension then had a cold 5 mL diethyl ether solution of NaHMDS (70 mg, 0.38 mmol, 1.05 equiv.) added dropwise over the course of 5 minutes and allowed to warm to room temperature and mix for 16 h. The resulting suspension was then cooled to -40 °C and allowed to settle over the course of several hours and then decanted and

filtrated. **L5**H, 130 mg, 0.311 mmol, 86%. ^{1}H NMR (400 MHz, $CDCl_3$) δ 8.08 (d, *J* = 8.0 Hz , 1H, *p*–Ph_{dipp}), 7.43–7.42 (d, *J* = 4.0 Hz, 2H, *m*–Ph_{dipp}), 7.34 (m, 5H, *m,p,o*–Ph), 5.74 (br s, H, —$NHCH_2C$–), 3.81 (s, 2H –$NHCH_2C$–), 3.67–3.66 (m, 2H, –OCH_2CH_2O–), 3.63-2.61 (m, 2H, –OCH_2CH_2O–), 2.81 (m, 2H, –$CCH(CH_3)_2$ Ph_{dipp}), 2.55 (s, 2H, –CCH_2C–), 1.71 (s, 6H, –$NC(CH_3)_2$–), 1.54 (s, 6H, –$CH_2C(CH_3)_2C$–), 1.35 (d, *J* = 8.0 Hz, 6H, –$CCH(CH_3)_2$ Ph_{dipp}), 1.17 (d, *J* = 8.0 Hz, 6H, –$CCH(CH_3)_2$ Ph_{dipp}). $^{13}C\{^1H\}$ NMR (100 MHz, , $CDCl_3$) 163.8, 148.9, 142.6, 134.8, 132.8, 128.9, 128.2, 128.0, 126.4, 124.9, 124.1, 122.9, 108.1, 61.8, 55.5, 52.0, 41.2, 30.6, 29.8, 29.7, 29.2, 28.9, 28.6, 26.3, 22.5 ppm. Anal. Calcd for $C_{28}H_{38}N_2O$ (%): C, 80.34; H, 9.15; N, 6.69. Found (%): C, 80.55; H, 8.90; N, 6.44.

4.9 General procedure for the synthesis of Zn(**L*x***)$_2$. A 20 mL vial was charged with **L*x***H (2.0 equiv.) was dissolved in DCM. $ZnEt_2$ (1.0 M in hexanes; 1.0 equiv., on an approximately 0.35-mmol scale) was added dropwise to **L*x***H. During this addition, gas was generated. The mixture was stirred for 16 h. Volatiles were then removed in vacuo, washed with pentane, and dried in vacuo, to further purify, the crude was washed with diethyl ether and dried in vacuo, resulting in yellow solids. Zn(**L1**)$_2$, 99.7 mg, 0.157 mmol, 90%. ^{1}H NMR (400 MHz, $CDCl_3$) δ 7.66 (d, *J* = 8.0 Hz, 2H, *o*–Ph), 7.27–7.23 (m, 2H, *m*–Ph), 7.08 (t, *J* = 8.0 Hz, 1H, –NCHC–), 6.39 (s, 2H, –NCHCHN–), 5.03–4.99 (m, 2H, –$NCHMe_2$), 1.27–1.21 ppm (m, 12H, –CH_3). $^{13}C\{^1H\}$ NMR (100 MHz, $CDCl_3$) δ 128.0, 127.8, 127.6, 127.5, 124.5, 123.5, 110.6, 106.8, 46.5, 22.6 ppm. Anal. Calcd for $C_{34}H_{44}N_6O_2Zn$ (%): C, 64.40; H, 6.99; N, 13.25. Found (%): C, 64.67; H, 6.83; N, 13.56. Zn(**L2**)$_2$, 38 mg, 0.073 mmol, 98%. ^{1}H NMR (400 MHz, $CDCl_3$) δ 7.68 (d, *J* = 8.0 Hz, 4H, *o*–Ph), 7.29–7.26 (m, 4H, *m*–Ph), 7.13 (t, *J* = 8.0 Hz, 2H, *p*–Ph), 6.65 (s, 1H, –NCHC–), 6.18 (s, 4H, –NCHCHN–), 3.49 ppm (s, 6H, –NMe). $^{13}C\{^1H\}$ NMR (100 MHz, $CDCl_3$) δ 149.3, 141.2, 127.8, 125.2, 123.8, 115.6, 105.7, 34.2, 29.8 ppm. Anal. Calcd for $C_{26}H_{28}N_6O_2Zn$ (%): C, 59.83; H, 5.41; N, 16.10. Found (%): C, 60.14; H, 5.67; N, 15.88. Zn(**L3**)$_2$, 60.0 mg, 0.106 mmol, 97%. ^{1}H NMR (400 MHz, $CDCl_3$) δ 7.71 (d, *J* = 8.0 Hz, 2H, *o*–Ph), 7.28–7.24 (m, 2H, *m*–Ph), 7.12 (t, *J* = 8.0 Hz, 1H, *p*–Ph), 6.20 (s, 1H, –NCHC–), 3.15 (s, 4H, –NCH_2–), 2.97 (s, 6H, –NMe), 1.91 ppm (t, *J* = 4.0 Hz, 2H, –$CH_2CH_2CH_2$–). $^{13}C\{^1H\}$ NMR (100 MHz, $CDCl_3$) δ 127.7, 125.3, 124.1, 107.2, 48.6, 38.7, 21.4 ppm. Anal. Calcd for $C_{28}H_{36}N_6O_2Zn$ (%): C, 60.70; H, 6.55; N, 15.17. Found (%): C, 60.94; H, 6.48; N, 15.43. Zn(**L4**)$_2$, 36.0 mg, 0.070 mmol, 75%. ^{1}H NMR (400 MHz, $CDCl_3$) δ 7.68 (d, *J* =8.0 Hz, 4H, *o*–Ph), 7.29–7.24 (m, 4H, *m*–Ph), 7.14 (t, *J* = 6.0 Hz, 2H, *p*–Ph), 6.29 (s, 1H, –NCHC–), 3.34 (s, 4H, –NCH_2CH_2N–), 2.93 ppm (s, 6H, –

NMe). $^{13}C\{^{1}H\}$ NMR (100 MHz, $CDCl_3$) δ 149.3, 141.2, 127.8, 125.2, 123.8, 115.6, 105.7, 34.2, 29.8 ppm. Anal. Calcd for $C_{26}H_{32}N_6O_2Zn$ (%): C, 59.37; H, 6.13; N, 15.98. Found (%): C, 59.19; H, 5.87; N, 16.34.

4.11 General procedure for the synthesis of Zn(**L*x***)Et. A 20 mL vial was charged with **L*x***H (1.0 equiv.) was dissolved in DCM. $ZnEt_2$ (1.0 M in hexanes; 1.5 equiv., on an approximately 0.35-mmol scale) was added dropwise to **L*x***H. During this addition, gas was generated. The mixture was stirred for 16 h. Volatiles were then removed in vacuo, washed with pentane, and dried in vacuo, to further purify, the crude was washed with diethyl ether and dried in vacuo, resulting in yellow solids. Zn(**L1**)Et, 64 mg, 0.17 mmol, 98%. ^{1}H NMR (400 MHz, C_6D_6) δ 7.92 (d, J = 12.0 Hz, 2H, *o*–Ph), 7.29 (t, J = 10.0 Hz, 2H, *m*–Ph), 7.10 (s, 1H, *p*–Ph), 6.67 (s, 1H, –NCHC–), 5.82 (s, 2H, –CHCHN–), 5.02 (br s, 2H, –$NCHMe_2$), 1.57–1.41 (br, s, 3H, –CH_2CH_3), 1.11–0.96 (br, 12H, –CH_3), 0.60–0.45 ppm (br, s, 2H, –CH_2CH_3). $^{13}C\{^{1}H\}$ NMR (100 MHz, C_6D_6) 150.1, 147.0, 141.5, 124.8, 123.7, 112.9, 110.6, 47.0, 30.2, 21.8, 14.0, –0.54 ppm. Anal. Calcd for $C_{19}H_{27}N_3OZn$ (%): C, 60.24; H, 7.18; N, 11.09. Found (%): C, 60.50; H, 6.91; N, 10.87. Zn(**L5**)Et, 64.3 mg, 0.170 mmol, 98%. ^{1}H NMR (400 MHz, CD_2Cl_2) δ 7.46 (t, J = 4.0 Hz, 1H, *p*–Ph_{dipp}), 7.32 (br, 2H, *m*–Ph_{dipp}), 7.06 (br, 3H, *o,p*–Ph), 6.99 (br, 2H, *m*–Ph), 6.09 (s, 1H, –NCHCPh–), 3.15 (s br, 2H, –$CCHMe_2$), 2.14 (s, 2H, Me_2CCH_2–), 1.77 (br, s, 6H, Me_2CCH_2–), 1.51 (br, 12H, –$CHCH_3$), 1.14 (br, s, 6H, Me_2CN–), 0.77 (br, 3H, –CH_2CH_3), -0.32 ppm (br, 2H, –CH_2CH_3). $^{13}C\{^{1}H\}$ NMR (100 MHz, , CD_2Cl_2) 164.2, 152.1, 147.6, 139.4, 136.1, 128.9, 128.7, 127.0, 125.9, 125.1, 124.9, 109.1, 65.2, 43.0, 29.5, 29.0, 24.3, 21.1, 12.5, 0.94. Anal. Calcd for $C_{30}H_{42}N_2OZn$ (%): C, 70.37; H, 8.27; N, 5.47. Found (%): C, 70.70; H, 7.99; N, 5.56.

4.12 Synthesis of $Zn(OBn)_2$. A 20 mL vial was charged with $ZnEt_2$ (1.0 M in hexanes; 1.0 equiv., 1.03 mmol) in dissolved in DCM was added dropwise to benzyl alcohol (2.5 equiv., 2.60 mmol) dissolved in DCM. The mixture was stirred for 1 h. Volatiles were then removed in vacuo, washed with pentane, and dried in vacuo, resulting in white solids (99 mg, 0.16 mmol, 90%.) ^{1}H NMR (400 MHz, $CDCl_3$) δ 7.38 (d, J = 4.0 Hz, 10H, Ar), 4.72 ppm (m, 4H, -CH_2-). $^{13}C\{^{1}H\}$ NMR (100 MHz, $CDCl_3$) δ 128.7, 127.8, 127.2, 29.9 ppm. Anal. Calcd for $C_{14}H_{14}O_2Zn$ (%): C, 6.13; H, 5.05. Found (%): C, 60.20; H, 4.88.

4.13 Synthesis of Al(**L1**)$_2$OBn. A 20 mL vial was charged with **L1**H (2.0 equiv.) dissolved in C_6D_6. $AlMe_3$ (2.0 M in toluene; 1.0 equiv., 90 mg, 0.26 mmol) was added dropwise to **L1**H.

During this addition, gas was generated. The mixture was stirred for 16 h. To which benzyl alcohol (1.0 equiv., 57 mg, 0.53 mmol)) dissolved in toluene was slowly added. The mixture was stirred for 16h. Volatiles were then removed in vacuo, washed with pentane, and dried in vacuo to yield dark brown solid (101 mg, 0.192 mmol, 73%). ^{1}H NMR (300 MHz, C_6D_6) δ 7.70 (d, 2H, o-Ph *J* = 8.00 MHz), 7.30 (t, 2H, m-Ph *J* = 8.00 MHz), 7.08 (m, 1H, - NCHC-), 6.60 (s, 1H, - NCHC-), 6.03 (s, 2H, - OCH2Bn), 5.72 (m, 2H, -NCHCHN-), 1.10 (d, 6H, -CH_3, *J* = 7.00 MHz) and 0.90 ppm (d, 6H, -CH_3, *J* = 7.00 MHz). ^{13}C{^{1}H}NMR (100 MHz, C_6D_6) δ 149.5, 146.5, 142.6, 140.7, 137.4, 125.1, 125.0, 123.4, 122.4, 120.8, 109.6, 109.2, 62.8, 44.8, 21.0, 19.8, 19.68, 19.40 ppm.

References

(1) Stürzel, M.; Mihan, S.; Mülhaupt, R. From Multisite Polymerization Catalysis to Sustainable Materials and All-Polyolefin Composites. *Chem. Rev.* **2016**, *116* (3), 1398–1433. https://doi.org/10.1021/acs.chemrev.5b00310.

(2) Geyer, R.; Jambeck, J. R.; Law, K. L. Production, Use, and Fate of All Plastics Ever Made. *Sci. Adv.* **2017**, *3* (7), e1700782. https://doi.org/10.1126/sciadv.1700782.

(3) Kaminsky, W. Trends in Polyolefin Chemistry. *Macromol. Chem. Phys.* **2008**, *209* (5), 459–466. https://doi.org/10.1002/macp.200700575.

(4) Scott, G. Polymers and the Environment. *R. Soc. Chem.* **1999**. https://doi.org/10.1039/9781847551726.

(5) Alamán-Díez, P.; García-Gareta, E.; Napal, P. F.; Arruebo, M.; Pérez, M. Á. In Vitro Hydrolytic Degradation of Polyester-Based Scaffolds under Static and Dynamic Conditions in a Customized Perfusion Bioreactor. *Materials* **2022**, *15* (7), 2572. https://doi.org/10.3390/ma15072572.

(6) Benyathiar, P.; Kumar, P.; Carpenter, G.; Brace, J.; Mishra, D. K. Polyethylene Terephthalate (PET) Bottle-to-Bottle Recycling for the Beverage Industry: A Review. *Polymers* **2022**, *14* (12), 2366. https://doi.org/10.3390/polym14122366.

(7) Benavides, P. T.; Dunn, J. B.; Han, J.; Biddy, M.; Markham, J. Exploring Comparative Energy and Environmental Benefits of Virgin, Recycled, and Bio-Derived PET Bottles. *ACS Sustain. Chem. Eng.* **2018**, *6* (8), 9725–9733. https://doi.org/10.1021/acssuschemeng.8b00750.

(8) De Oliveira, P. Z.; Vandenberghe, L. P. D. S.; Soccol, C. R. Lactic Acid Production Using Sugarcane Juice as an Alternative Substrate and Purification through Ion-Exchange Resins. *Fermentation* **2023**, *9* (10), 879. https://doi.org/10.3390/fermentation9100879.

(9) Alves De Oliveira, R.; Schneider, R.; Hoss Lunelli, B.; Vaz Rossell, C. E.; Maciel Filho, R.; Venus, J. A Simple Biorefinery Concept to Produce 2G-Lactic Acid from Sugar Beet Pulp (SBP): A High-Value Target Approach to Valorize a Waste Stream. *Molecules* **2020**, *25* (9), 2113. https://doi.org/10.3390/molecules25092113.

(10) Jiang, S.; Xu, P.; Tao, F. L-Lactic Acid Production by Bacillus Coagulans through Simultaneous Saccharification and Fermentation of Lignocellulosic Corncob Residue. *Bioresour. Technol. Rep.* **2019**, *6*, 131–137. https://doi.org/10.1016/j.biteb.2019.02.005.

(11) Rezvani Ghomi, E. R.; Khosravi, F.; Saedi Ardahaei, A. S.; Dai, Y.; Neisiany, R. E.; Foroughi, F.; Wu, M.; Das, O.; Ramakrishna, S. The Life Cycle Assessment for Polylactic Acid (PLA) to Make It a Low-Carbon Material. *Polymers* **2021**, *13* (11), 1854. https://doi.org/10.3390/polym13111854.

(12) Dorgan, J. R.; Lehermeier, H. J.; Palade, L.-I.; Cicero, J. Polylactides: Properties and Prospects of an Environmentally Benign Plastic from Renewable Resources. *Macromol. Symp.* **2001**, *175* (1), 55–66. https://doi.org/10.1002/1521-3900(200110)175:1<55::AID-MASY55>3.0.CO;2-K.

(13) Naser, A. Z.; Deiab, I.; Darras, B. M. Poly(Lactic Acid) (PLA) and Polyhydroxyalkanoates (PHAs), Green Alternatives to Petroleum-Based Plastics: A Review. *RSC Adv.* **2021**, *11* (28), 17151–17196. https://doi.org/10.1039/D1RA02390J.

(14) Dos Santos Vieira, I.; Herres-Pawlis, S. Lactide Polymerisation with Complexes of Neutral N-Donors – New Strategies for Robust Catalysts. *Eur. J. Inorg. Chem.* **2012**, *2012* (5), 765–774. https://doi.org/10.1002/ejic.201101131.

(15) Jamshidian, M.; Tehrany, E. A.; Imran, M.; Jacquot, M.; Desobry, S. Poly-Lactic Acid: Production, Applications, Nanocomposites, and Release Studies. *Compr. Rev. Food Sci. Food Saf.* **2010**, *9* (5), 552–571. https://doi.org/10.1111/j.1541-4337.2010.00126.x.
(16) Sun, C.; Wei, S.; Tan, H.; Huang, Y.; Zhang, Y. Progress in Upcycling Polylactic Acid Waste as an Alternative Carbon Source: A Review. *Chem. Eng. J.* **2022**, *446*, 136881. https://doi.org/10.1016/j.cej.2022.136881.
(17) Inkinen, S.; Hakkarainen, M.; Albertsson, A.-C.; Södergård, A. From Lactic Acid to Poly(Lactic Acid) (PLA): Characterization and Analysis of PLA and Its Precursors. *Biomacromolecules* **2011**, *12* (3), 523–532. https://doi.org/10.1021/bm101302t.
(18) Abedi, E.; Hashemi, S. M. B. Lactic Acid Production – Producing Microorganisms and Substrates Sources-State of Art. *Heliyon* **2020**, *6* (10), e04974. https://doi.org/10.1016/j.heliyon.2020.e04974.
(19) Khan, B. S. Neutral Bidendate Guanidine-Based Zinc Complexes for the Ring Opening Polymerization of Lactide. *York University* **2022**, 1–110. http://hdl.handle.net/10315/40601.
(20) Cunha, B. L. C.; Bahú, J. O.; Xavier, L. F.; Crivellin, S.; De Souza, S. D. A.; Lodi, L.; Jardini, A. L.; Filho, R. M.; Schiavon, M. I. R. B.; Concha, V. O. C.; Severino, P.; Souto, E. B. Lactide: Production Routes, Properties, and Applications. *Bioengineering* **2022**, *9* (4), 164. https://doi.org/10.3390/bioengineering9040164.
(21) Ceppatelli, M.; Frediani, M.; Bini, R. High-Pressure Reactivity of L , L -Lactide. *J. Phys. Chem. B* **2011**, *115* (10), 2173–2184. https://doi.org/10.1021/jp1110136.
(22) Stanford, M. J.; Dove, A. P. Stereocontrolled Ring-Opening Polymerisation of Lactide. *Chem Soc Rev* **2010**, *39* (2), 486–494. https://doi.org/10.1039/B815104K.
(23) Li, Y.; Wang, S.; Qian, S.; Liu, Z.; Weng, Y.; Zhang, Y. Depolymerization and Re/Upcycling of Biodegradable PLA Plastics. *ACS Omega* **2024**, *9* (12), 13509–13521. https://doi.org/10.1021/acsomega.3c08674.
(24) Gupta, A. P.; Kumar, V. New Emerging Trends in Synthetic Biodegradable Polymers – Polylactide: A Critique. *Eur. Polym. J.* **2007**, *43* (10), 4053–4074. https://doi.org/10.1016/j.eurpolymj.2007.06.045.
(25) Quirk, R. P. Stereochemistry and Macromolecules: Principles and Applications. *J. Chem. Educ.* **1981**, *58* (7), 540. https://doi.org/10.1021/ed058p540.
(26) Michell, R. M.; Ladelta, V.; Da Silva, E.; Müller, A. J.; Hadjichristidis, N. Poly(Lactic Acid) Stereocomplexes Based Molecular Architectures: Synthesis and Crystallization. *Prog. Polym. Sci.* **2023**, *146*, 101742. https://doi.org/10.1016/j.progpolymsci.2023.101742.
(27) Ovitt, T. M.; Coates, G. W. Stereochemistry of Lactide Polymerization with Chiral Catalysts: New Opportunities for Stereocontrol Using Polymer Exchange Mechanisms. *J. Am. Chem. Soc.* **2002**, *124* (7), 1316–1326. https://doi.org/10.1021/ja012052+.
(28) Teixeira, S.; Eblagon, K. M.; Miranda, F.; R. Pereira, M. F.; Figueiredo, J. L. Towards Controlled Degradation of Poly(Lactic) Acid in Technical Applications. *C* **2021**, *7* (2), 42. https://doi.org/10.3390/c7020042.
(29) Pan, P.; Inoue, Y. Polymorphism and Isomorphism in Biodegradable Polyesters. *Prog. Polym. Sci.* **2009**, *34* (7), 605–640. https://doi.org/10.1016/j.progpolymsci.2009.01.003.
(30) Tschan, M. J.-L.; Gauvin, R. M.; Thomas, C. M. Controlling Polymer Stereochemistry in Ring-Opening Polymerization: A Decade of Advances Shaping the Future of Biodegradable Polyesters. *Chem. Soc. Rev.* **2021**, *50* (24), 13587–13608. https://doi.org/10.1039/D1CS00356A.
(31) Ovitt, T. M.; Coates, G. W. Stereoselective Ring-Opening Polymerization of Rac-Lactide with a Single-Site, Racemic Aluminum Alkoxide Catalyst: Synthesis of Stereoblock Poly(Lactic

Acid). *J. Polym. Sci. Part Polym. Chem.* **2000**, *38* (S1, 2000), 4686–4692. https://doi.org/10.1002/1099-0518(200012)38:1+<4686::AID-POLA80>3.0.CO;2-0.
(32) Widhianto, Y. W.; Yamamoto, M.; Masutani, K.; Kimura, Y.; Yamane, H. Thermal Properties of the Multi-Stereo Block Poly(Lactic Acid)s with Various Block Lengths. *Polym. Degrad. Stab.* **2017**, *142*, 188–197. https://doi.org/10.1016/j.polymdegradstab.2017.06.016.
(33) Park, H.-S.; Hong, C.-K. Relationship between the Stereocomplex Crystallization Behavior and Mechanical Properties of PLLA/PDLA Blends. *Polymers* **2021**, *13* (11), 1851. https://doi.org/10.3390/polym13111851.
(34) Hirata, M.; Kimura, Y. Thermomechanical Properties of Stereoblock Poly(Lactic Acid)s with Different PLLA/PDLA Block Compositions. *Polymer* **2008**, *49* (11), 2656–2661. https://doi.org/10.1016/j.polymer.2008.04.014.
(35) Belleney, J.; Wisniewski, M.; Le Borgne, A. Influence of the Nature of the Ligand on the Microstructure of Poly d,l-Lactides Prepared with Organoaluminum Initiators. *Eur. Polym. J.* **2004**, *40* (3), 523–530. https://doi.org/10.1016/j.eurpolymj.2003.11.001.
(36) Zell, M. T.; Padden, B. E.; Paterick, A. J.; Thakur, K. A. M.; Kean, R. T.; Hillmyer, M. A.; Munson, E. J. Unambiguous Determination of the ^{13}C and ^{1}H NMR Stereosequence Assignments of Polylactide Using High-Resolution Solution NMR Spectroscopy. *Macromolecules* **2002**, *35* (20), 7700–7707. https://doi.org/10.1021/ma0204148.
(37) Chisholm, M. H.; Iyer, S. S.; McCollum, D. G.; Pagel, M.; Werner-Zwanziger, U. Microstructure of Poly(Lactide). Phase-Sensitive HETCOR Spectra of Poly(*Meso* -Lactide), Poly(*r Ac* -Lactide), and Atactic Poly(Lactide). *Macromolecules* **1999**, *32* (4), 963–973. https://doi.org/10.1021/ma9806864.
(38) Whitehorne, T. J. J.; Schaper, F. NacnacBnCuOiPr: A Strained Geometry Resulting in Very High Lactide Polymerization Activity. *Chem. Commun.* **2012**, *48* (83), 10334. https://doi.org/10.1039/c2cc34247b.
(39) Fortun, S.; Daneshmand, P.; Schaper, F. Isotactic *Rac* -Lactide Polymerization with Copper Complexes: The Influence of Complex Nuclearity. *Angew. Chem. Int. Ed.* **2015**, *54* (46), 13669–13672. https://doi.org/10.1002/anie.201505674.
(40) Chan, C. H.; Chen, J.-T.; Farrell, W. S.; Fellows, C. M.; Keddie, D. J.; Luscombe, C. K.; Matson, J. B.; Merna, J.; Moad, G.; Russell, G. T.; Théato, P.; Topham, P. D.; Sosa Vargas, L. Reconsidering Terms for Mechanisms of Polymer Growth: The “Step-Growth” and “Chain-Growth” Dilemma. *Polym. Chem.* **2022**, *13* (16), 2262–2270. https://doi.org/10.1039/D2PY00086E.
(41) Jasinski, F.; Rannée, A.; Schweitzer, J.; Fischer, D.; Lobry, E.; Croutxé-Barghorn, C.; Schmutz, M.; Le Nouen, D.; Criqui, A.; Chemtob, A. Thiol–Ene Linear Step-Growth Photopolymerization in Miniemulsion: Fast Rates, Redox-Responsive Particles, and Semicrystalline Films. *Macromolecules* **2016**, *49* (4), 1143–1153. https://doi.org/10.1021/acs.macromol.5b02512.
(42) Hu, Y.; Daoud, W.; Cheuk, K.; Lin, C. Newly Developed Techniques on Polycondensation, Ring-Opening Polymerization and Polymer Modification: Focus on Poly(Lactic Acid). *Materials* **2016**, *9* (3), 133. https://doi.org/10.3390/ma9030133.
(43) Platel, R.; Hodgson, L.; Williams, C. Biocompatible Initiators for Lactide Polymerization. *Polym. Rev.* **2008**, *48* (1), 11–63. https://doi.org/10.1080/15583720701834166.
(44) Yokoyama, A.; Yokozawa, T. Converting Step-Growth to Chain-Growth Condensation Polymerization. *Macromolecules* **2007**, *40* (12), 4093–4101. https://doi.org/10.1021/ma061357b.
(45) Ito, S. Chain-Growth Polymerization Enabling Formation/Introduction of Arylene Groups into Polymer Main Chains. *Polym. J.* **2016**, *48* (6), 667–677. https://doi.org/10.1038/pj.2016.18.

(46) Storey, R. F. Fundamental Aspects of Living Polymerization. *Fundam. Control. Radic. Polym.* **2013**, 60–77. https://doi.org/10.1039/9781849737425-00060.
(47) Yokozawa, T.; Yokoyama, A. Chain-Growth Polycondensation: Living Polymerization Nature in Polycondensation and Approach to Condensation Polymer Architecture. *Polym J* **2004**, *36* (2). https://doi.org/10.1002/chin.200430250.
(48) Ajellal, N.; Carpentier, J. F.; Guillaume, C.; Guillaume, S. M.; Helou, M.; Poirier, V.; Sarazina, Y.; Trifonov, A. Bridging the Gap in Catalysis via Multidisciplinary Approaches. *Dalton Trans.* **2010**, *39* (36), 8354. https://doi.org/10.1039/c0dt90044c.
(49) Sun, Y.; Cui, Y.; Xiong, J.; Dai, Z.; Tang, N.; Wu, J. Different Mechanisms at Different Temperatures for the Ring-Opening Polymerization of Lactide Catalyzed by Binuclear Magnesium and Zinc Alkoxides. *Dalton Trans.* **2015**, *44* (37), 16383–16391. https://doi.org/10.1039/C5DT01784J.
(50) Balla, E.; Daniilidis, V.; Karlioti, G.; Kalamas, T.; Stefanidou, M.; Bikiaris, N. D.; Vlachopoulos, A.; Koumentakou, I.; Bikiaris, D. N. Poly(Lactic Acid): A Versatile Biobased Polymer for the Future with Multifunctional Properties—From Monomer Synthesis, Polymerization Techniques and Molecular Weight Increase to PLA Applications. *Polymers* **2021**, *13* (11), 1822. https://doi.org/10.3390/polym13111822.
(51) Dechy-Cabaret, O.; Martin-Vaca, B.; Bourissou, D. Controlled Ring-Opening Polymerization of Lactide and Glycolide. *Chem. Rev.* **2004**, *104* (12), 6147–6176. https://doi.org/10.1021/cr040002s.
(52) Connor, E. F.; Nyce, G. W.; Myers, M.; Möck, A.; Hedrick, J. L. First Example of N-Heterocyclic Carbenes as Catalysts for Living Polymerization: Organocatalytic Ring-Opening Polymerization of Cyclic Esters. *J. Am. Chem. Soc.* **2002**, *124* (6), 914–915. https://doi.org/10.1021/ja0173324.
(53) Munzeiwa, W. A.; Omondi, B. O.; Nyamori, V. O. A Perspective into Ring-Opening Polymerization of ε-Caprolactone and Lactides: Effect of, Ligand, Catalyst Structure and System Dynamics, on Catalytic Activity and Polymer Properties. *Polym. Bull.* **2024**, *81* (11), 9419–9464. https://doi.org/10.1007/s00289-024-05149-5.
(54) Itzinger, R.; Schwarzinger, C.; Paulik, C. Investigation of the Influence of Impurities on the Ring-Opening Polymerisation of L-Lactide from Biogenous Feedstock. *J. Polym. Res.* **2020**, *27* (12), 383. https://doi.org/10.1007/s10965-020-02339-3.
(55) Chuma, A.; Horn, H. W.; Swope, W. C.; Pratt, R. C.; Zhang, L.; Lohmeijer, B. G. G.; Wade, C. G.; Waymouth, R. M.; Hedrick, J. L.; Rice, J. E. The Reaction Mechanism for the Organocatalytic Ring-Opening Polymerization of L -Lactide Using a Guanidine-Based Catalyst: Hydrogen-Bonded or Covalently Bound? *J. Am. Chem. Soc.* **2008**, *130* (21), 6749–6754. https://doi.org/10.1021/ja0764411.
(56) Pratt, R. C.; Lohmeijer, B. G. G.; Long, D. A.; Waymouth, R. M.; Hedrick, J. L. Triazabicyclodecene: A Simple Bifunctional Organocatalyst for Acyl Transfer and Ring-Opening Polymerization of Cyclic Esters. *J. Am. Chem. Soc.* **2006**, *128* (14), 4556–4557. https://doi.org/10.1021/ja060662+.
(57) Weidner, S. M.; Kricheldorf, H. R. The Role of Transesterification in SnOct2-Catalyzed Polymerizations of Lactides. *Macromol. Chem. Phys.* **2017**, *218* (3), 1600331. https://doi.org/10.1002/macp.201600331.
(58) Penczek, S.; Szymanski, R.; Duda, A.; Baran, J. Living Polymerization of Cyclic Esters– a Route to(Bio)Degradable Polymers. Influence of Chain Transfer to Polymer on Livingness. *Macromol. Symp.* **2003**, *201* (1), 261–270. https://doi.org/10.1002/masy.200351129.

(59) Shaver, M. P.; Cameron, D. J. A. Tacticity Control in the Synthesis of Poly(Lactic Acid) Polymer Stars with Dipentaerythritol Cores. *Biomacromolecules* **2010**, *11* (12), 3673–3679. https://doi.org/10.1021/bm101140d.
(60) Karidi, K.; Pladis, P.; Kiparissides, C. A Theoretical and Experimental Kinetic Investigation of the ROP of L, L - L Actide in the Presence of Polyalcohols. *Macromol. Symp.* **2013**, *333* (1), 206–215. https://doi.org/10.1002/masy.201300040.
(61) Rittinghaus, R. D.; Schäfer, P. M.; Albrecht, P.; Conrads, C.; Hoffmann, A.; Ksiazkiewicz, A. N.; Bienemann, O.; Pich, A.; Herres-Pawlis, S. New Kids in Lactide Polymerization: Highly Active and Robust Iron Guanidine Complexes as Superior Catalysts. *ChemSusChem* **2019**, *12* (10), 2161–2165. https://doi.org/10.1002/cssc.201900481.
(62) Jędrzkiewicz, D.; Adamus, G.; Kwiecień, M.; John, Ł.; Ejfler, J. Lactide as the Playmaker of the ROP Game: Theoretical and Experimental Investigation of Ring-Opening Polymerization of Lactide Initiated by Aminonaphtholate Zinc Complexes. *Inorg. Chem.* **2017**, *56* (3), 1349–1365. https://doi.org/10.1021/acs.inorgchem.6b02439.
(63) Hermann, A.; Hill, S.; Metz, A.; Heck, J.; Hoffmann, A.; Hartmann, L.; Herres-Pawlis, S. Next Generation of Zinc Bisguanidine Polymerization Catalysts towards Highly Crystalline, Biodegradable Polyesters. *Angew. Chem. Int. Ed.* **2020**, *59* (48), 21778–21784. https://doi.org/10.1002/anie.202008473.
(64) Ebrahimi, T.; Mamleeva, E.; Yu, I.; Hatzikiriakos, S. G.; Mehrkhodavandi, P. The Role of Nitrogen Donors in Zinc Catalysts for Lactide Ring-Opening Polymerization. *Inorg. Chem.* **2016**, *55* (18), 9445–9453. https://doi.org/10.1021/acs.inorgchem.6b01722.
(65) Chamberlain, B. M.; Cheng, M.; Moore, D. R.; Ovitt, T. M.; Lobkovsky, E. B.; Coates, G. W. Polymerization of Lactide with Zinc and Magnesium β-Diiminate Complexes: Stereocontrol and Mechanism. *J. Am. Chem. Soc.* **2001**, *123* (14), 3229–3238. https://doi.org/10.1021/ja003851f.
(66) Williams, C. K.; Breyfogle, L. E.; Choi, S. K.; Nam, W.; Young, V. G.; Hillmyer, M. A.; Tolman, W. B. A Highly Active Zinc Catalyst for the Controlled Polymerization of Lactide. *J. Am. Chem. Soc.* **2003**, *125* (37), 11350–11359. https://doi.org/10.1021/ja0359512.
(67) Fuchs, M.; Schmitz, S.; Schäfer, P. M.; Secker, T.; Metz, A.; Ksiazkiewicz, A. N.; Pich, A.; Kögerler, P.; Monakhov, K. Yu.; Herres-Pawlis, S. Mononuclear Zinc(II) Schiff Base Complexes as Catalysts for the Ring-Opening Polymerization of Lactide. *Eur. Polym. J.* **2020**, *122*, 109302. https://doi.org/10.1016/j.eurpolymj.2019.109302.
(68) Du, H.; Velders, A. H.; Dijkstra, P. J.; Sun, J.; Zhong, Z.; Chen, X.; Feijen, J. Chiral Salan Aluminium Ethyl Complexes and Their Application in Lactide Polymerization. *Chem. – Eur. J.* **2009**, *15* (38), 9836–9845. https://doi.org/10.1002/chem.200900799.
(69) Degée, Ph.; Dubois, Ph.; Jacobsen, S.; Fritz, H. -G.; Jérôme, R. Beneficial Effect of Triphenylphosphine on the Bulk Polymerization of L , L -lactide Promoted by 2-ethylhexanoic Acid Tin (II) Salt. *J. Polym. Sci. Part Polym. Chem.* **1999**, *37* (14), 2413–2420. https://doi.org/10.1002/(SICI)1099-0518(19990715)37:14<2413::AID-POLA15>3.0.CO;2-#.
(70) Dubois, P.; Jacobs, C.; Jerome, R.; Teyssie, P. Macromolecular Engineering of Polylactones and Polylactides. 4. Mechanism and Kinetics of Lactide Homopolymerization by Aluminum Isopropoxide. *Macromolecules* **1991**, *24* (9), 2266–2270. https://doi.org/10.1021/ma00009a022.
(71) Le Borgne, A.; Vincens, V.; Jouglard, M.; Spassky, N. Ring-opening Oligomerization Reactions Using Aluminium Complexes of Schiff's Bases as Initiators. *Makromol. Chem. Macromol. Symp.* **1993**, *73* (1), 37–46. https://doi.org/10.1002/masy.19930730106.

(72) Spassky, N.; Wisniewski, M.; Pluta, C.; Le Borgne, A. Highly Stereoelective Polymerization of *Rac* -(D , L)-lactide with a Chiral Schiff's Base/Aluminium Alkoxide Initiator. *Macromol. Chem. Phys.* **1996**, *197* (9), 2627–2637. https://doi.org/10.1002/macp.1996.021970902.
(73) Ovitt, T. M.; Coates, G. W. Stereoselective Ring-Opening Polymerization of *Meso* -Lactide: Synthesis of Syndiotactic Poly(Lactic Acid). *J. Am. Chem. Soc.* **1999**, *121* (16), 4072–4073. https://doi.org/10.1021/ja990088k.
(74) Iwasa, N.; Fujiki, M.; Nomura, K. Ring-Opening Polymerization of Various Cyclic Esters by Al Complex Catalysts Containing a Series of Phenoxy-Imine Ligands: Effect of the Imino Substituents for the Catalytic Activity. *J. Mol. Catal. Chem.* **2008**, *292* (1–2), 67–75. https://doi.org/10.1016/j.molcata.2008.06.009.
(75) Masuda, J. D.; Martin, D.; Lyon-Saunier, C.; Baceiredo, A.; Donnadieu, B.; Bertrand, G. Stable P-Heterocyclic Carbenes: Scope and Limitations. *Chem. Asian J.* **2008**, *2* (1), 178–187. https://doi.org/10.1002/asia.200600300.
(76) McGuinness, D. Alkene Oligomerisation and Polymerisation with Metal-NHC Based Catalysts. *Dalton Trans.* **2009**, No. 35, 6915. https://doi.org/10.1039/b906479f.
(77) Huang, J.; Schanz, H.-J.; Stevens, E. D.; Nolan, S. P. Stereoelectronic Effects Characterizing Nucleophilic Carbene Ligands Bound to the Cp*RuCl (Cp* = η^5-C_5Me_5) Moiety: A Structural and Thermochemical Investigation. *Organometallics* **1999**, *18* (12), 2370–2375. https://doi.org/10.1021/om990054l.
(78) Tamm, M.; Petrovic, D.; Randoll, S.; Beer, S.; Bannenberg, T.; Jones, P. G.; Grunenberg, J. Structural and Theoretical Investigation of 2-Iminoimidazolines ? Carbene Analogues of Iminophosphoranes. *Org. Biomol. Chem.* **2007**, *5* (3), 523. https://doi.org/10.1039/b615418b.
(79) Doddi, A.; Peters, M.; Tamm, M. N-Heterocyclic Carbene Adducts of Main Group Elements and Their Use as Ligands in Transition Metal Chemistry. *Chem. Rev.* **2019**, *119* (12), 6994–7112. https://doi.org/10.1021/acs.chemrev.8b00791.
(80) Petrovic, D.; Bannenberg, T.; Randoll, S.; Jones, P. G.; Tamm, M. Synthesis and Reactivity of Copper(i) Complexes Containing a Bis(Imidazolin-2-Imine) Pincer Ligand. *Dalton Trans.* **2007**, No. 26, 2812. https://doi.org/10.1039/b703183a.
(81) Tamm, M.; Randoll, S.; Bannenberg, T.; Herdtweck, E. Titanium Complexes with Imidazolin-2-Iminato Ligands. *Chem. Commun.* **2004**, No. 7, 876. https://doi.org/10.1039/b401041h.
(82) Huynh, S.; Arrowsmith, M.; Meier, L.; Dietz, M.; Härterich, M.; Michel, M.; Gärtner, A.; Braunschweig, H. Cyclic Alkyl(Amino)Iminates (CAAIs) as Strong 2σ,4π-Electron Donor Ligands for the Stabilisation of Boranes and Diboranes(4): A Synthetic and Computational Study. *Dalton Trans.* **2023**, *52* (12), 3869–3876. https://doi.org/10.1039/D3DT00298E.
(83) Ochiai, T.; Franz, D.; Inoue, S. Applications of N-Heterocyclic Imines in Main Group Chemistry. *Chem. Soc. Rev.* **2016**, *45* (22), 6327–6344. https://doi.org/10.1039/C6CS00163G.
(84) Shoken, D.; Sharma, M.; Botoshansky, M.; Tamm, M.; Eisen, M. S. Mono(Imidazolin-2-Iminato) Titanium Complexes for Ethylene Polymerization at Low Amounts of Methylaluminoxane. *J. Am. Chem. Soc.* **2013**, *135* (34), 12592–12595. https://doi.org/10.1021/ja406925z.
(85) Schäfer, P. M.; Fuchs, M.; Ohligschläger, A.; Rittinghaus, R.; McKeown, P.; Akin, E.; Schmidt, M.; Hoffmann, A.; Liauw, M. A.; Jones, M. D.; Herres-Pawlis, S. Highly Active N,O Zinc Guanidine Catalysts for the Ring-Opening Polymerization of Lactide. *Chem Sus Chem* **2017**, *10* (18), 3547–3556. https://doi.org/10.1002/cssc.201701237.

(86) Larocque, T. G.; Dastgir, S.; Lavoie, G. G. Coordination and Reactivity Study of Titanium and Zirconium Complexes of the First Imidazol-2-Imine Ethenolate Ligand. *Organometallics* **2013**, *32* (15), 4314–4320. https://doi.org/10.1021/om4004708.
(87) Khan, B. S.; Flores-Romero, V.; LeBlanc, J.; Lavoie, G. G. Lactide Polymerization Using Zinc Dichloride Complexes Containing a Neutral Bidentate Ligand with a Diacylated Cyclic Guanidine. *Organometallics* **2022**, *41* (19), 2668–2677. https://doi.org/10.1021/acs.organomet.2c00254.
(88) Melaimi, M.; Jazzar, R.; Soleilhavoup, M.; Bertrand, G. Cyclic (Alkyl)(Amino)Carbenes (CAACs): Recent Developments. *Angew. Chem. Int. Ed.* **2017**, *56* (34), 10046–10068. https://doi.org/10.1002/anie.201702148.
(89) Back, O.; Henry-Ellinger, M.; Martin, C. D.; Martin, D.; Bertrand, G. ^{31}P NMR Chemical Shifts of Carbene–Phosphinidene Adducts as an Indicator of the π-Accepting Properties of Carbenes. *Angew. Chem. Int. Ed.* **2013**, *52* (10), 2939–2943. https://doi.org/10.1002/anie.201209109.
(90) Pyykkö, P.; Atsumi, M. Molecular Double-Bond Covalent Radii for Elements Li–E112. *Chem. Eur. J.* **2009**, *15* (46), 12770–12779. https://doi.org/10.1002/chem.200901472.
(91) Payne, J.; McKeown, P.; Mahon, M. F.; Emanuelsson, E. A. C.; Jones, M. D. Mono- and Dimeric Zinc(II) Complexes for PLA Production and Degradation into Methyl Lactate – a Chemical Recycling Method. *Polym. Chem.* **2020**, *11* (13), 2381–2389. https://doi.org/10.1039/D0PY00192A.
(92) Addison, A. W.; Rao, T. N.; Reedijk, J.; van Rijn, J.; Verschoor, G. C. Synthesis, Structure, and Spectroscopic Properties of Copper(11) Compounds Containing Nitrogen-Sulphur Donor Ligands ;the Crystal and Molecular Structure of Aqua[l,7-Bis(N-Methylbenzimidazol-2'-Yl)-2,6-Dithiaheptane]Copper(Ii) Perchlorate t. *Dalton Int. J. Inorg. Chem.* **1984**, *7*, 1349–1356. https://doi.org/10.1039/DT9840001349.
(93) Neuba, A.; Haase, R.; Bernard, M.; Flörke, U.; Herres-Pawlis, S. Systematische Studie zu den Koordinationseigenschaften des Guanidin-Liganden N^1,N^2-Bis(1,3-dimethylimidazolidin-2-yliden)-ethan-1,2-diamin mit den Metallen Mn, Co, Ni, Ag und Cu. *Z. Für Anorg. Allg. Chem.* **2008**, *634* (14), 2511–2517. https://doi.org/10.1002/zaac.200800335.
(94) Jiang, Y. Phenoxy-Imine/-Amide Aluminum Complexes with Pendant or Coordinated Pyridine Moieties: Solvent Effects on Structural Type and Catalytic Capability for the ROP of Cyclic Esters. *Polym. Guilford* **2022**, *242*, 124602. https://doi.org/10.1016/j.polymer.2022.124602.
(95) Fish, H.; Hart, S.; Lamb, K. J.; North, M.; Quek, S. C. Z.; Whitwood, A. C.; Woods, B.; Wu, X. Structural Analysis of Five-Coordinate Aluminium(Salen) Complexes and Its Relationship to Their Catalytic Activity. *Dalton Trans.* **2021**, *50* (2), 587–598. https://doi.org/10.1039/D0DT03598J.
(96) Espartero, J. L.; Rashkov, I.; Li, S. M.; Manolova, N.; Vert, M. NMR Analysis of Low Molecular Weight Poly(Lactic Acid)s. *Macromolecules* **1996**, *29* (10), 3535–3539. https://doi.org/10.1021/ma950529u.
(97) Lewinski, P.; Sosnowski, S.; Kazmierski, S.; Penczek, S. L-Lactide Polymerization Studied by ^{1}H NMR with Diffusion-Ordered Spectroscopy (DOSY): A "One NMR Tube Experiment" Providing Data on Monomer Conversion, Polymer Structure, M_n and M_w. *Polym. Chem.* **2015**, *6* (24), 4353–4357. https://doi.org/10.1039/C5PY00455A.
(98) Petrus, R.; Bykowski, D.; Sobota, P. Solvothermal Alcoholysis Routes for Recycling Polylactide Waste as Lactic Acid Esters. *ACS Catal.* **2016**, *6* (8), 5222–5235. https://doi.org/10.1021/acscatal.6b01009.

(99) Chen, H.-Y.; Tang, H.-Y.; Lin, C.-C. Ring-Opening Polymerization of Lactides Initiated by Zinc Alkoxides Derived from NNO-Tridentate Ligands. *Macromolecules* **2006**, *39* (11), 3745–3752. https://doi.org/10.1021/ma060471r.
(100) Florczak, M.; Michalski, A.; Kacprzak, A.; Brzeziński, M.; Biedroń, T.; Pająk, A.; Kubisa, P.; Biela, T. MALDI-TOF Analysis of Lactide Oligomers with Functional End Groups. *React. Funct. Polym.* **2016**, *104*, 71–77. https://doi.org/10.1016/j.reactfunctpolym.2016.05.010.
(101) Flores-Romero, V.; LeBlanc, J.; Chen, Z.; Lavoie, G. G. Ti and Zr Complexes Bearing Guanidine-Phenolate Ligands: Coordination Chemistry and Polymerization Studies. *RSC Adv.* **2024**, *14* (35), 25889–25899. https://doi.org/10.1039/D4RA05146G.
(102) Borda, J.; Bodnar, I.; Keki, S.; Sipos, L.; Zsuga, M. Optimum Conditions for the Synthesis of Linear Polylactic Acid-Based Urethanes. *J. Polym. Sci. Part Polym. Chem.* **2000**, *38* (16), 2925–2933. https://doi.org/10.1002/1099-0518(20000815)38:16<2925::AID-POLA100>3.0.CO;2-E.
(103) Bonnet, F.; Stoffelbach, F.; Fontaine, G.; Bourbigot, S. Continuous Cyclo-Polymerisation of L -Lactide by Reactive Extrusion Using Atoxic Metal-Based Catalysts: Easy Access to Well-Defined Polylactide Macrocycles. *RSC Adv.* **2015**, *5* (40), 31303–31310. https://doi.org/10.1039/C4RA16634E.
(104) Mao, X.; Xian, J.; Wang, R.; Han, X.; Pan, X.; Wu, J. Synthesis of Linear to Cyclic Polylactide *via* a One-Pot Step-Wise Ring-Opening Polymerization and Back-Biting Reaction of Ring Closure Using Magnesium Complexes. *Inorg. Chem.* **2022**, *61* (28), 10722–10730. https://doi.org/10.1021/acs.inorgchem.2c00935.
(105) Yu, Y.; Storti, G.; Morbidelli, M. Kinetics of Ring-Opening Polymerization of L, L-Lactide. *Ind. Eng. Chem. Res.* **2011**, *50* (13), 7927–7940. https://doi.org/10.1021/ie200117n.
(106) Schrempp, D. F.; Kaifer, E.; Wadepohl, H.; Himmel, H.-J. Copper Complexes of New Redox-Active 4,5-Bisguanidino-Substituted Benzodioxole Ligands: Control of the Electronic Structure by Counter-Ligands, Solvent, and Temperature. *Chem. – Eur. J.* **2016**, *22* (45), 16187–16199. https://doi.org/10.1002/chem.201602402.
(107) Jungbauer, S. H.; Huber, S. M. Cationic Multidentate Halogen-Bond Donors in Halide Abstraction Organocatalysis: Catalyst Optimization by Preorganization. *J. Am. Chem. Soc.* **2015**, *137* (37), 12110–12120. https://doi.org/10.1021/jacs.5b07863.
(108) Gao, Y.; Liu, J.; Li, Z.; Guo, T.; Xu, S.; Zhu, H.; Wei, F.; Chen, S.; Gebru, H.; Guo, K. Dichloroimidazolidinedione-Activated Beckmann Rearrangement of Ketoximes for Accessing Amides and Lactams. *J. Org. Chem.* **2018**, *83* (4), 2040–2049. https://doi.org/10.1021/acs.joc.7b02983.
(109) Wang, Y.-Q.; Lu, S.-M.; Zhou, Y.-G. Palladium-Catalyzed Asymmetric Hydrogenation of Functionalized Ketones. *Org. Lett.* **2005**, *7* (15), 3235–3238. https://doi.org/10.1021/ol051007u.

Appendix

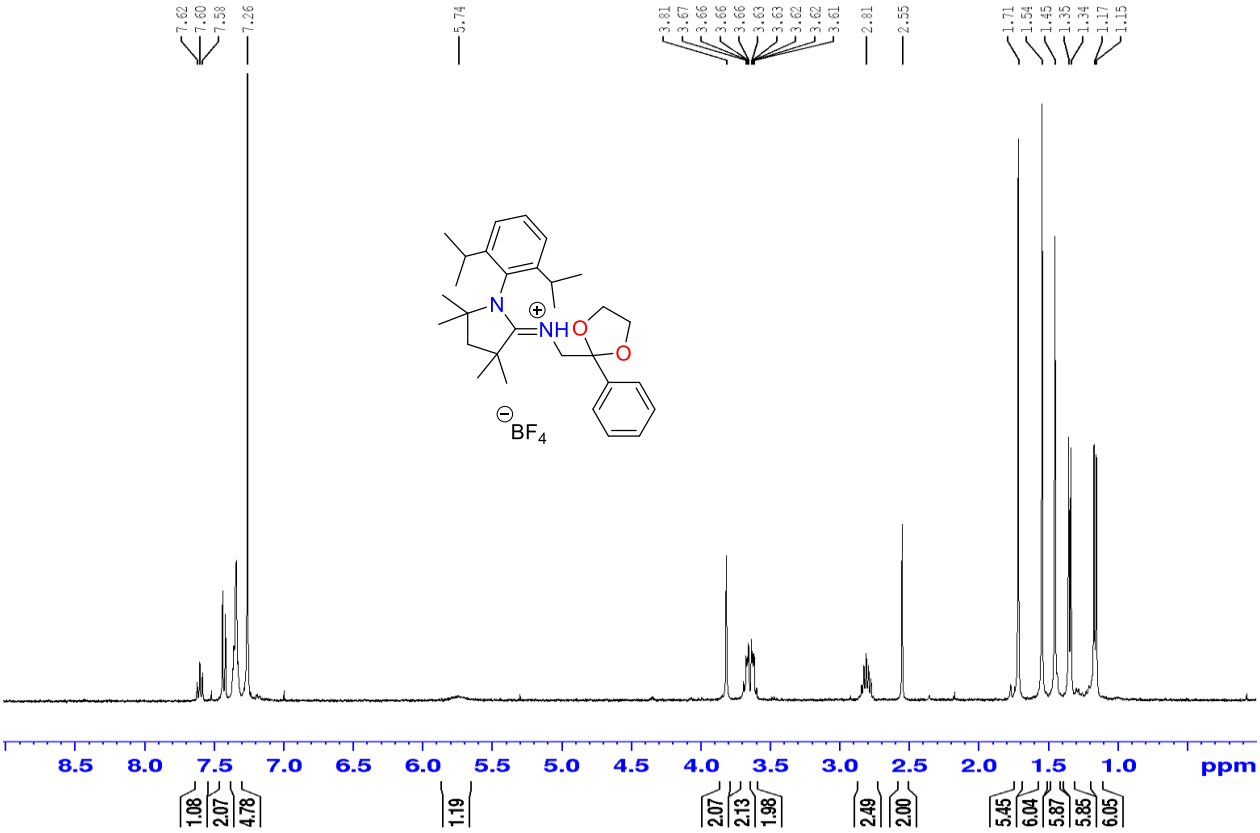

Figure A1.^{1}H NMR spectrum of **L5''**•HBF_4 (400 MHz, $CDCl_3$)

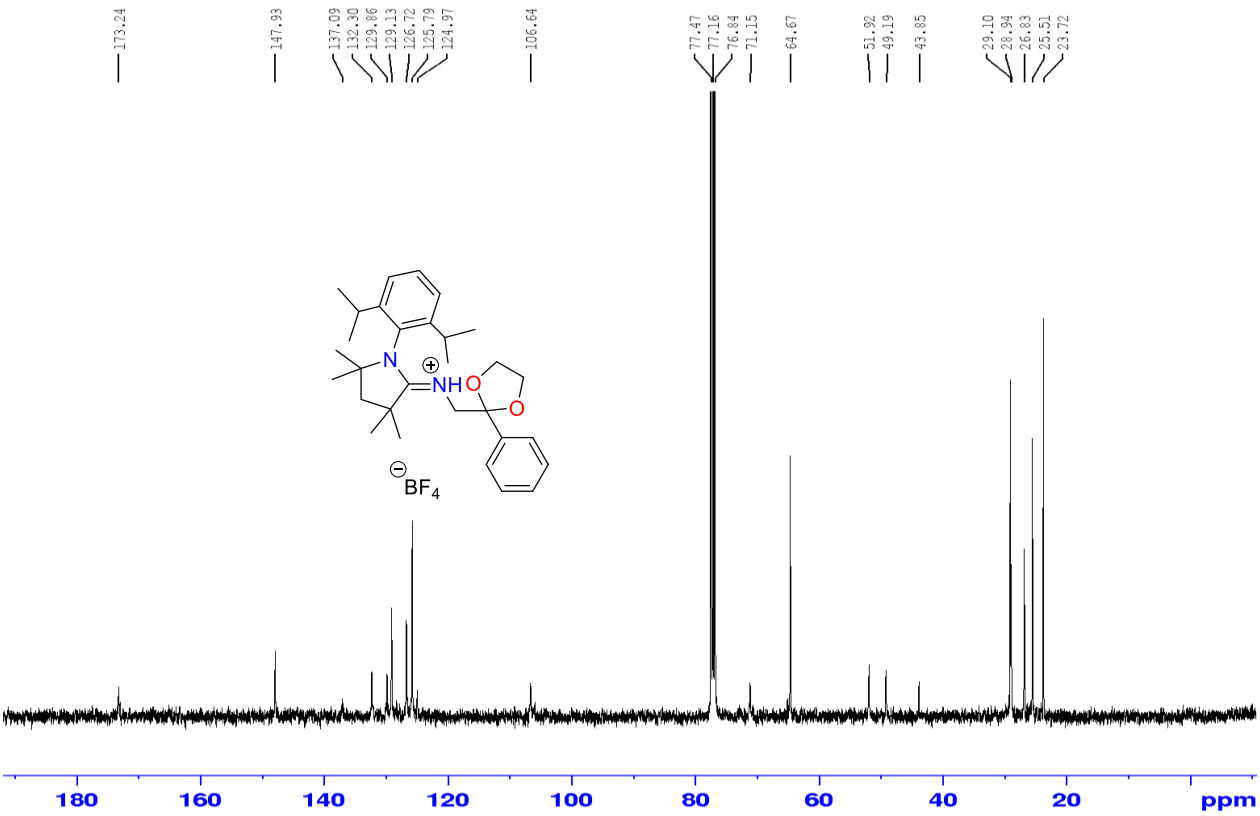

Figure A2 $^{13}C\{^{1}H\}$ NMR spectrum of **L5''**•HBF_4 (100 MHz, $CDCl_3$)

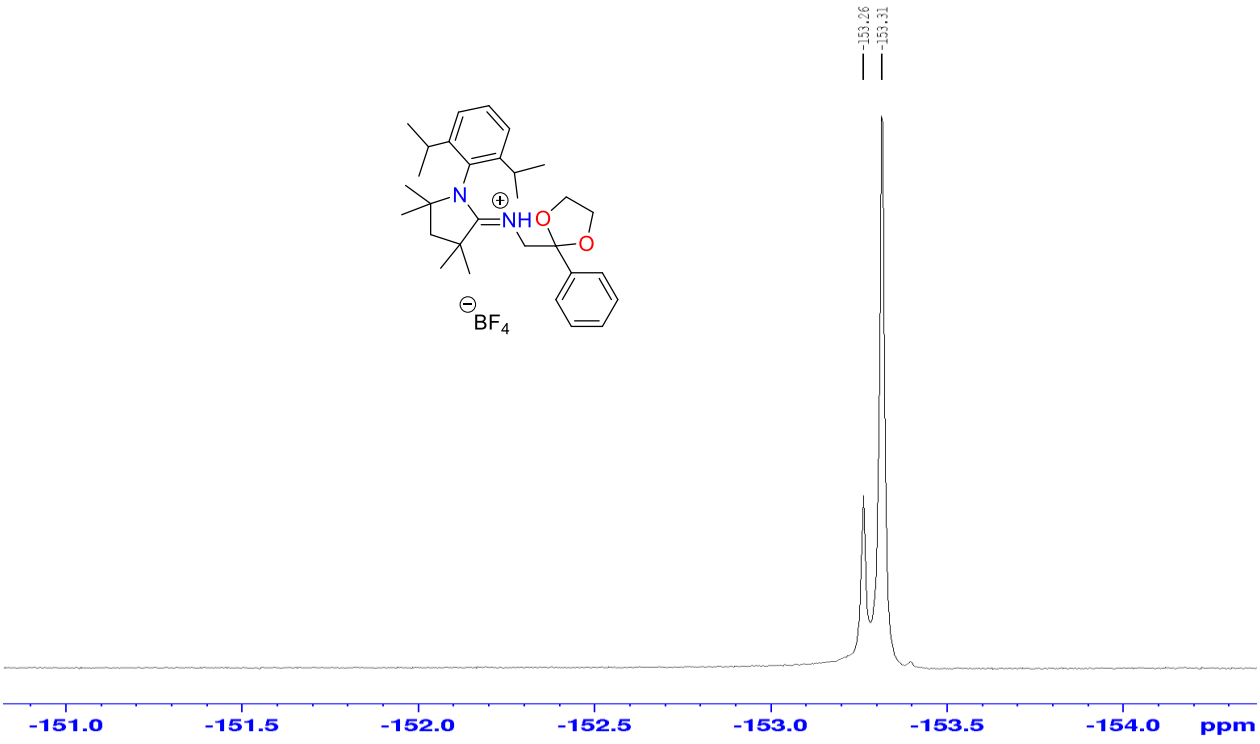

Figure A3. $^{19}F\{^{1}H\}$ NMR spectrum of **L5''**•HBF_4 (377 MHz, $CDCl_3$)

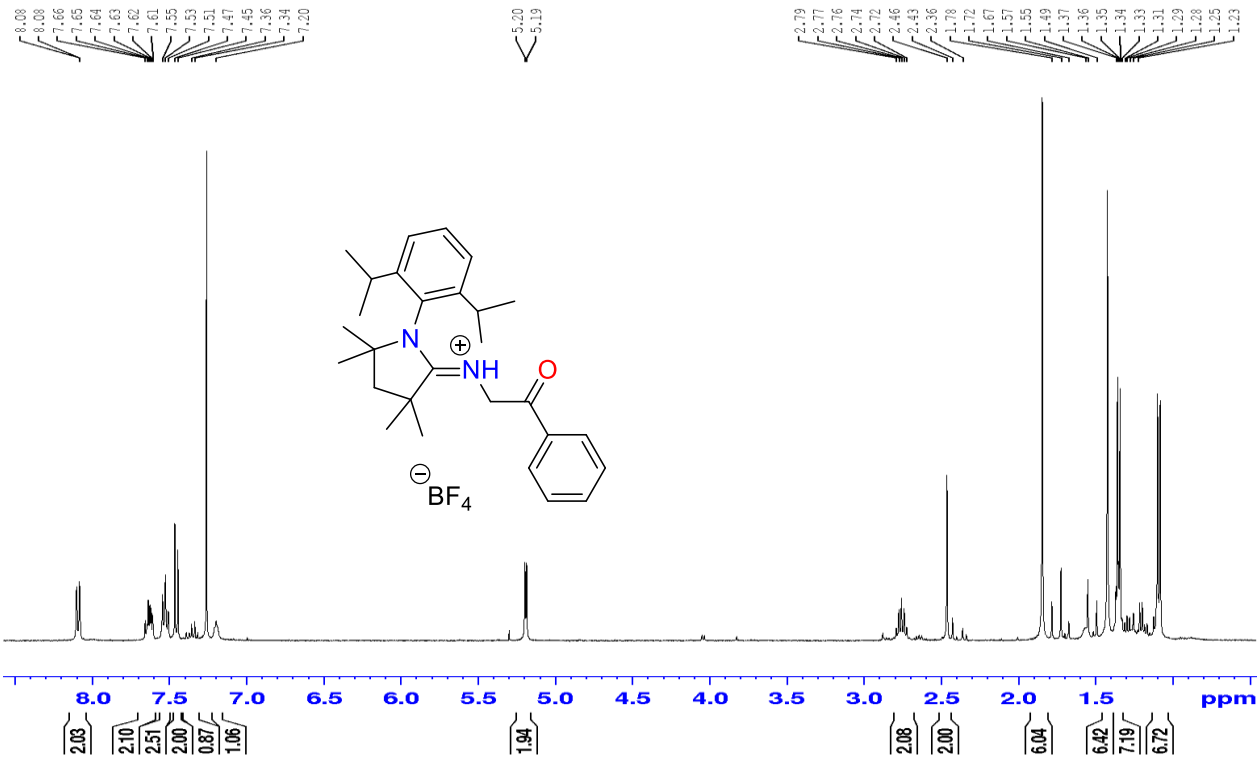

Figure A4. ^{1}H NMR spectrum of **L5'**•HBF_4 (400 MHz, $CDCl_3$)

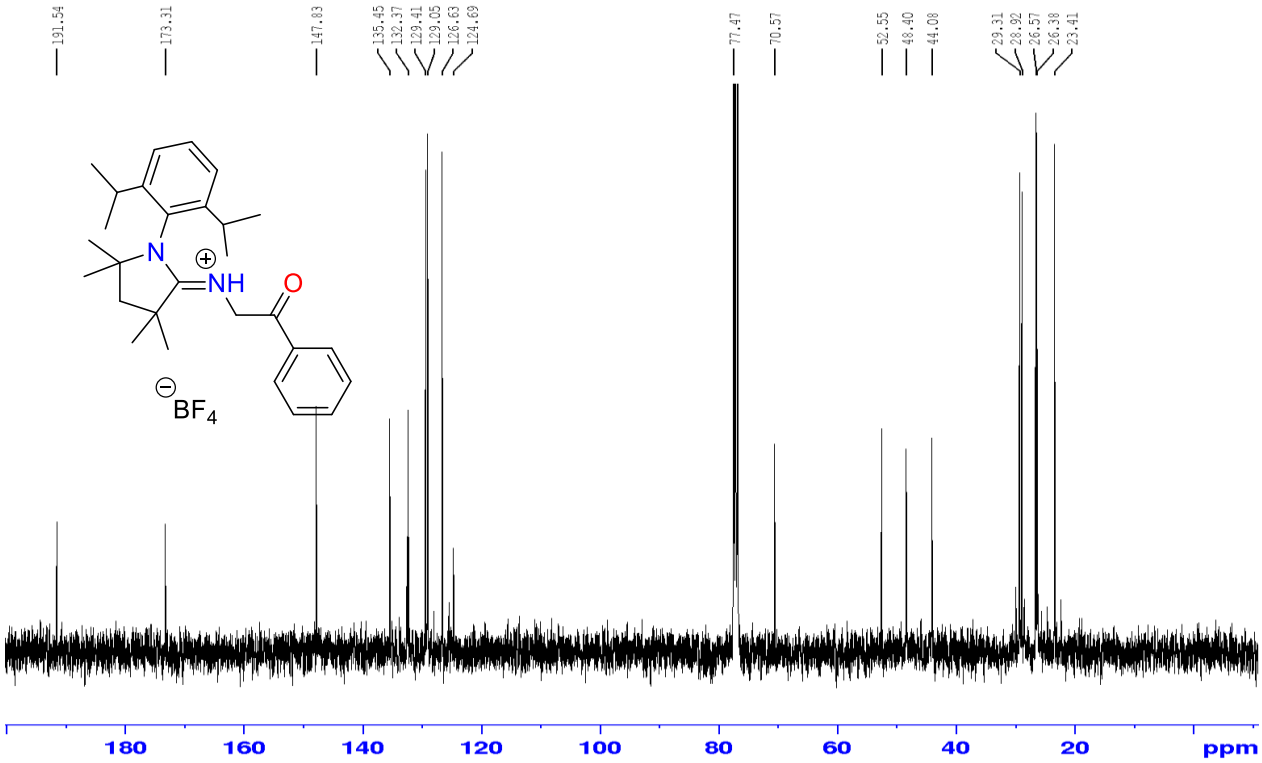

Figure A5. $^{13}C\{^{1}H\}$ NMR spectrum of **L5'**•HBF_4 (100 MHz, $CDCl_3$)

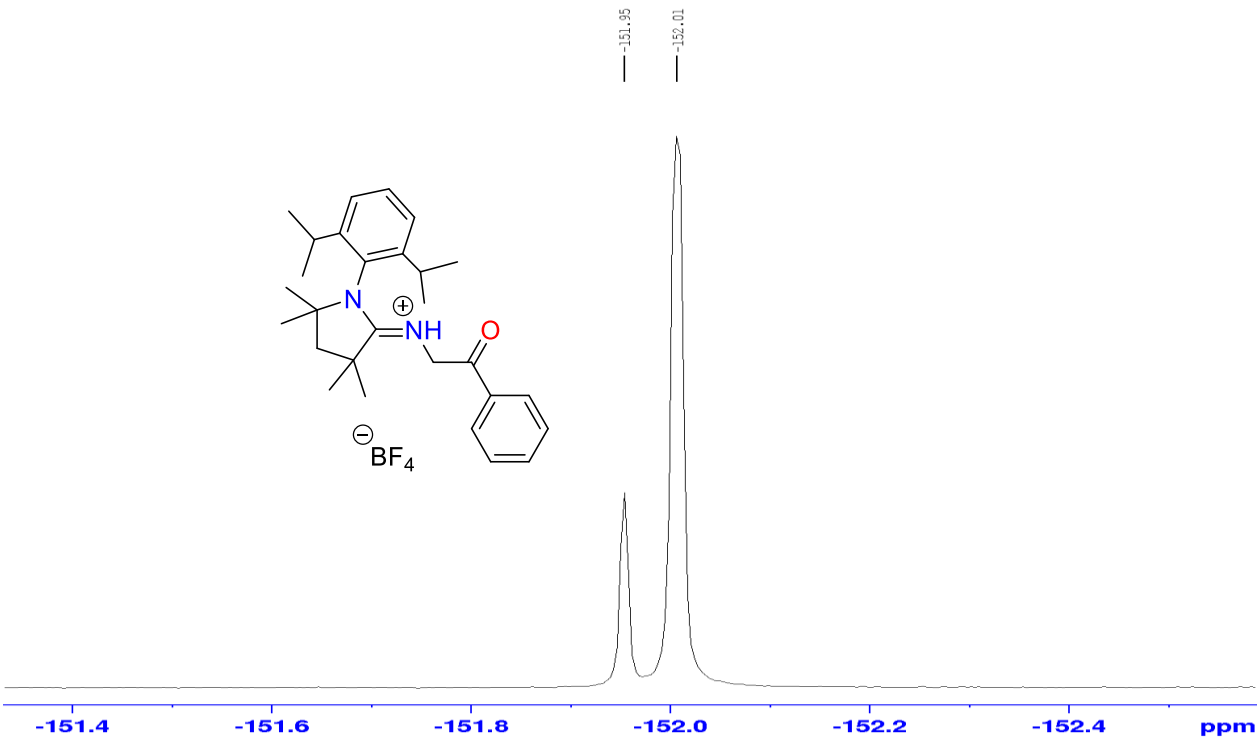

Figure A6. $^{19}F\{^{1}H\}$ NMR spectrum of **L5'**•HBF_4 (377 MHz, $CDCl_3$)

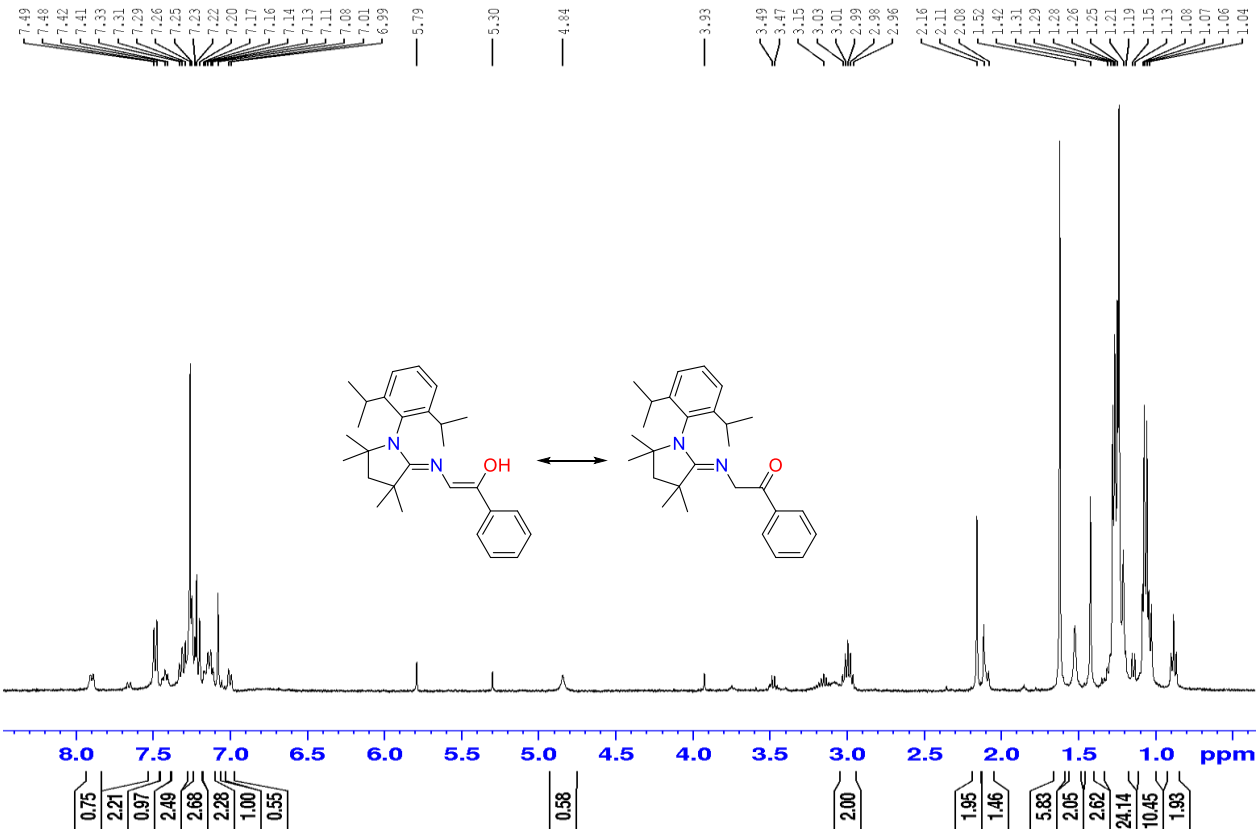

Figure A7. ^{1}H NMR spectrum of **L5**H (400 MHz, $CDCl_3$)

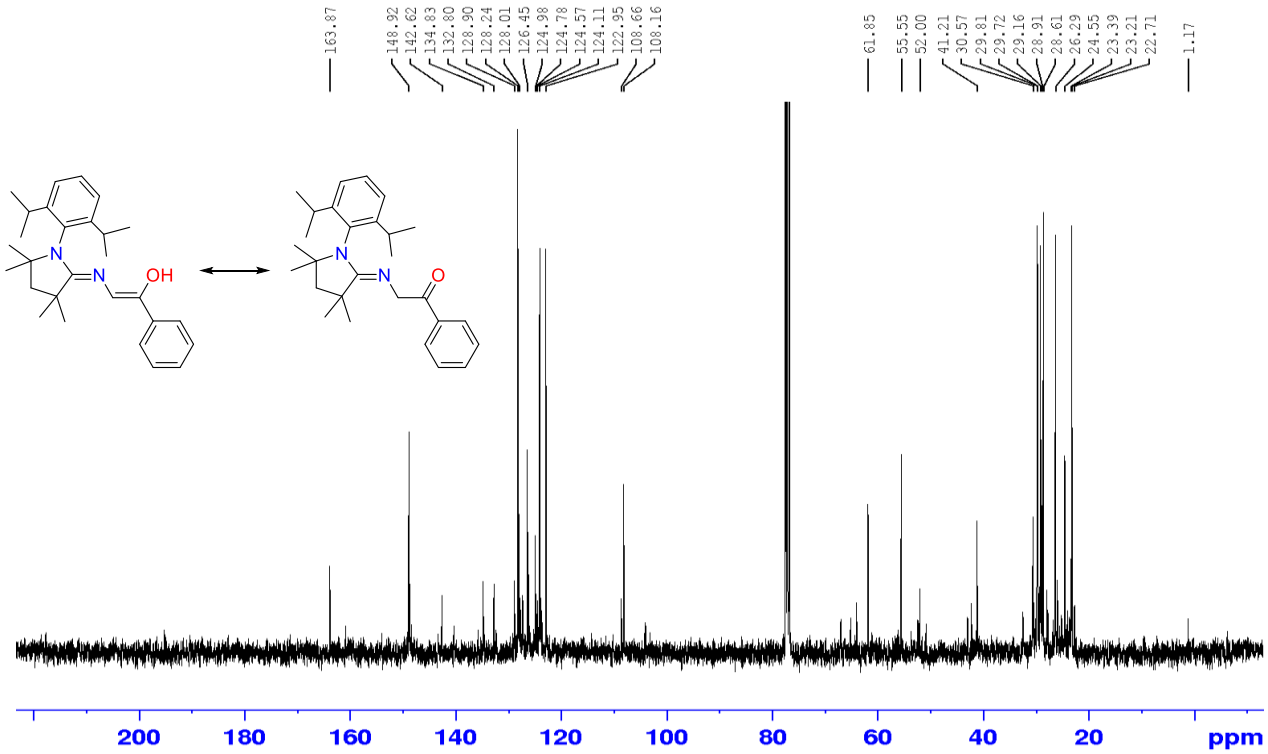

Figure A8. $^{13}C\{^{1}H\}$ NMR spectrum of **L1**H (100 MHz, $CDCl_3$)

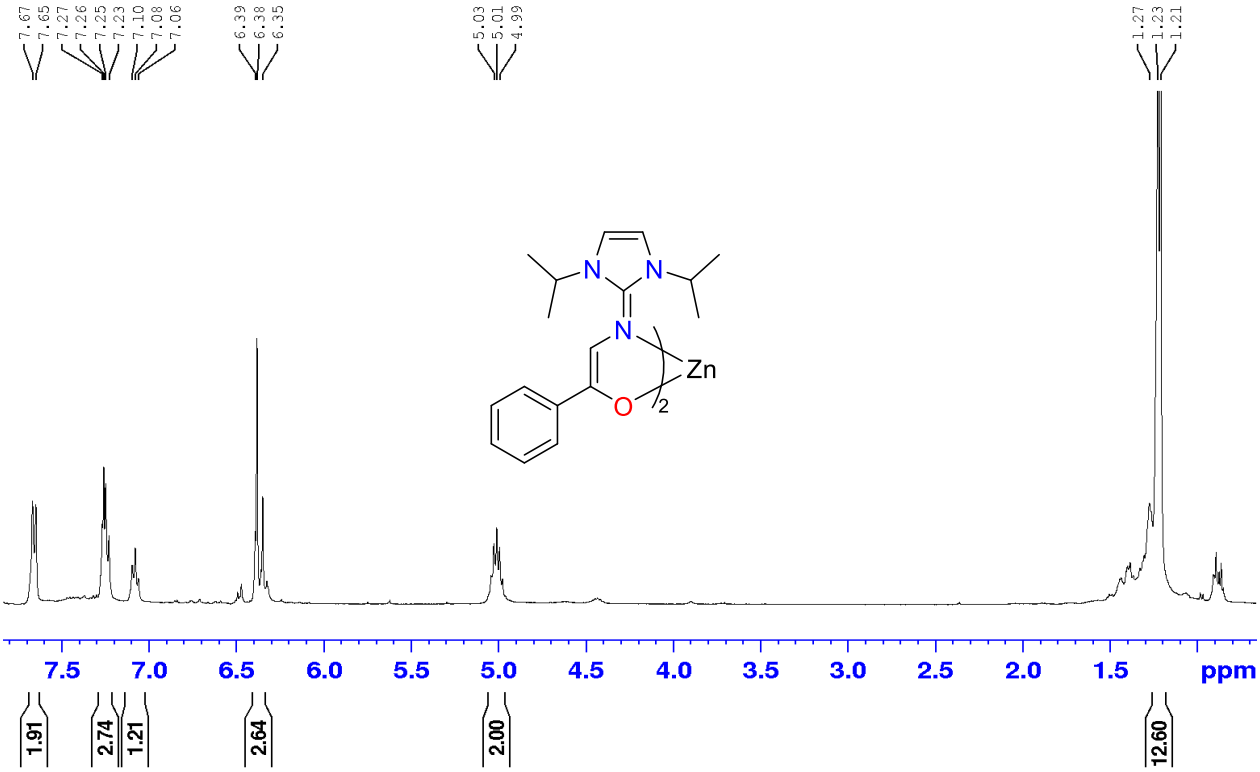

Figure A9. ^{1}H NMR spectrum of Zn(**L1**)$_2$ (400 MHz, $CDCl_3$)

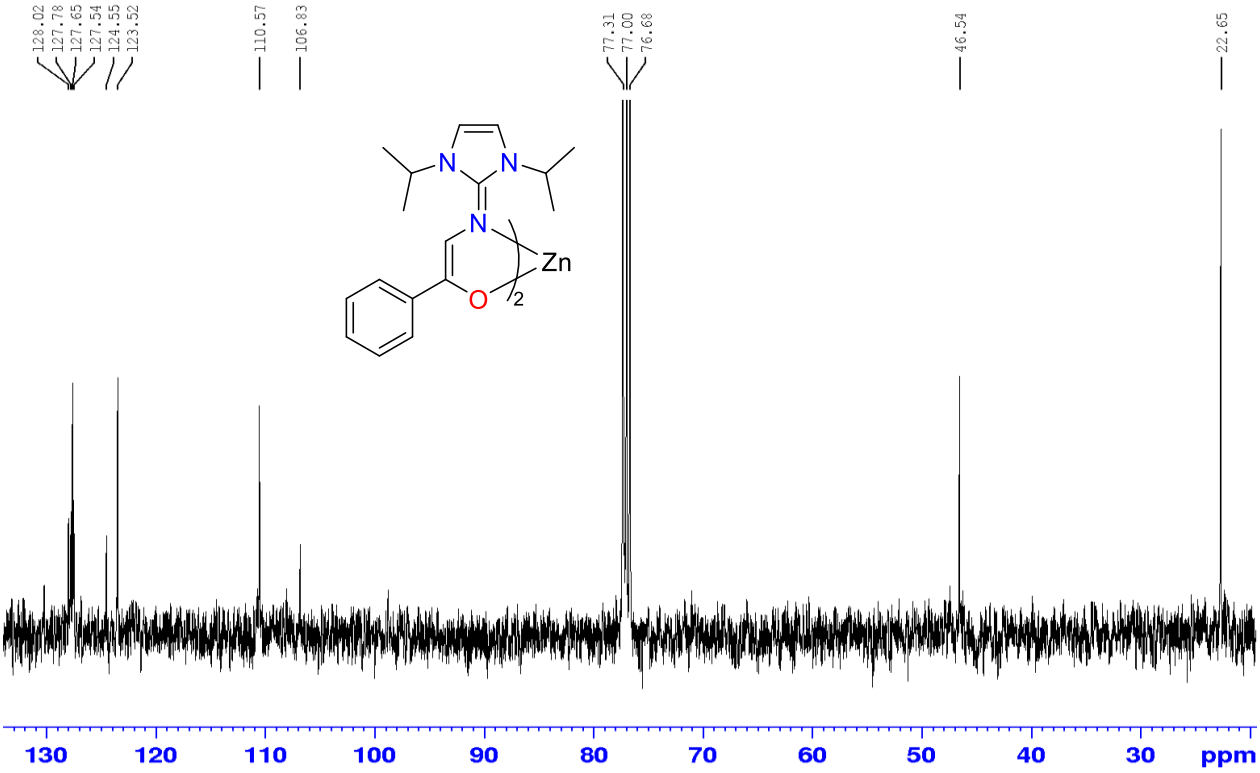

Figure A10. $^{13}C\{^{1}H\}$ NMR spectrum of Zn(**L1**)$_2$ (100 MHz, $CDCl_3$)

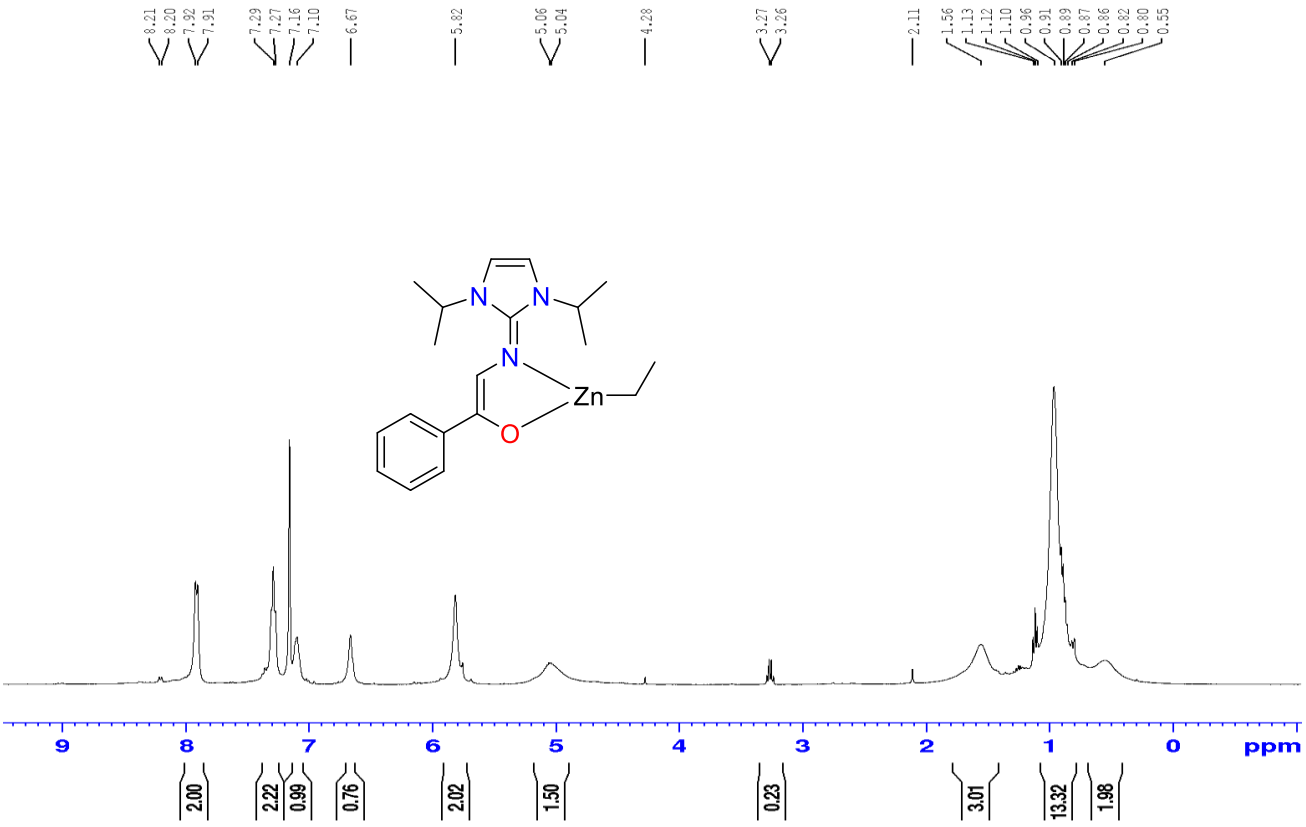

Figure A11. ^{1}H NMR spectrum of Zn(**L1**)Et (400 MHz, C_6D_6)

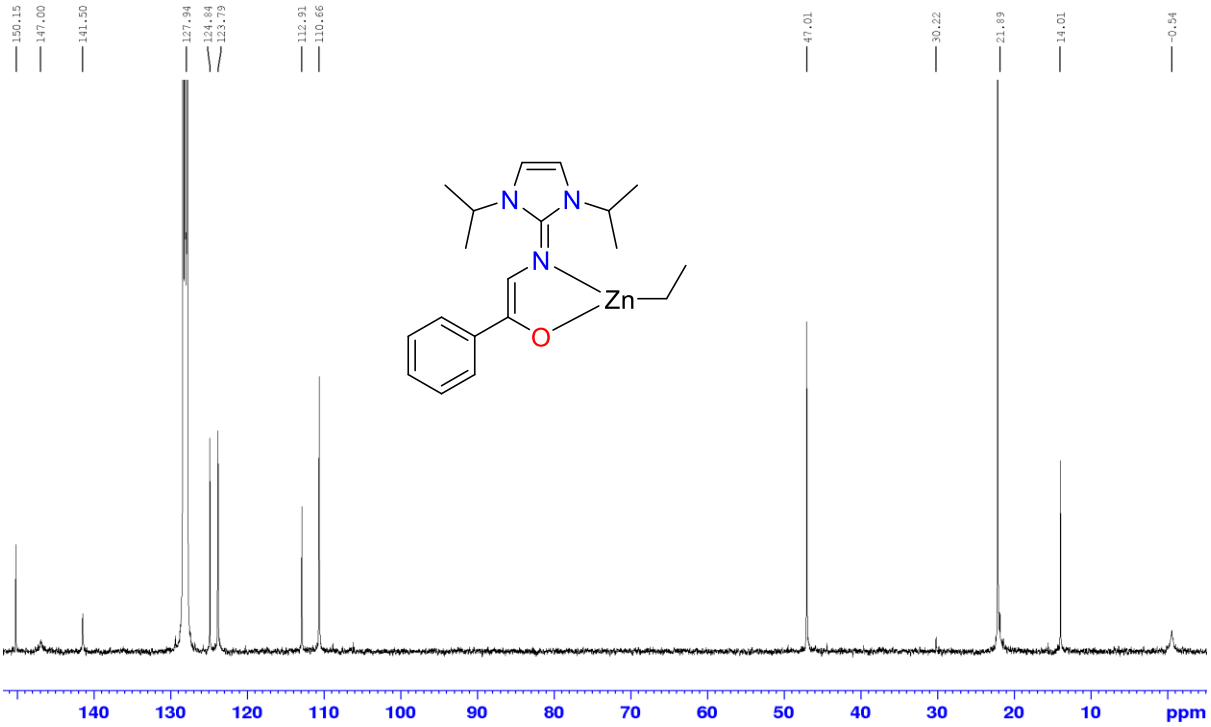

Figure A12. ^{13}C NMR spectrum of Zn(**L1**)Et (100 MHz, C_6D_6)

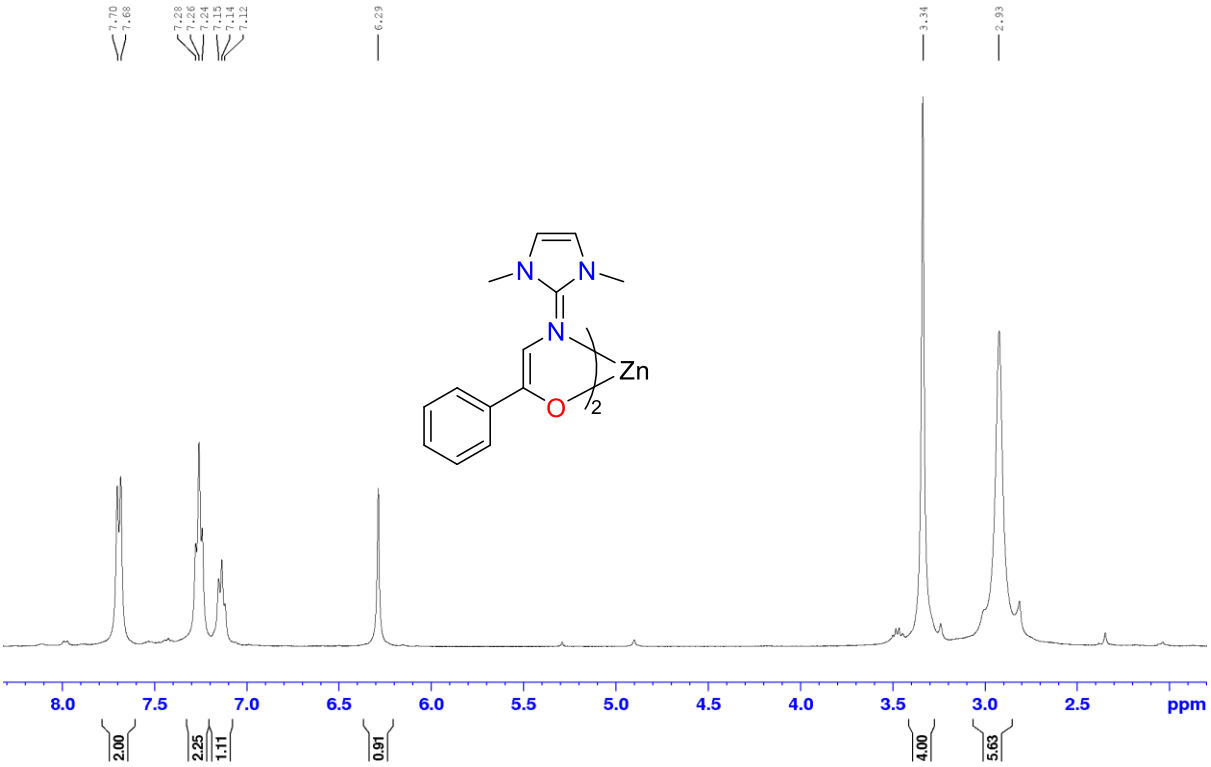

Figure A13. ^{1}H NMR spectrum of Zn(**L2**)$_2$ (400 MHz, $CDCl_3$)

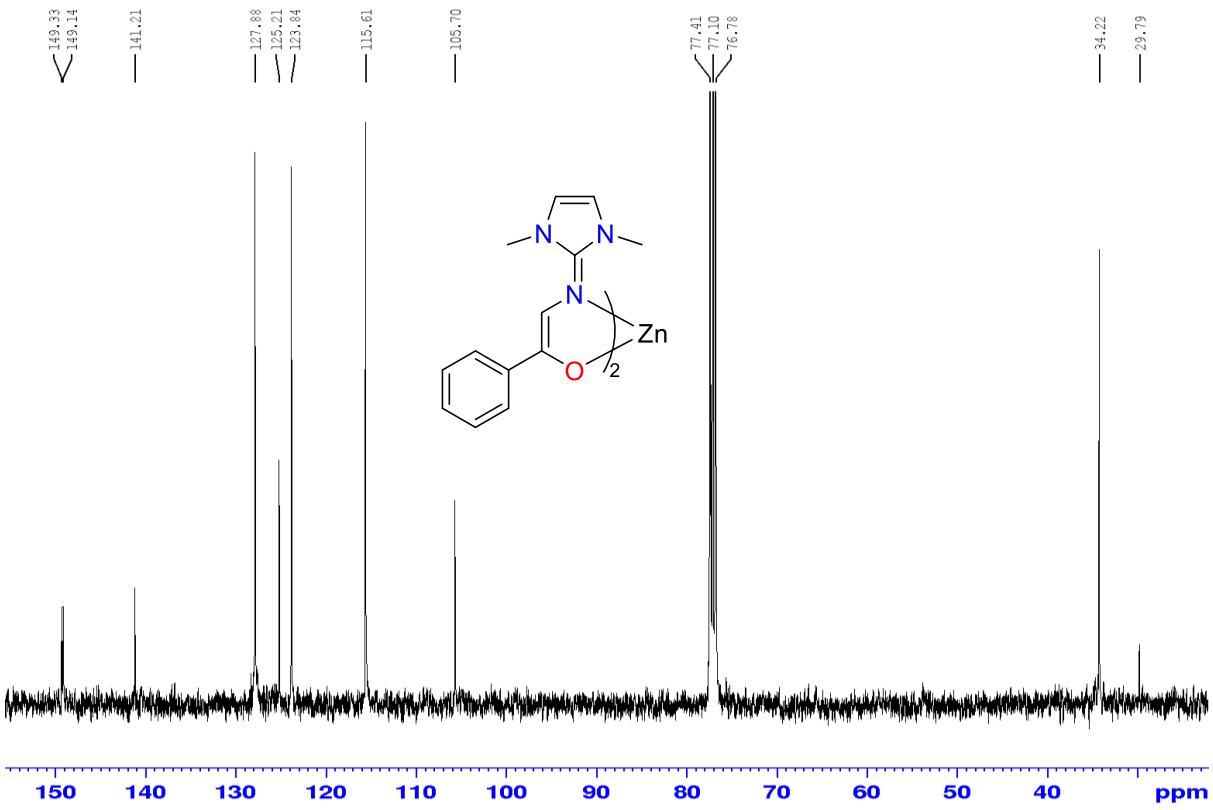

Figure A14. $^{13}C\{^{1}H\}$ NMR spectrum of Zn(**L2**)$_2$ (100 MHz, $CDCl_3$)

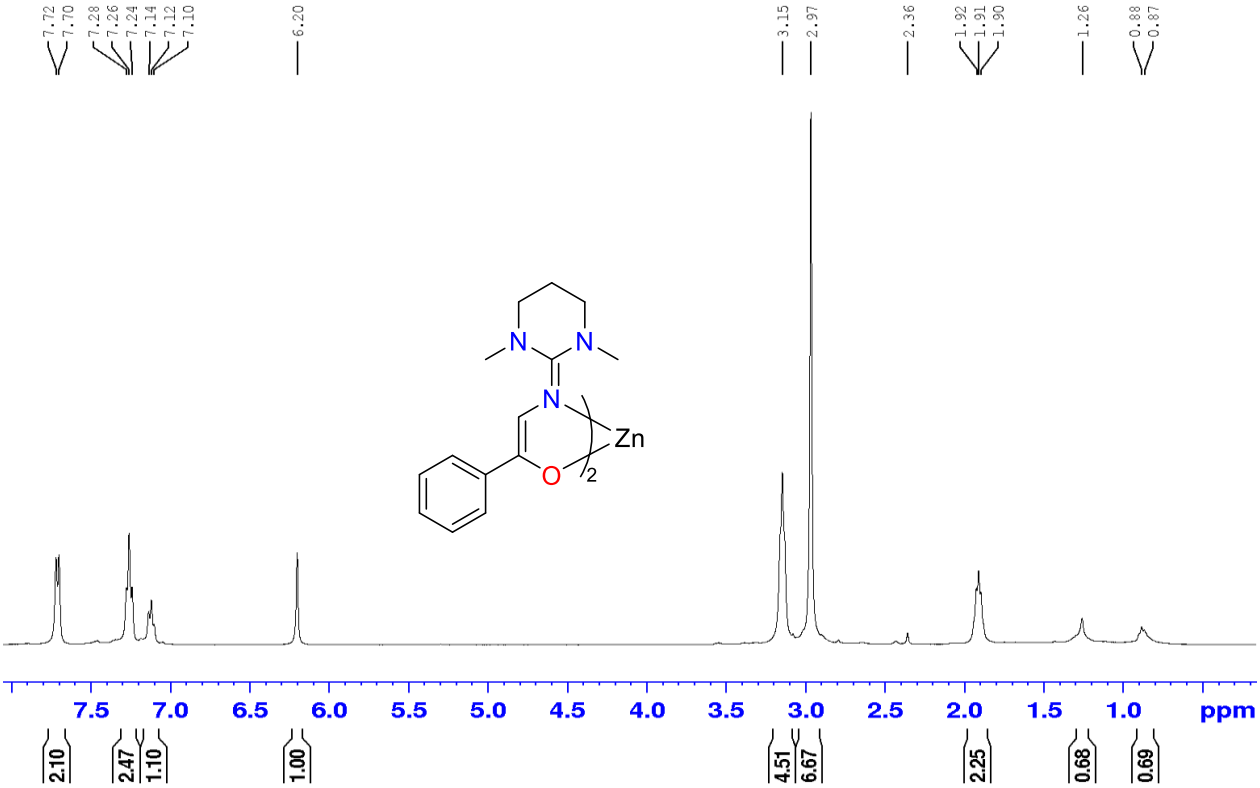

Figure A15. ^{1}H NMR spectrum of Zn(**L3**)$_2$ (400 MHz, $CDCl_3$)

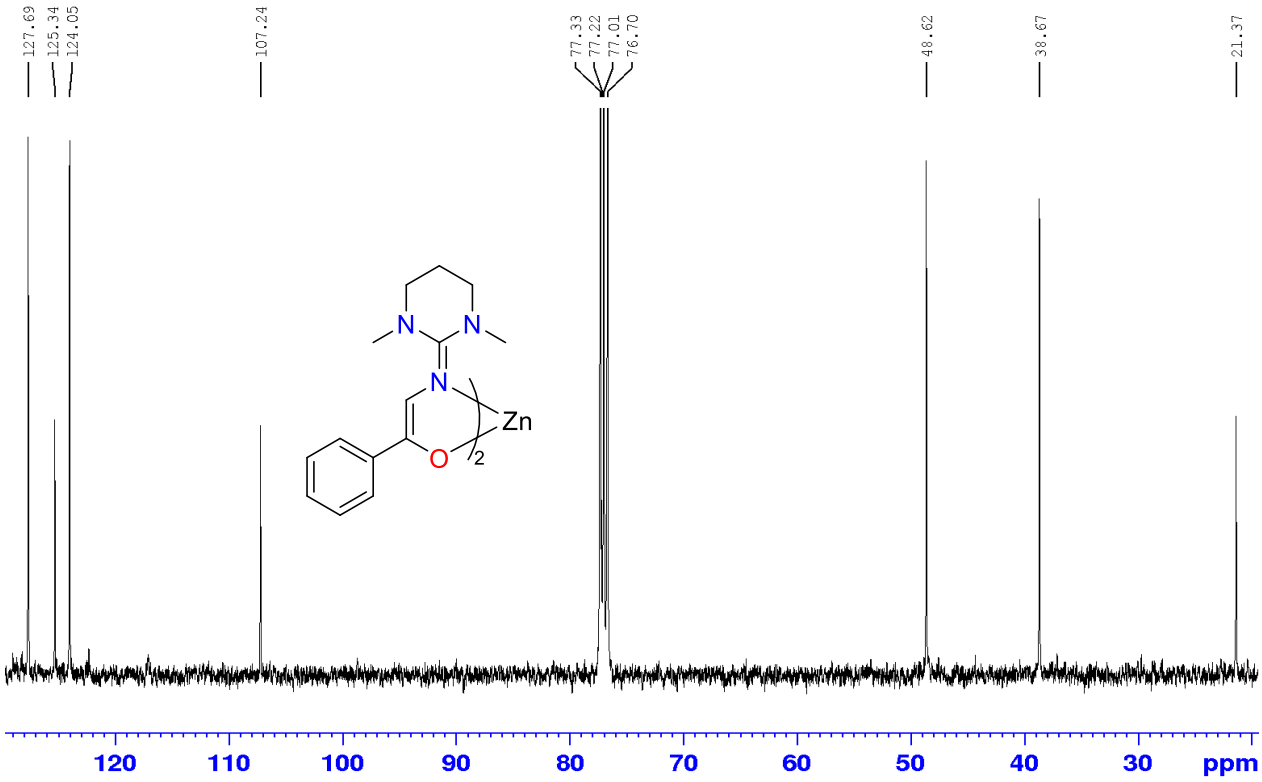

Figure A16. $^{13}C\{^{1}H\}$ NMR spectrum of Zn(**L3**)$_2$ (100 MHz, $CDCl_3$)

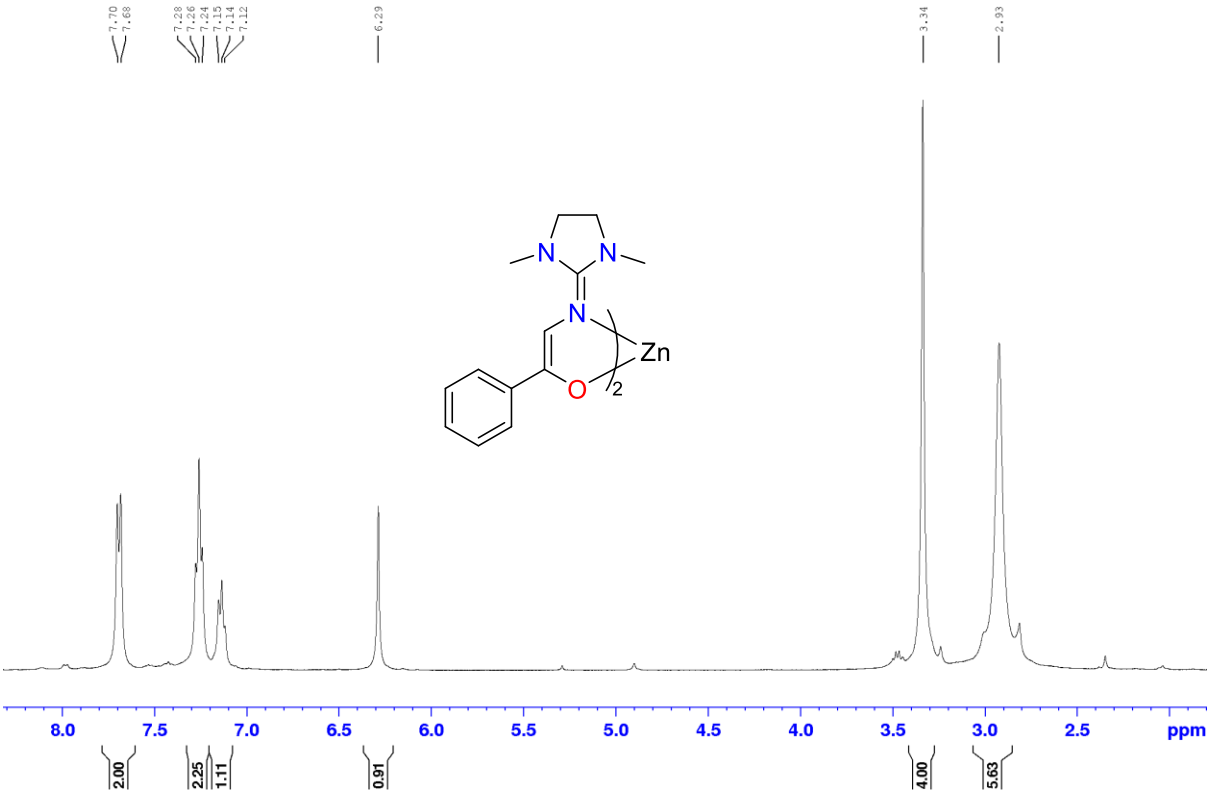

Figure A17. ^{1}H NMR spectrum of Zn(**L4**)$_2$ (400 MHz, $CDCl_3$)

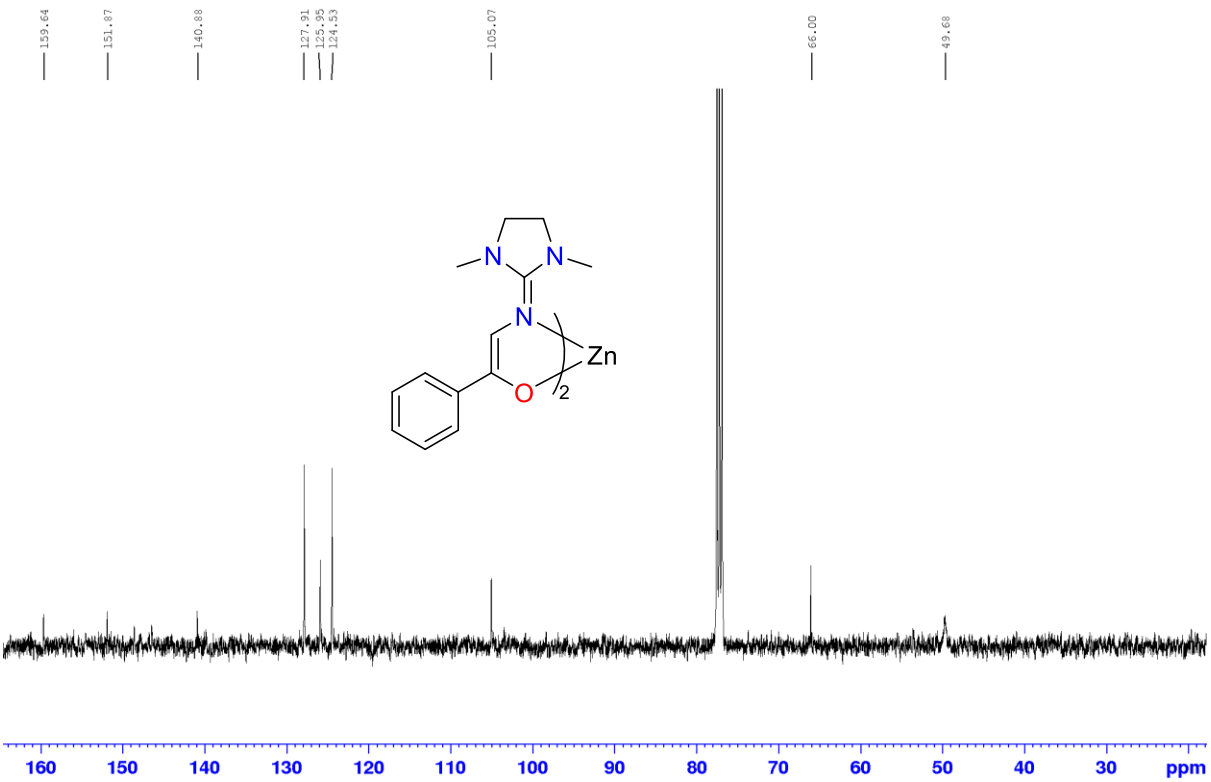

Figure A18. $^{13}C\{^{1}H\}$ NMR spectrum of Zn(**L4**)$_2$ (100 MHz, $CDCl_3$)

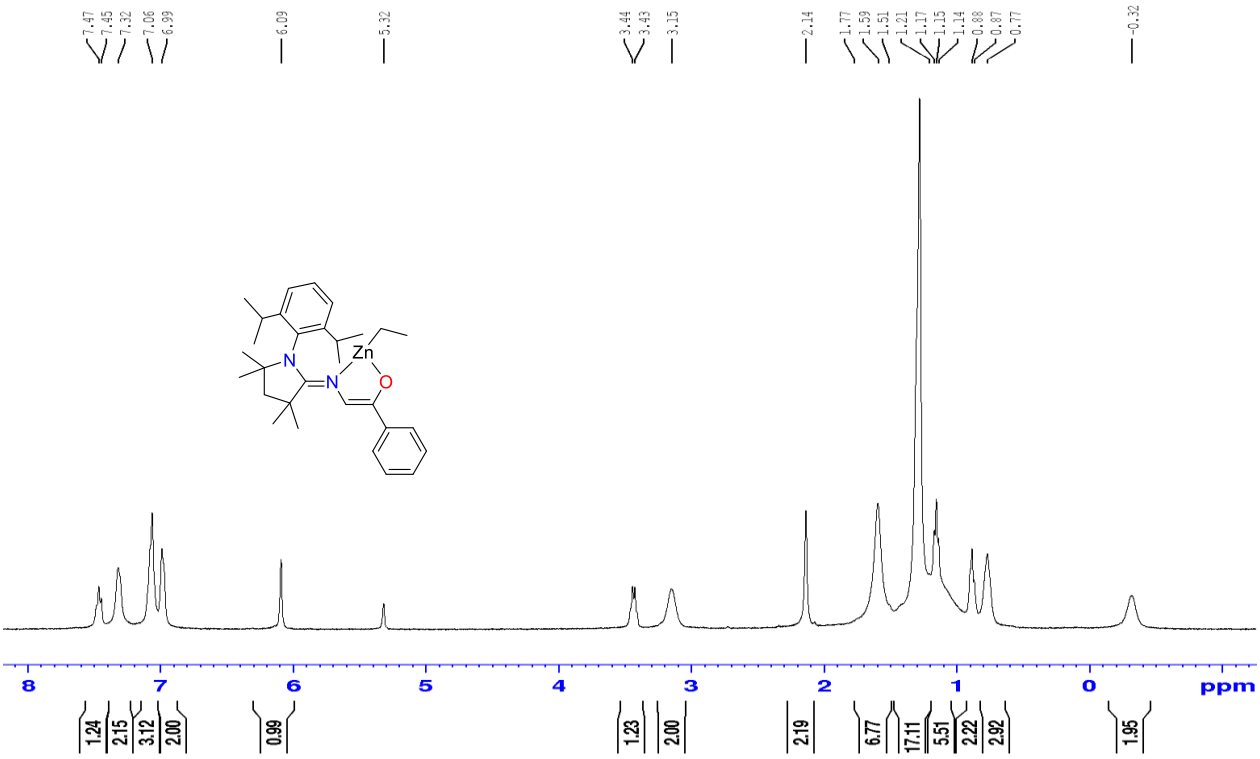

Figure A19. ^{1}H NMR spectrum of Zn(**L5**)Et (400 MHz, CD_2Cl_2)

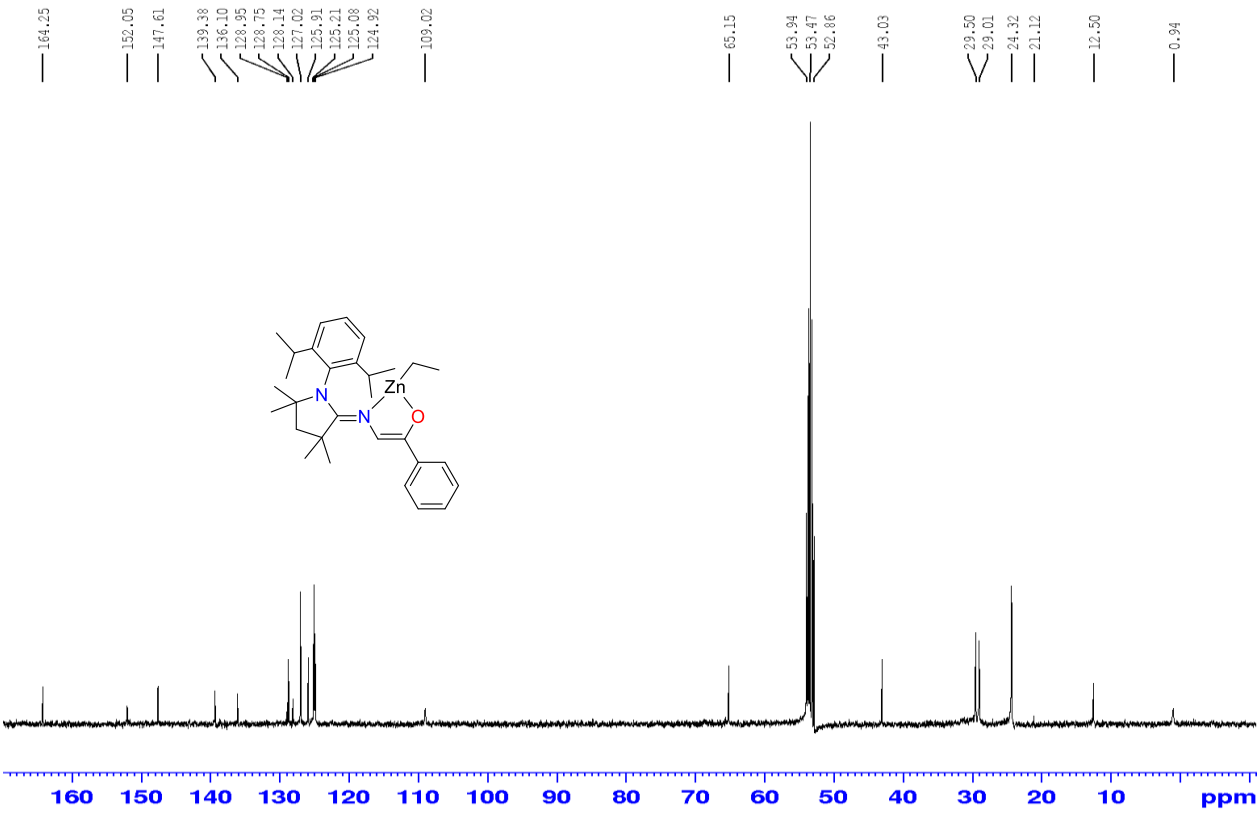

Figure A20. $^{13}C\{^{1}H\}$ NMR spectrum of Zn(**L5**)Et (100 MHz, CD_2Cl_2)

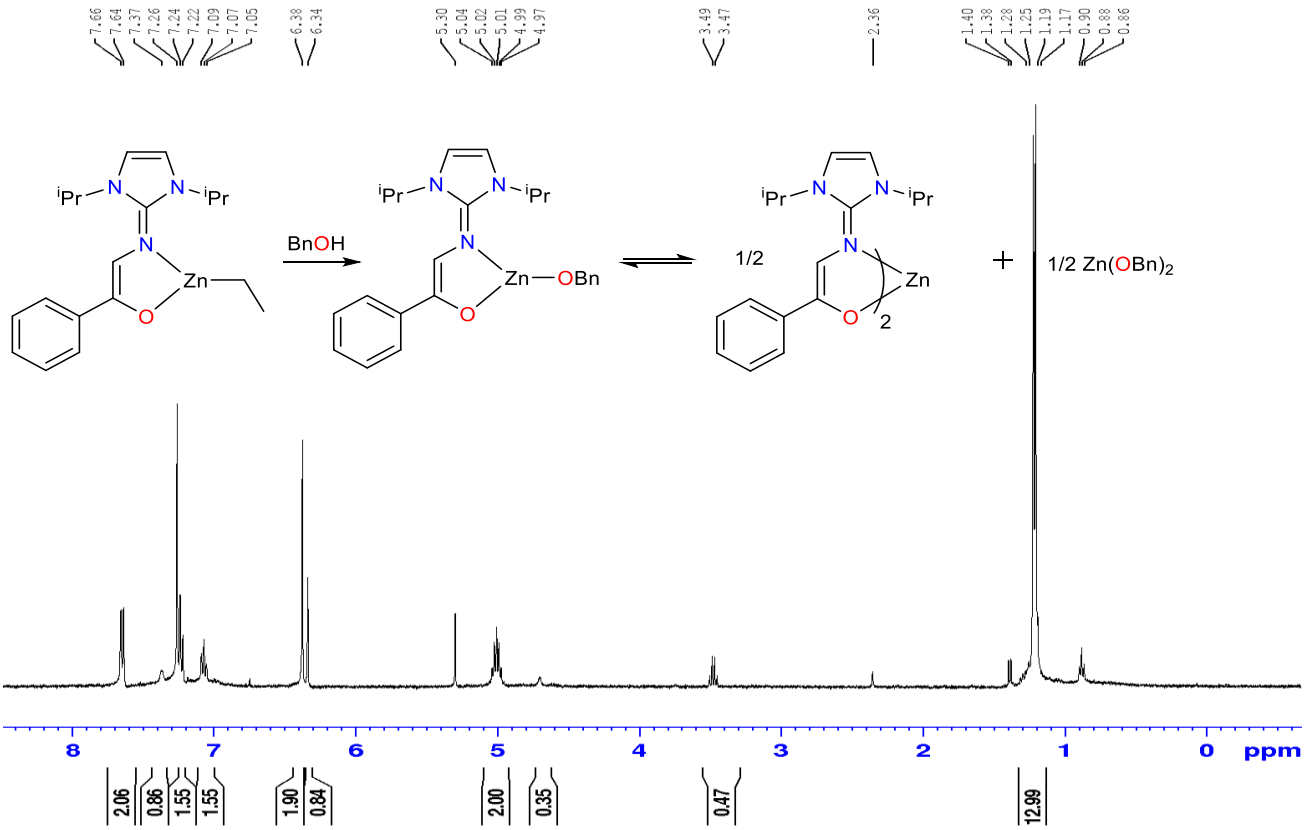

Figure A21. ^{1}H NMR spectrum of Zn(**L1**)$_2$ disproportionation product of Zn(**L1**)Et + BnOH (400 MHz, $CDCl_3$)

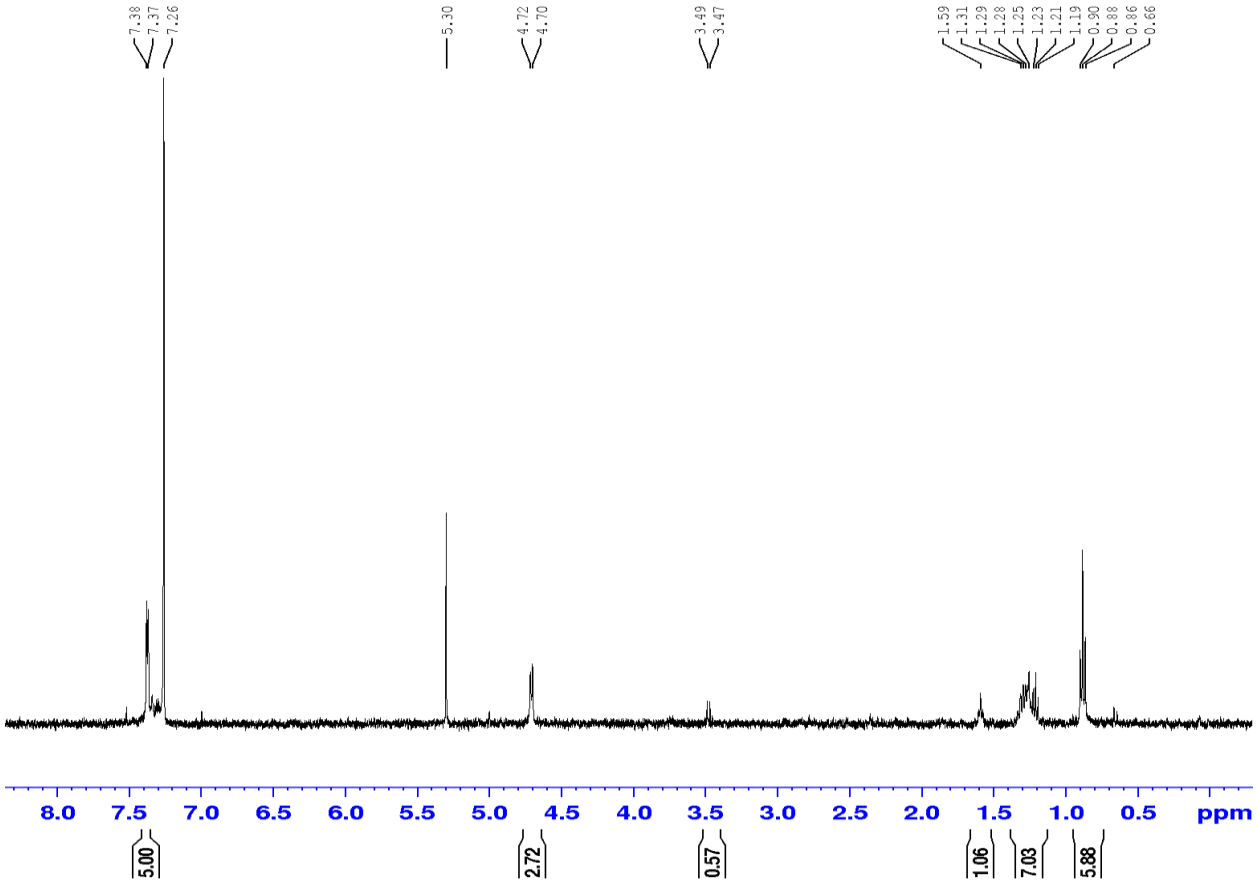

Figure A22. ^{1}H NMR spectrum of Zn(**OBn**)$_2$ (400 MHz, $CDCl_3$)

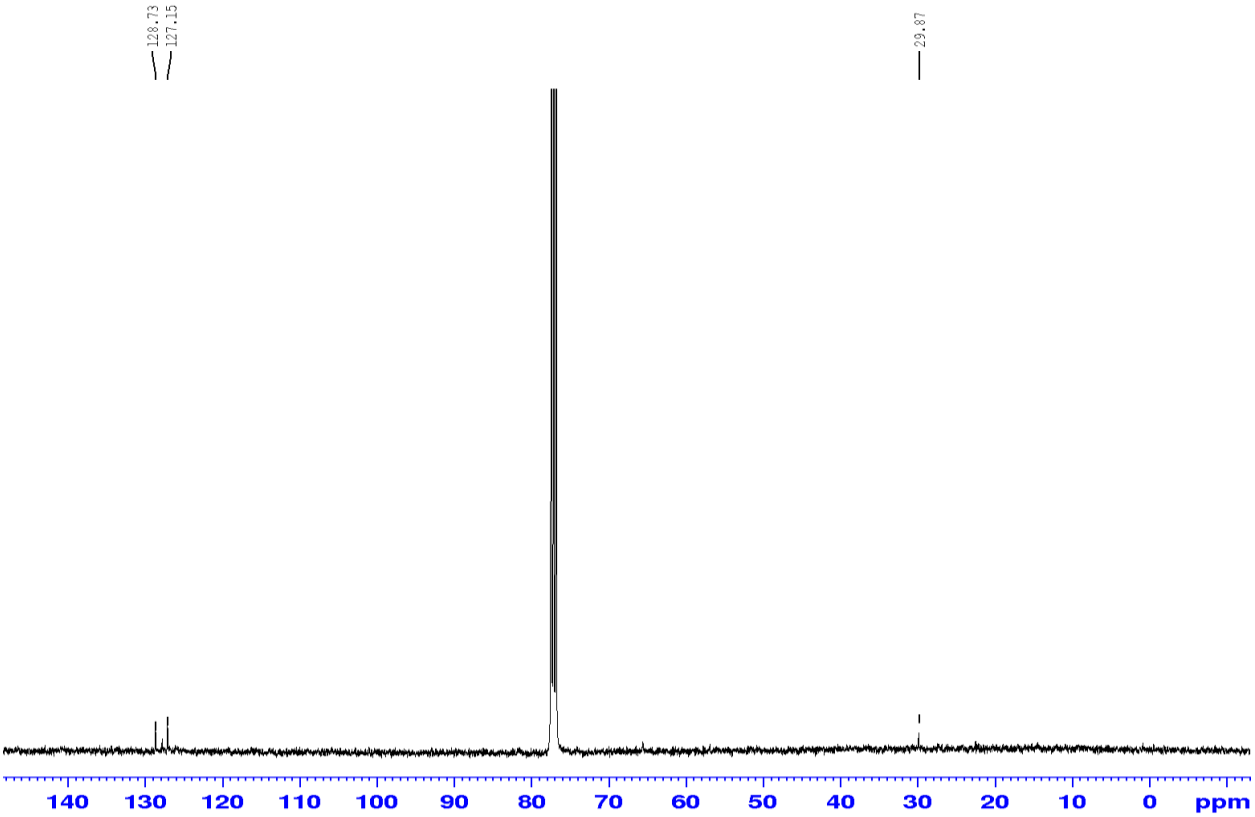

Figure A23. $^{13}C\{^{1}H\}$ NMR spectrum of Zn(**OBn**)$_2$ (100 MHz, $CDCl_3$)

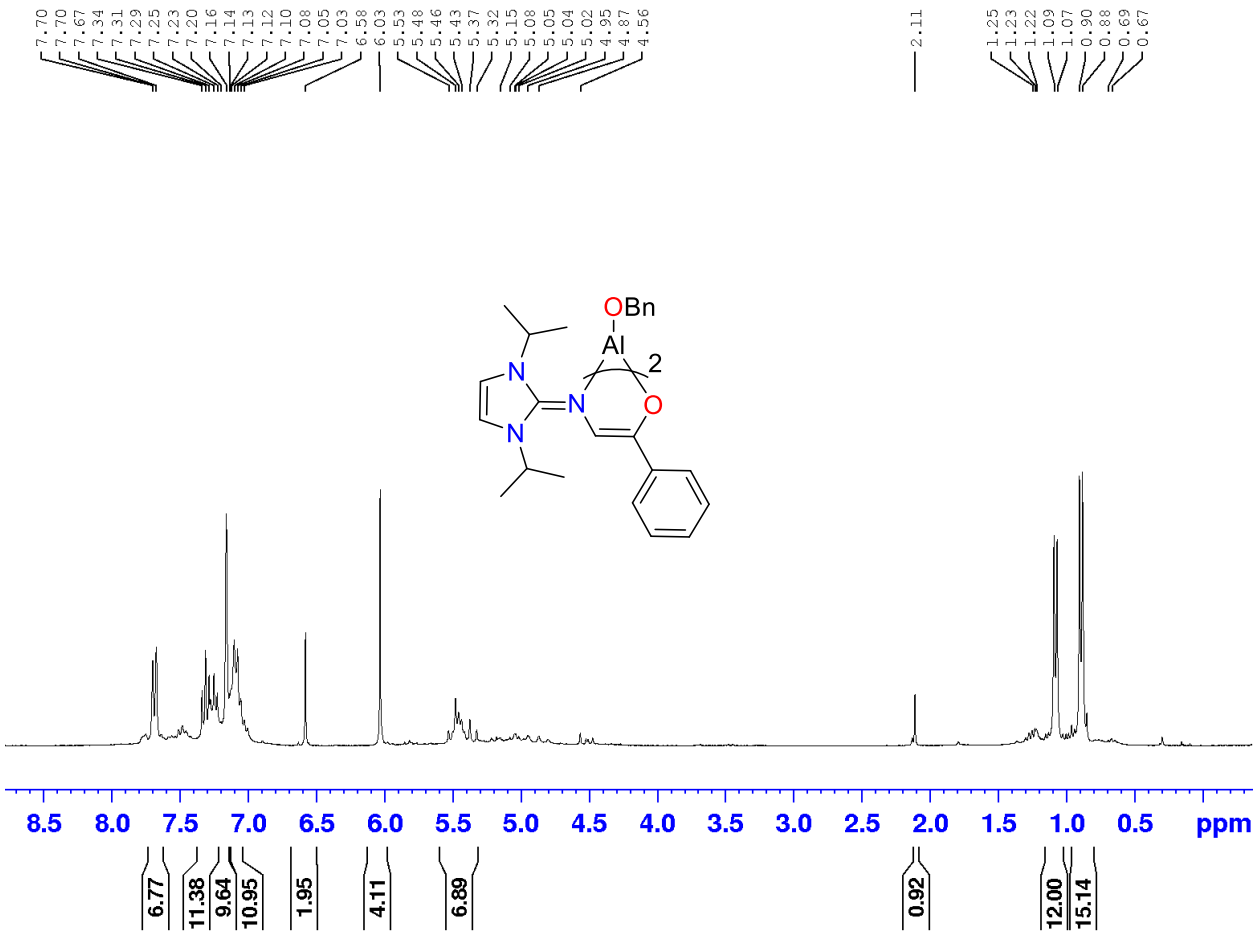

Figure A24. ^{1}H NMR spectrum of Al(**L1**)$_2$OBn (300 MHz, C_6D_6)

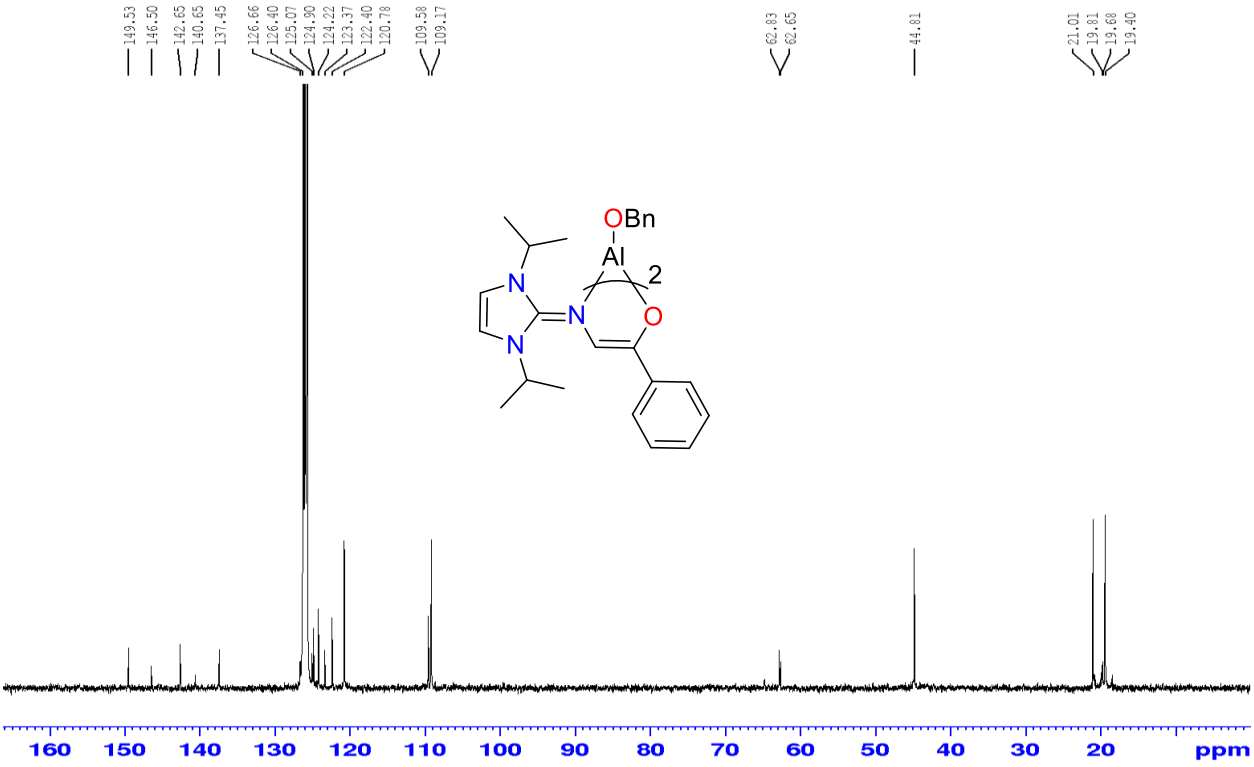

Figure A25. $^{13}C\{^{1}H\}$ NMR spectrum of Al(**L1**)$_2$OBn (100 MHz, C_6D_6)

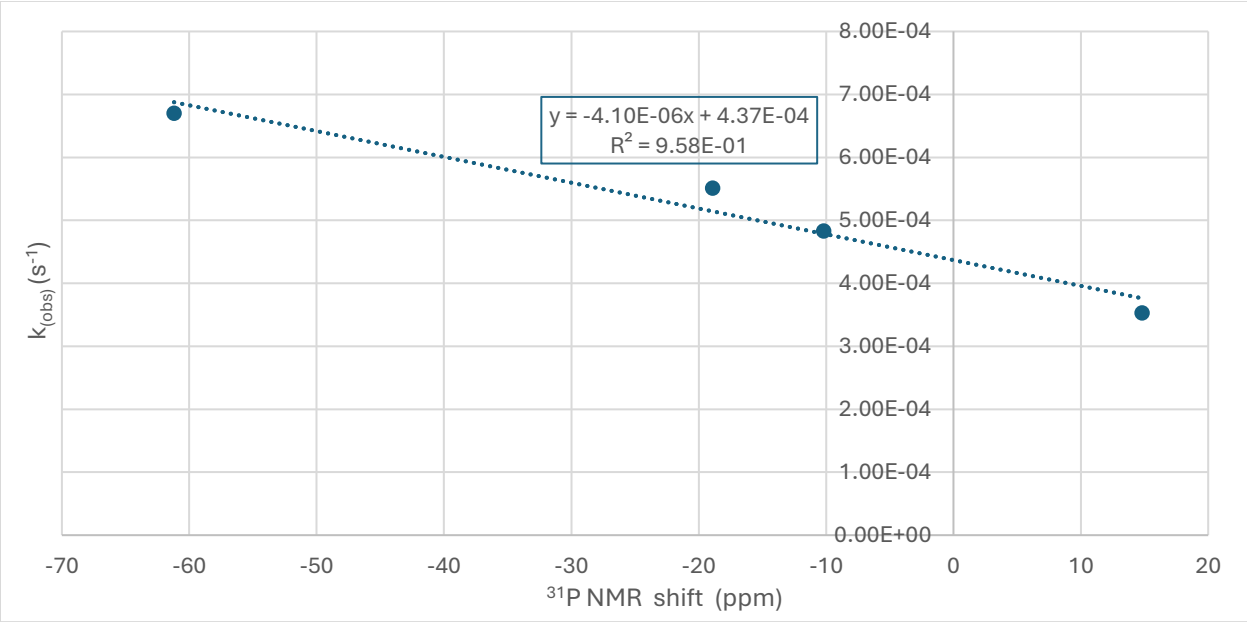

Figure A26. ^{31}P NMR shift of PPH adducts vs k_{obs} of Zn(**L1-L4**)$_2$ complexes at 130°C in a 100:1 stoichiometric ratio of lactide to catalyst.

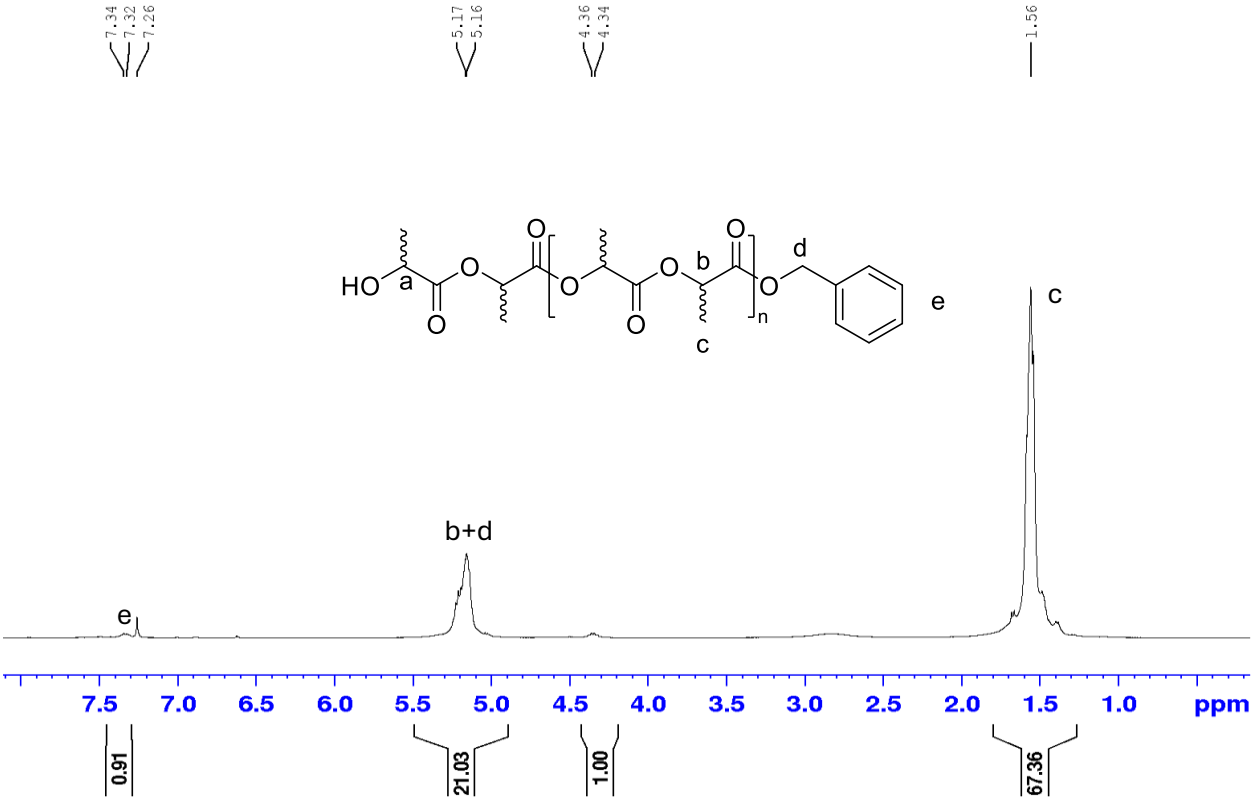

Figure A27. ^{1}H NMR spectrum (400 MHz, $CDCl_3$) of the polymer produced with Zn(**L1**)$_2$ using BnOH as co-initiator at 130°C in a 100::11 stoichiometric ratio of lactide to catalyst to co-initiator (entry 1).

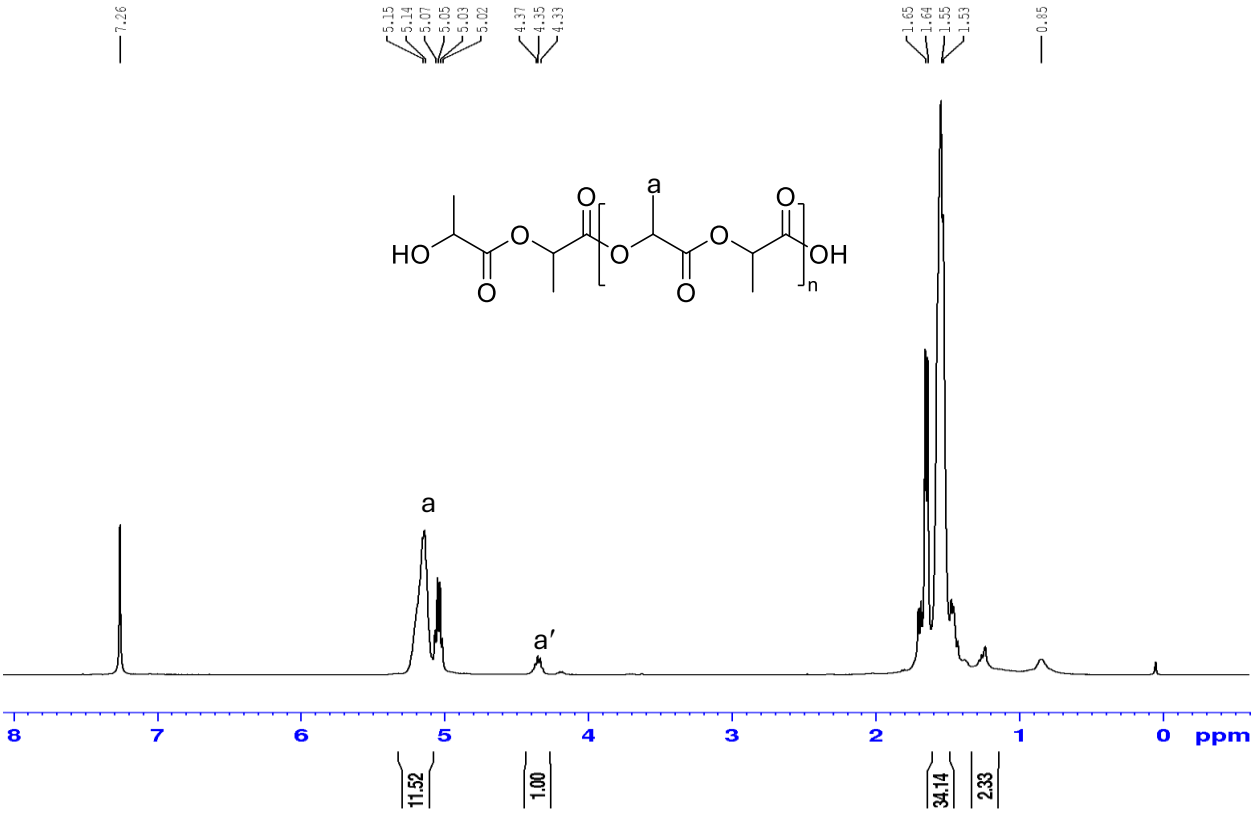

Figure A28. ^{1}H NMR spectrum (400 MHz, $CDCl_3$) of the polymer produced with Zn(**L1**)$_2$ at 130°C in a 500:1 stoichiometric ratio of lactide to catalyst (entry 1).

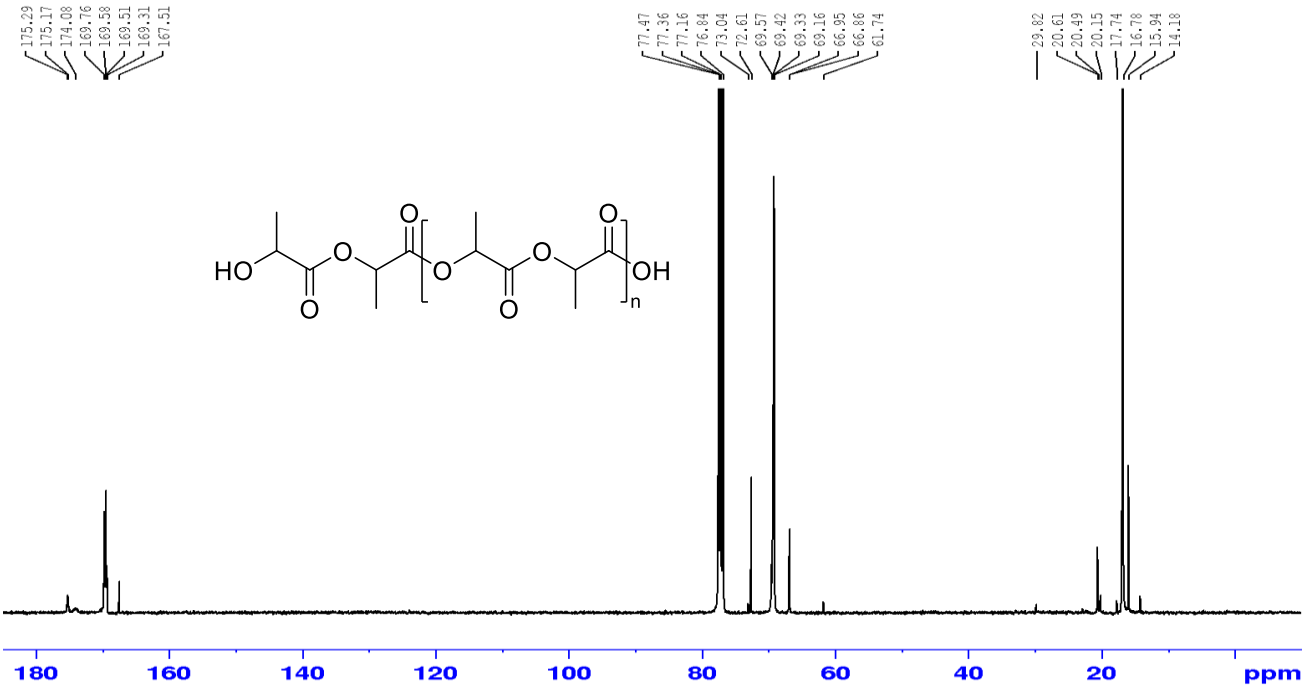

Figure A29. $^{13}C\{^{1}H\}$ NMR spectrum of the polymer produced with Zn(**L1**)$_2$ at 130°C in a 500:1 stoichiometric ratio of lactide to catalyst (entry 1).

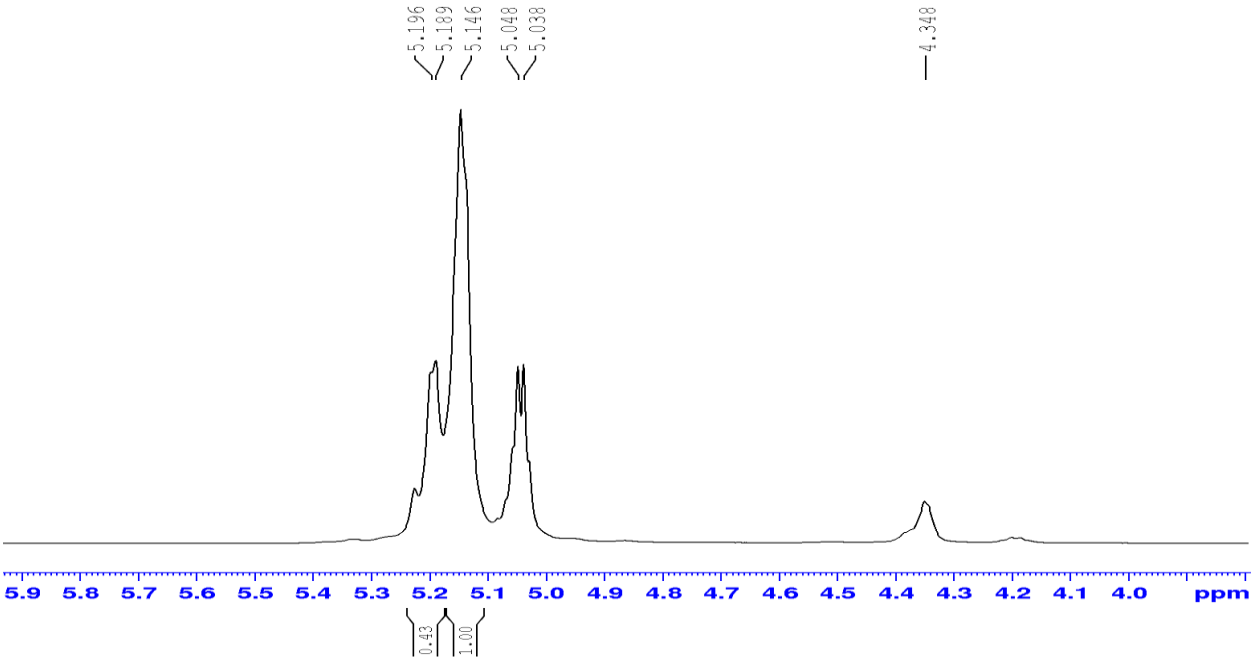

Figure A30**.** Homonuclear-decoupled ^{1}H NMR spectrum of the polymer produced with Zn(**L1**)$_2$ at 130°C in a 500:1 stoichiometric ratio of lactide to catalyst (entry 1).

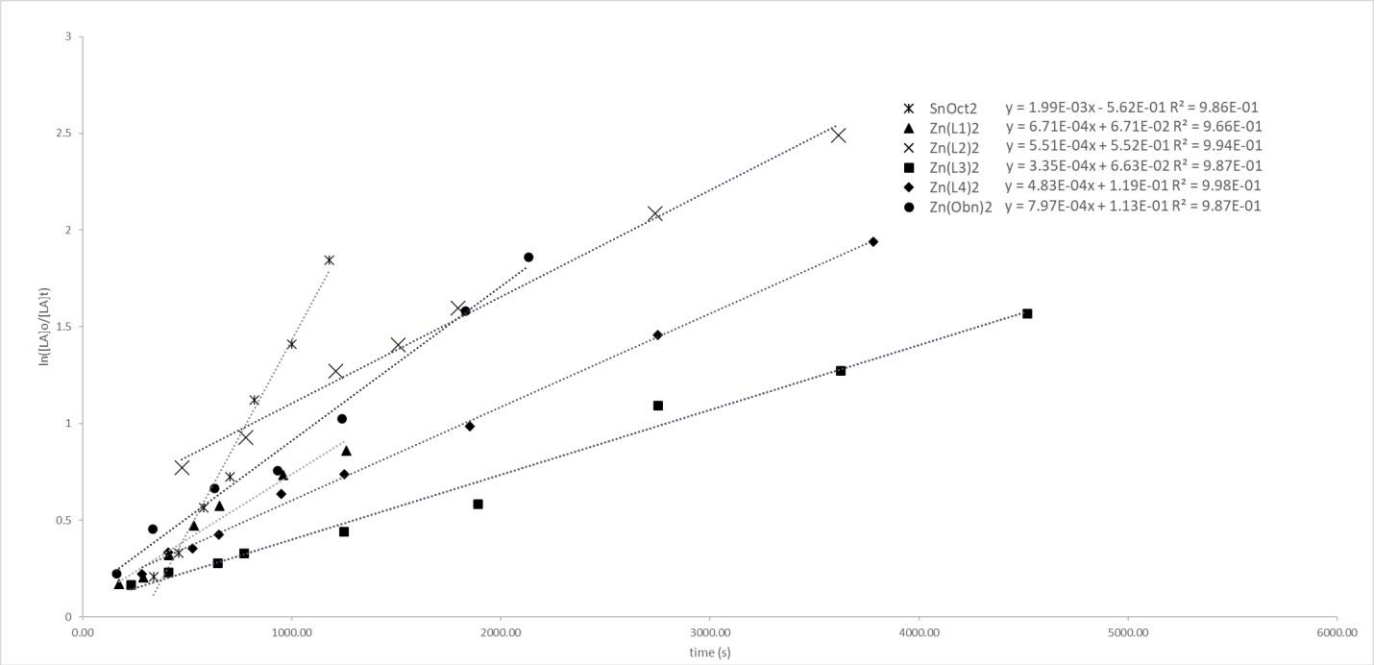

Figure A31**.** Kinetic plot for the polymerization of rac-lactide by $Sn(Oct)_2$, $Zn(\mathbf{L1})_2$, $Zn(\mathbf{L2})_2$, $Zn(\mathbf{L3})_2$, $Zn(\mathbf{L4})_2$, and $Zn(OBn)_2$ at 130°C in a 500:1 stoichiometric ratio of lactide to catalyst.

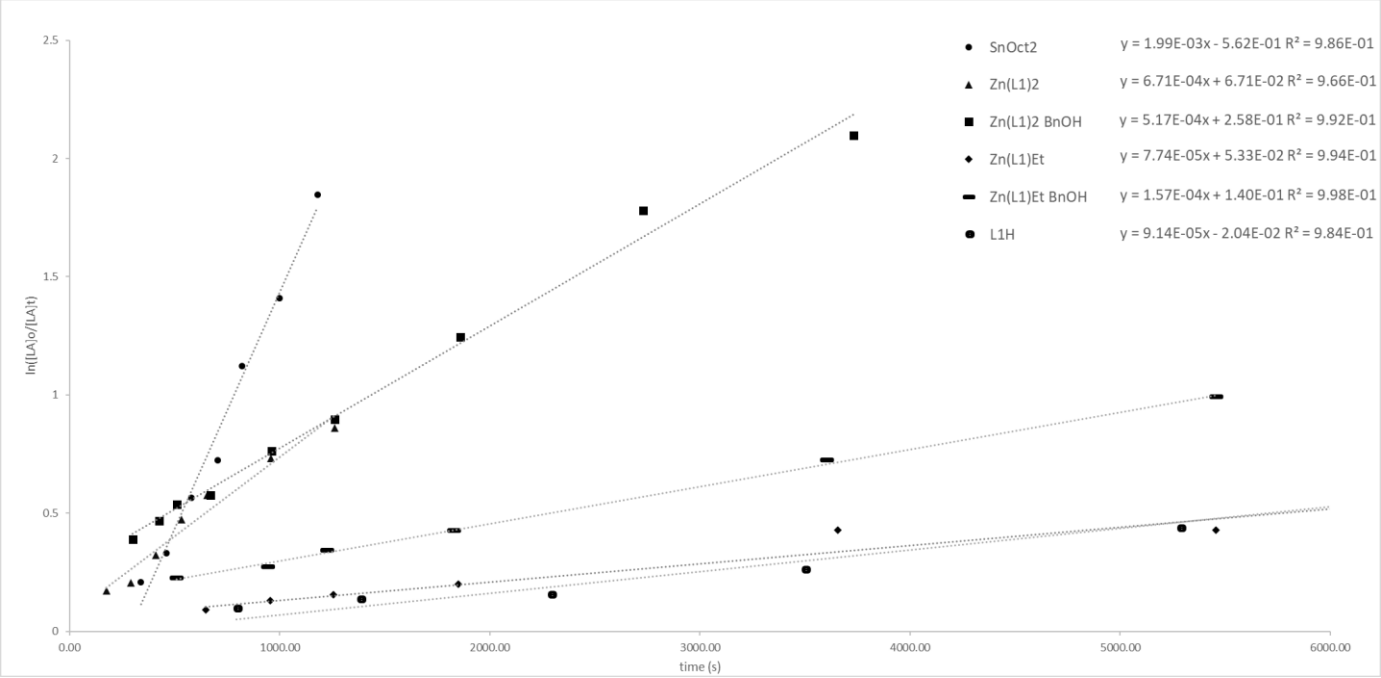

Figure A32**.** Kinetic plot for the polymerization of rac-lactide by $Sn(Oct)_2$, Zn(**L1**)$_2$, Zn(**L1**)$_2$ with BnOH as a co-initiator, Zn(**L1**)Et, Zn(**L1**)Et with BnOH as a co-initiator, and **L1**H at 130°C in a 500:1 stoichiometric ratio of lactide to catalyst.

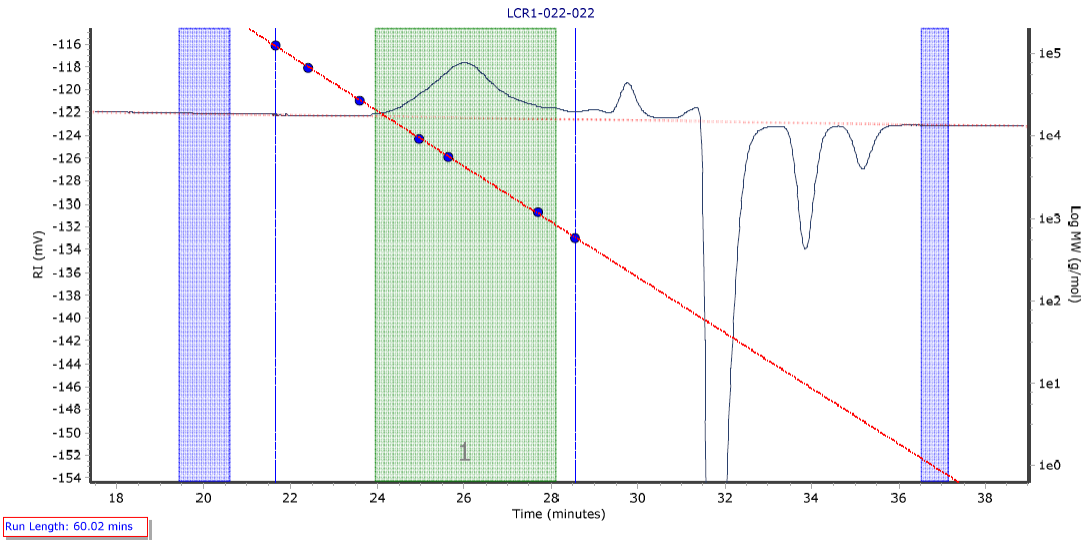

Figure A33**.** GPC chromatogram plot of the polymer obtained using complex Zn(**L1**)$_2$ (Table 4, entry 2) at 130°C in a 100:1 stoichiometric ratio of lactide to catalyst.

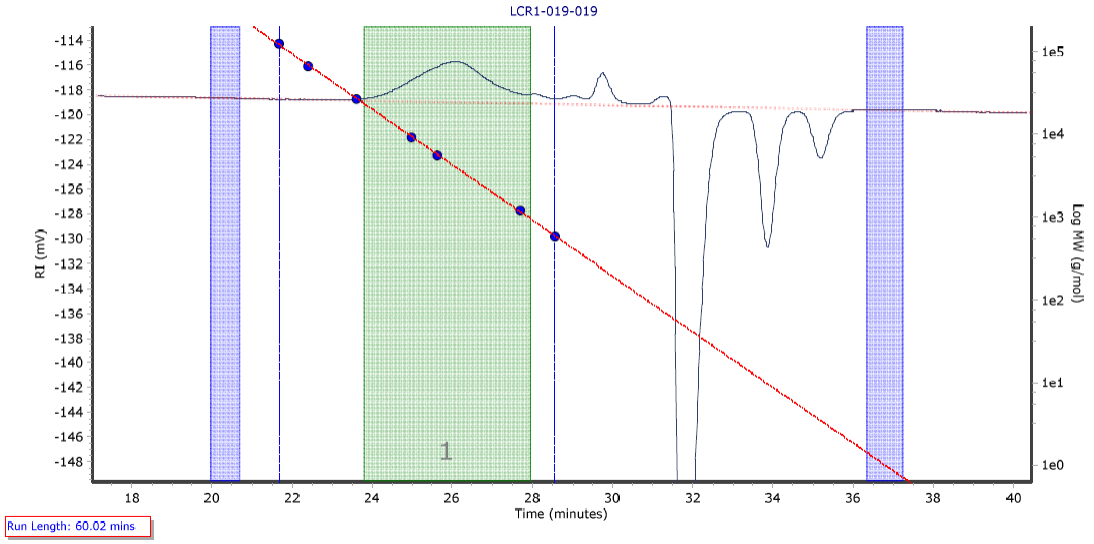

Figure A34**.** GPC chromatogram plot of the polymer obtained using complex Zn(**L1**)$_2$ (Table 4, entry 3) at 130°C in a 100:1:1 stoichiometric ratio of lactide to catalyst to BnOH.

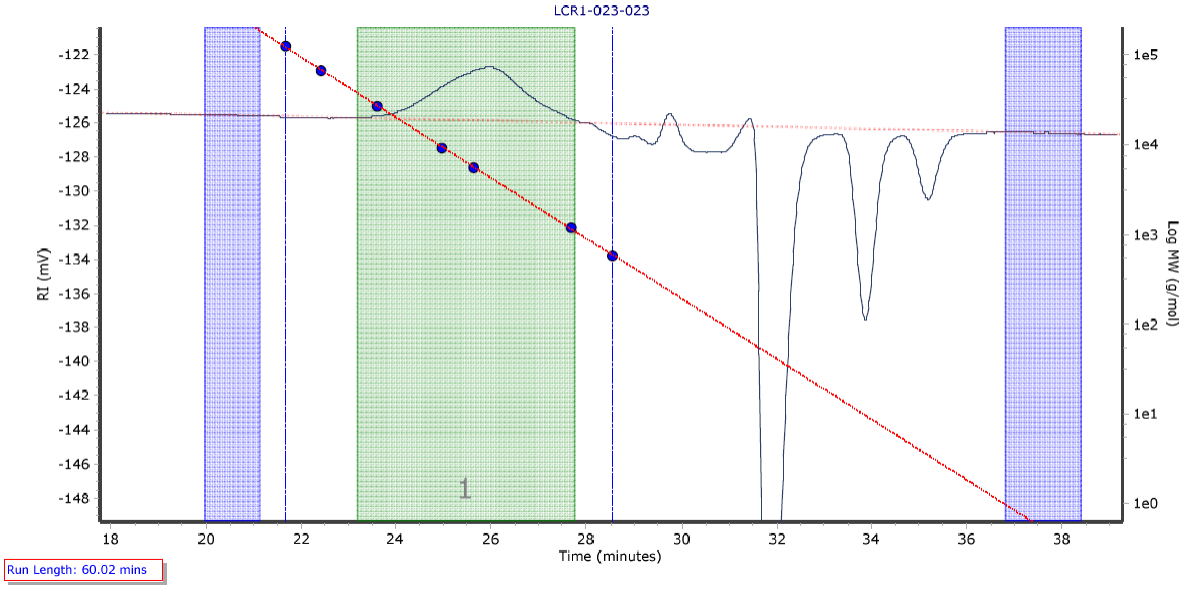

Figure A35. GPC chromatogram plot of the polymer obtained using complex Zn(**L1**)Et (Table 4, entry 4) at 130°C in a 100:1 stoichiometric ratio of lactide to catalyst.

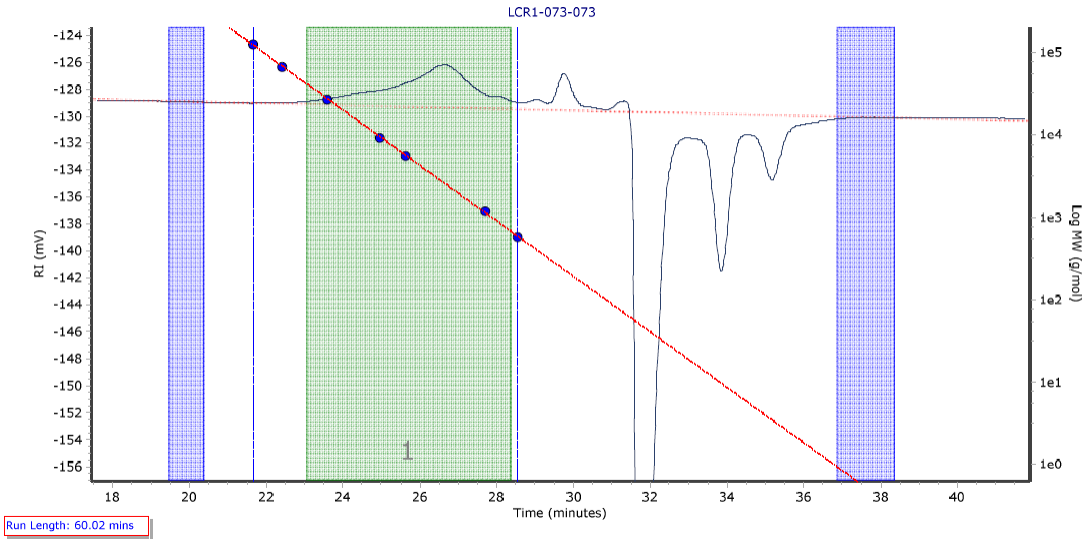

Figure A36**.** GPC chromatogram plot of the polymer obtained using complex Zn(**L1**)Et (Table 4, entry 5) at 130°C in a 100:1:1 stoichiometric ratio of lactide to catalyst to BnOH.

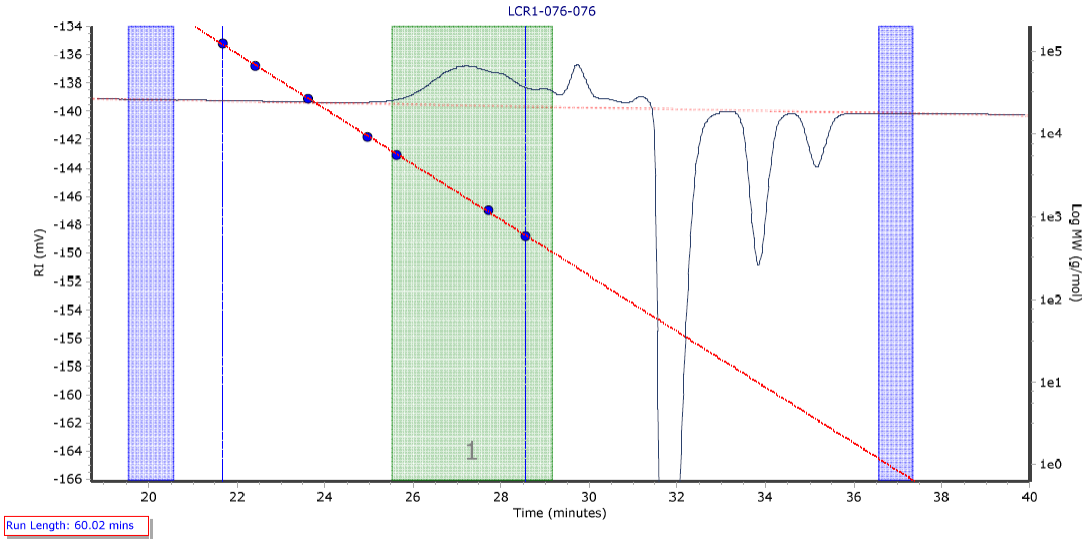

Figure A37**.** GPC chromatogram plot of the polymer obtained using complex Zn(**L2**)$_2$ (Table 4, entry 7) at 130°C in a 100:1 stoichiometric ratio of lactide to catalyst.

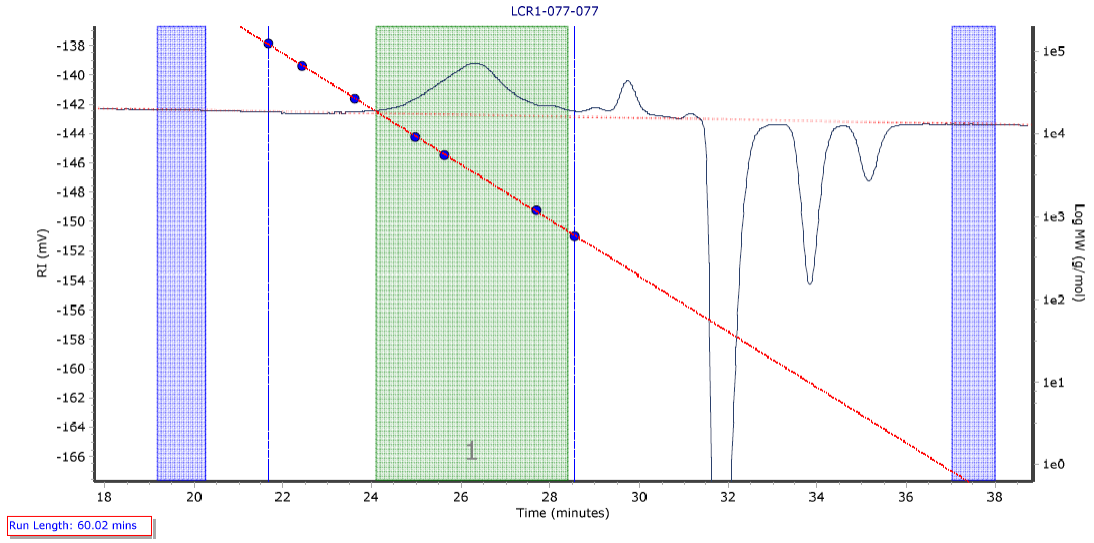

Figure A38**.** GPC chromatogram plot of the polymer obtained using complex Zn(**L2**)$_2$ (Table 4, entry 8) at 130°C in a 100:1:1 stoichiometric ratio of lactide to catalyst to BnOH.

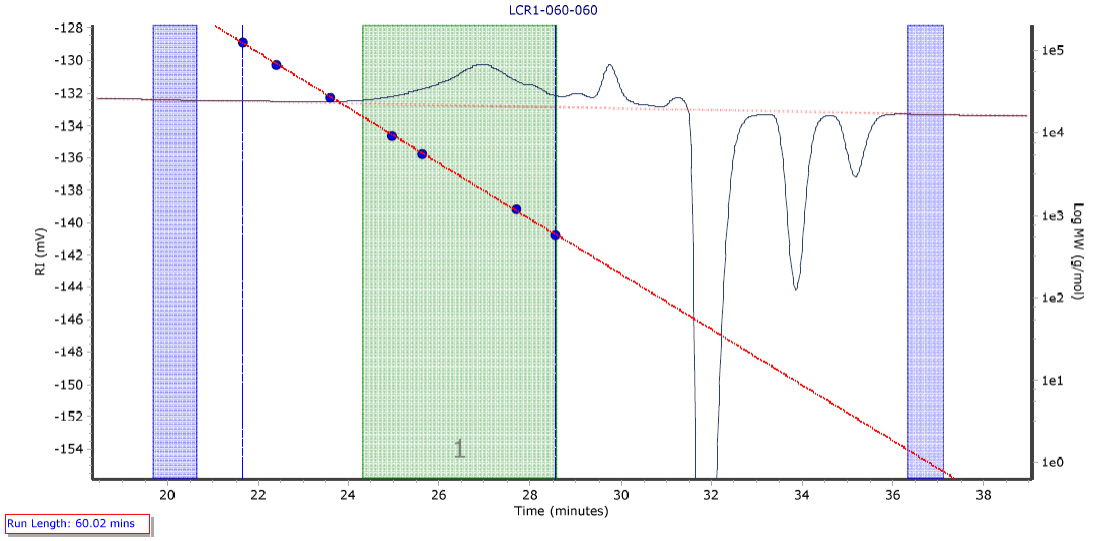

Figure A39**.** GPC chromatogram plot of the polymer obtained using complex Zn(**L3**)$_2$ (Table 4, entry 10) at 130°C in a 100:1 stoichiometric ratio of lactide to catalyst.

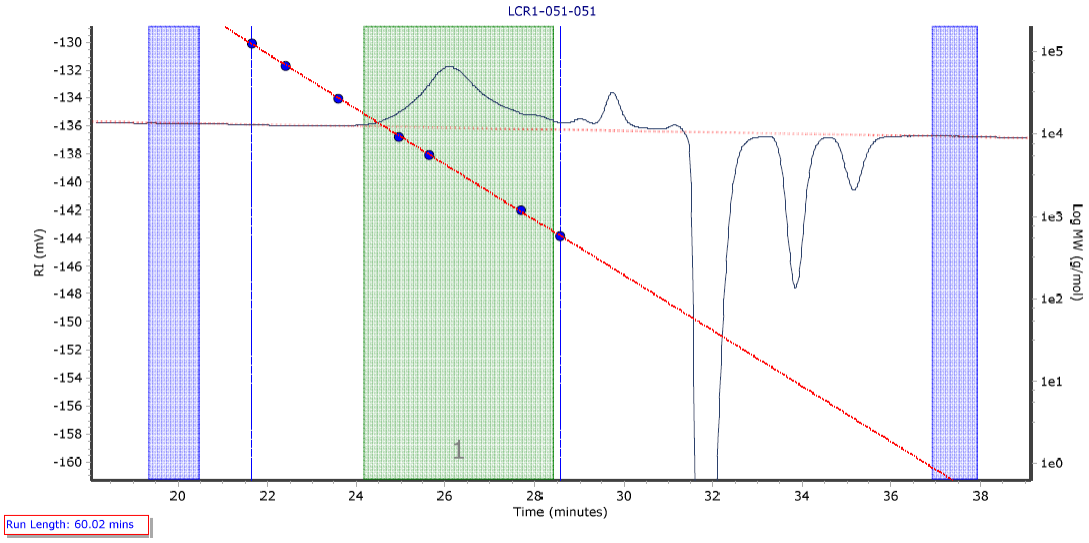

Figure A40**.** GPC chromatogram plot of the polymer obtained using complex Zn(**L3**)$_2$ (Table 4, entry 11) at 130°C in a 100:1:1 stoichiometric ratio of lactide to catalyst to BnOH.

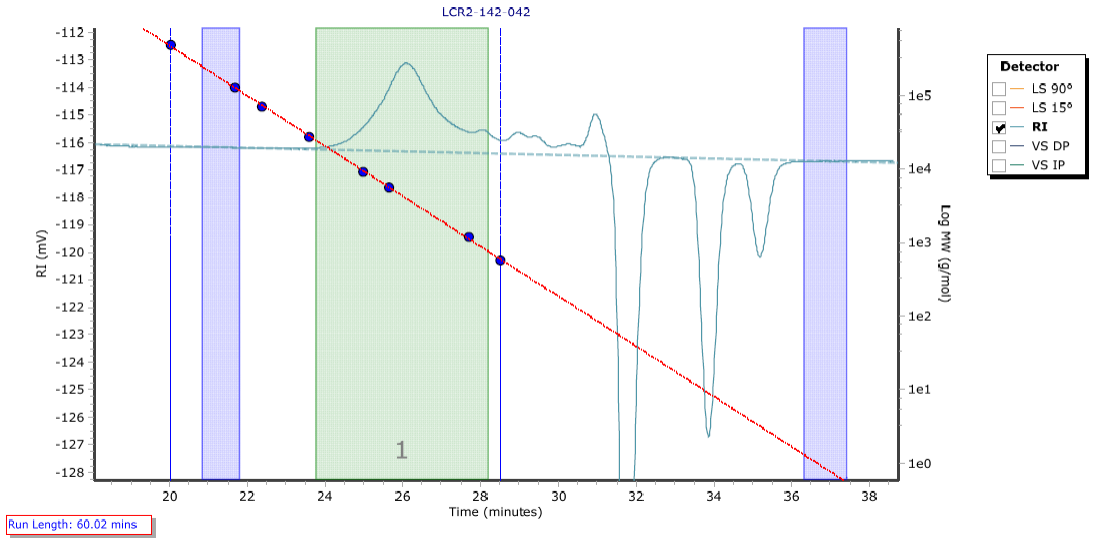

Figure A41. GPC chromatogram plot of the polymer obtained using complex Zn(**L4**)$_2$ (Table 4, entry 13) at 130°C in a 100:1 stoichiometric ratio of lactide to catalyst.

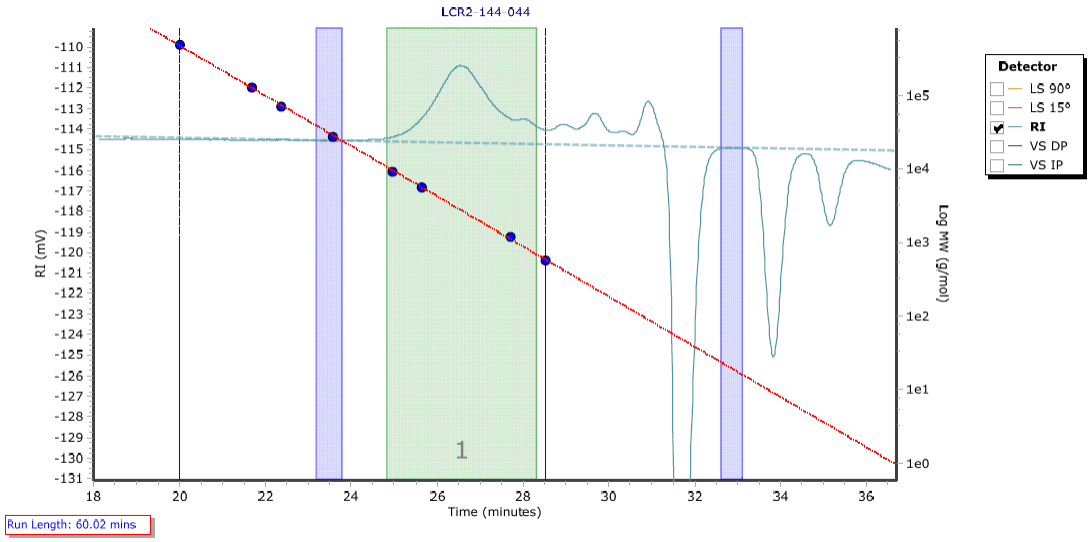

Figure A42**.** GPC chromatogram plot of the polymer obtained using complex Zn(**L4**)$_2$ (Table 4, entry 14) at 130°C in a 100:1:1 stoichiometric ratio of lactide to catalyst to BnOH.

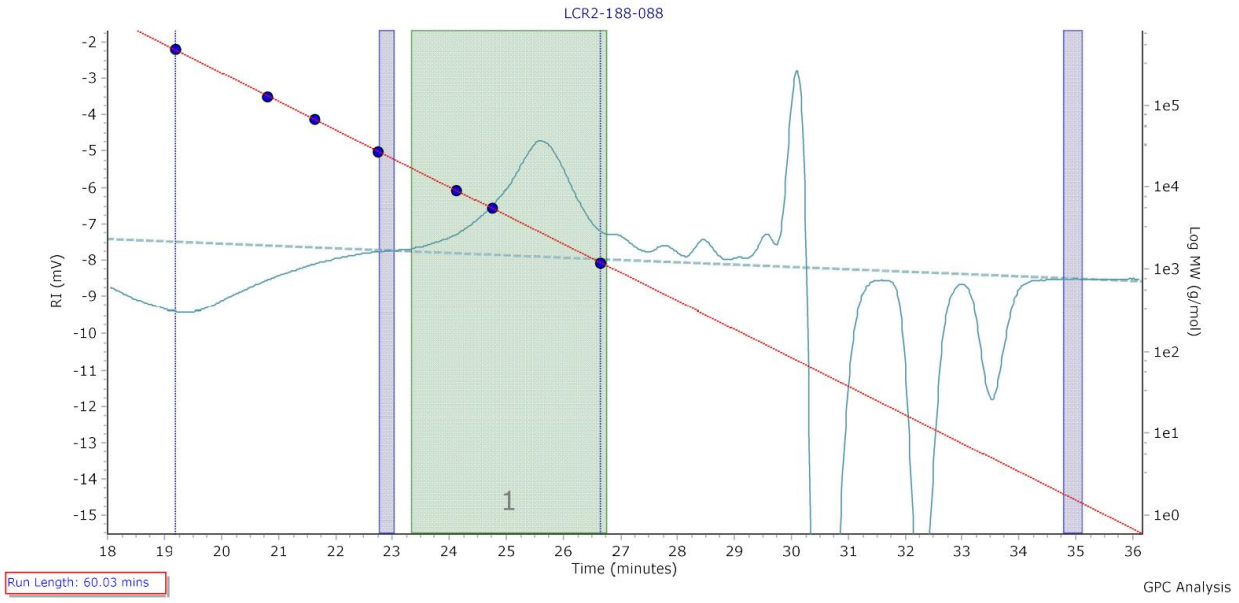

Figure A43. GPC chromatogram plot of the polymer obtained using complex Zn(**L5**)Et (Table 4, entry 15) at 130°C in a 100:1:1 stoichiometric ratio of lactide to catalyst to BnOH.

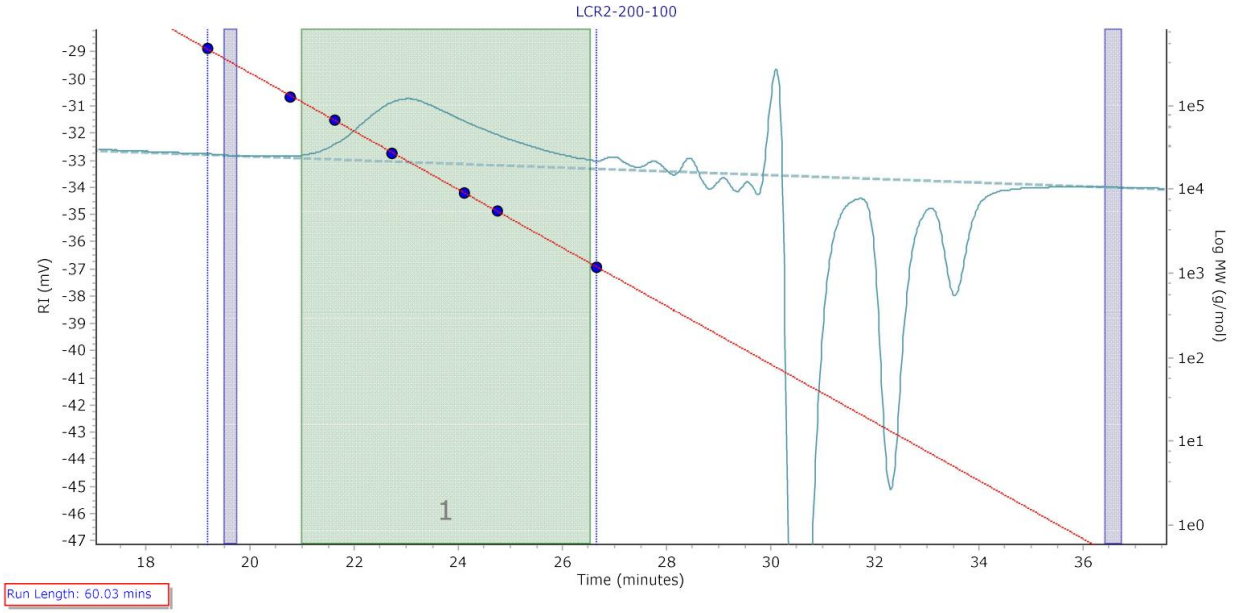

Figure A44**.** GPC chromatogram plot of the polymer obtained using complex Zn(**OBn**)$_2$ (Table 4, entry 16) at 130°C in a 100:1 stoichiometric ratio of lactide to catalyst.

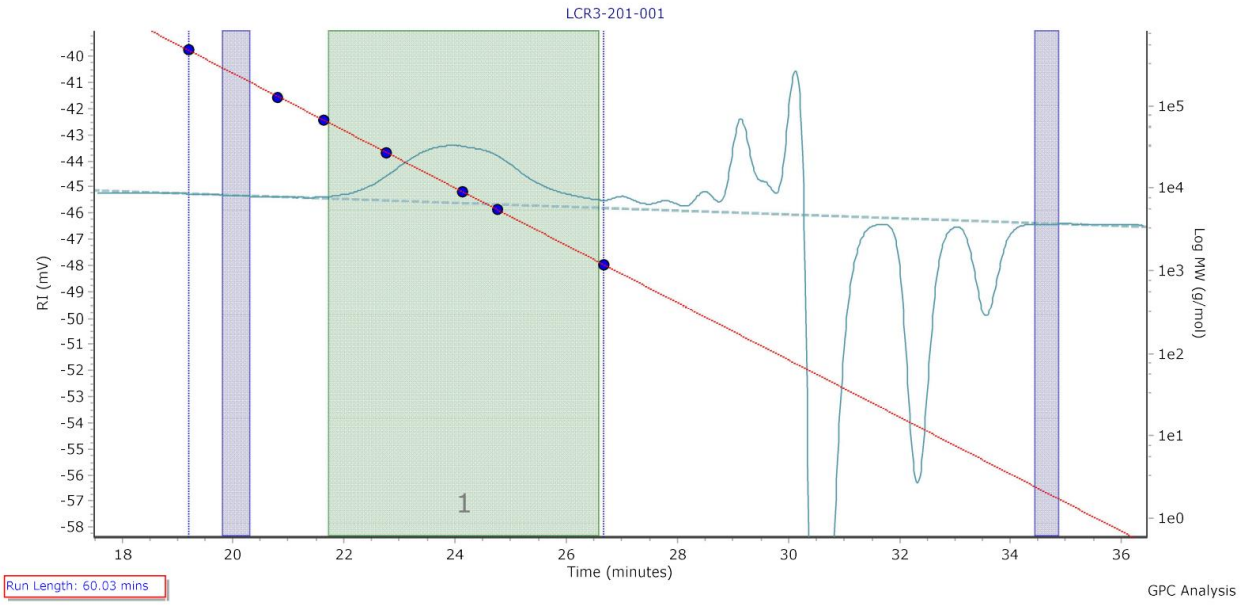

Figure A45. GPC chromatogram plot of the polymer obtained using complex $Zn(OBn)_2$ (Table 4**,** entry 17) at 130°C in a 100:1:1 stoichiometric ratio of lactide to catalyst to BnOH.

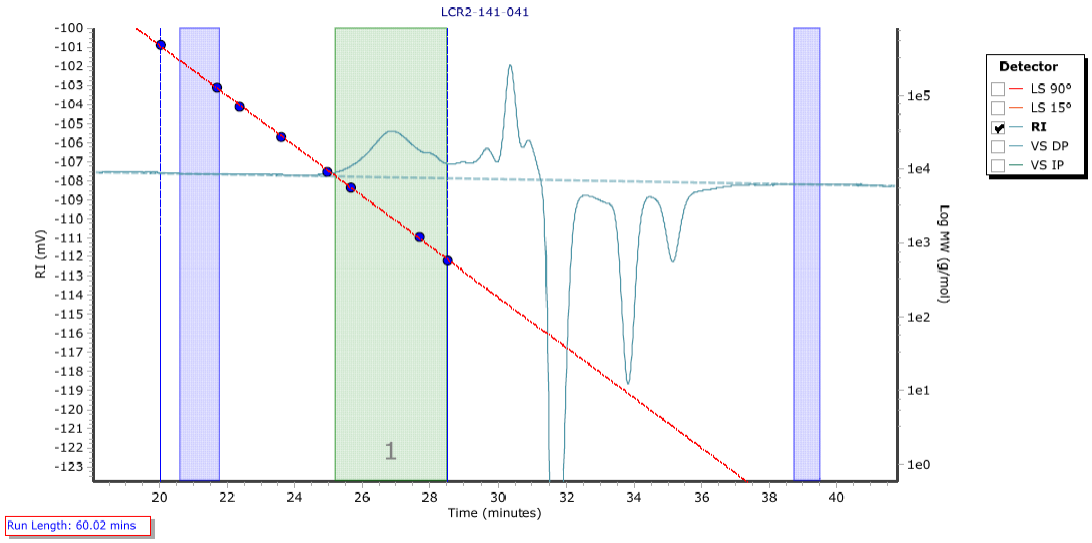

Figure A46**.** GPC chromatogram plot of the polymer obtained using complex **L1**H (Table 4, entry 19) at 130°C in a 100:1 stoichiometric ratio of lactide to catalyst.

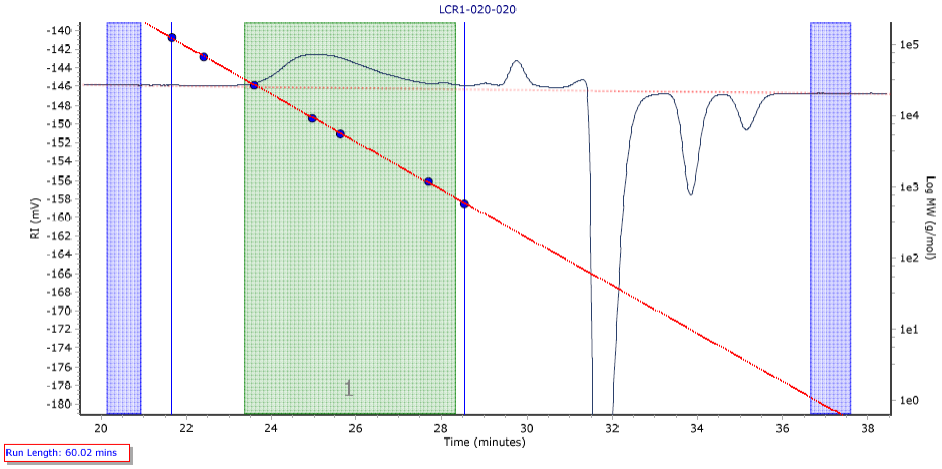

Figure A47**.** GPC chromatogram plot of the polymer obtained using complex $Sn(Oct)_2$ (Table 4, entry 20) at 130°C in a 100:1 stoichiometric ratio of lactide to catalyst.

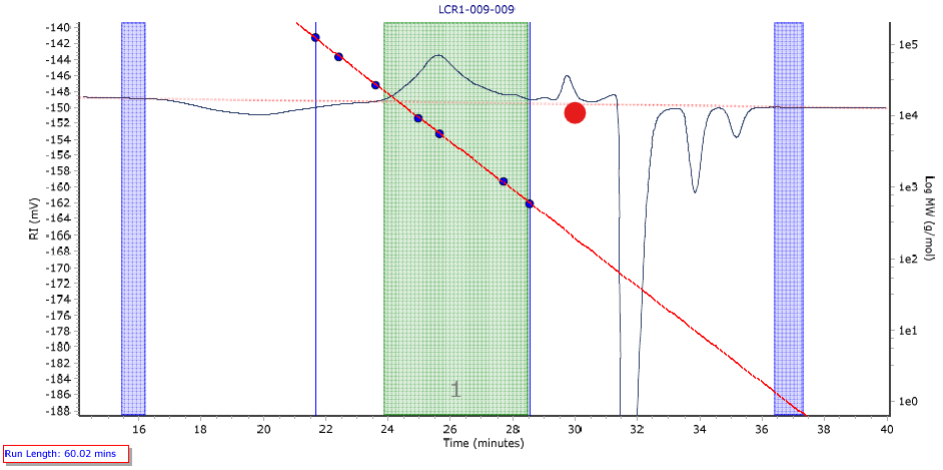

Figure A48**.** GPC chromatogram plot of the polymer obtained using complex $Sn(Oct)_2$ (Table 4, entry 21) at 130°C in a 100:1:1 stoichiometric ratio of lactide to catalyst to BnOH.

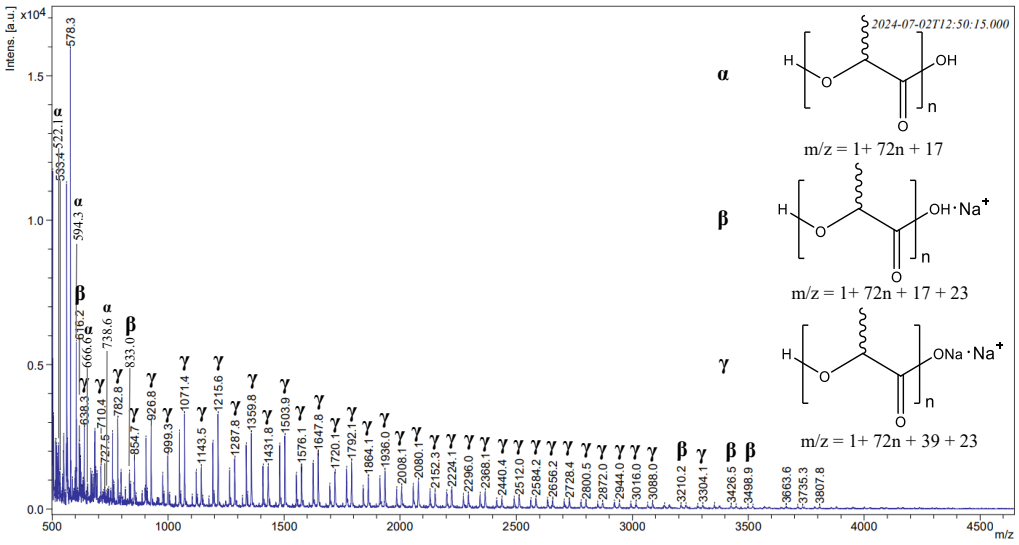

Figure A49**.** MALDI-TOF mass spectrum of PLA generated from **L1**H (Table 4, entry 19) at 130°C in a 100:1:0 stoichiometric ratio of lactide to catalyst to BnOH. All peaks can be found in Table A1.

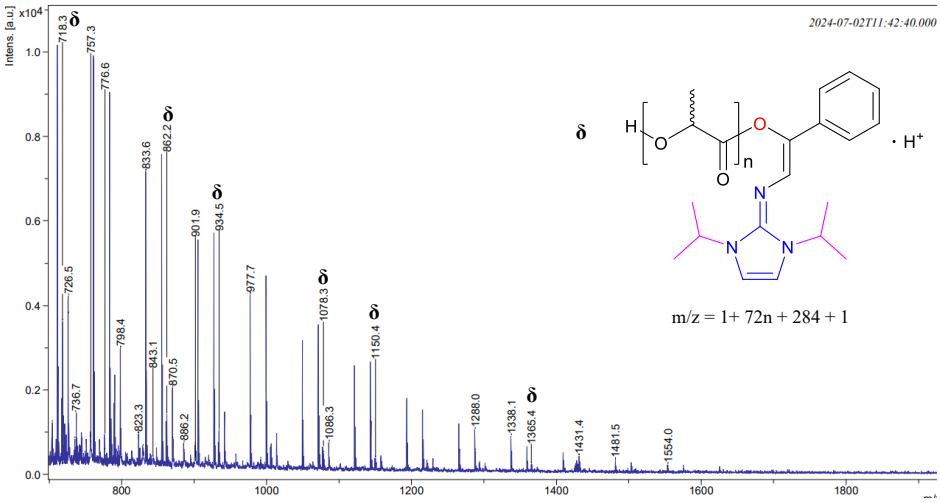

Figure A50**.** MALDI-TOF mass spectrum of PLA generated from Zn(**L1**)$_2$ (Table 4, entry 2) at 130°C in a 100:1:0 stoichiometric ratio of lactide to catalyst to BnOH. All peaks can be found in Table A2.

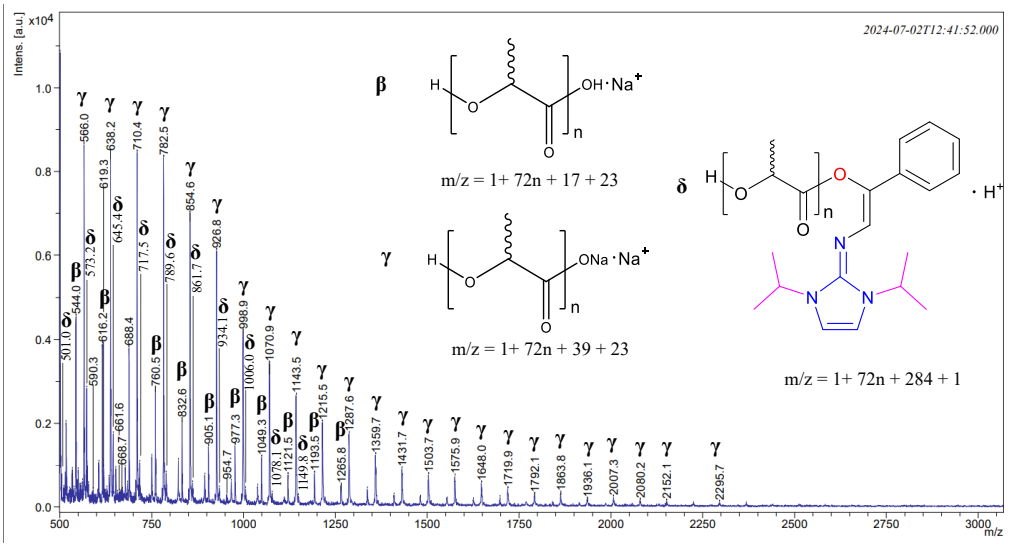

Figure A51. MALDI-TOF mass spectrum of PLA generated from Zn(**L1**)$_2$ (Table 4, entry 3) at 130°C in a 100:1:1 stoichiometric ratio of lactide to catalyst to BnOH. All peaks can be found in Table A3.

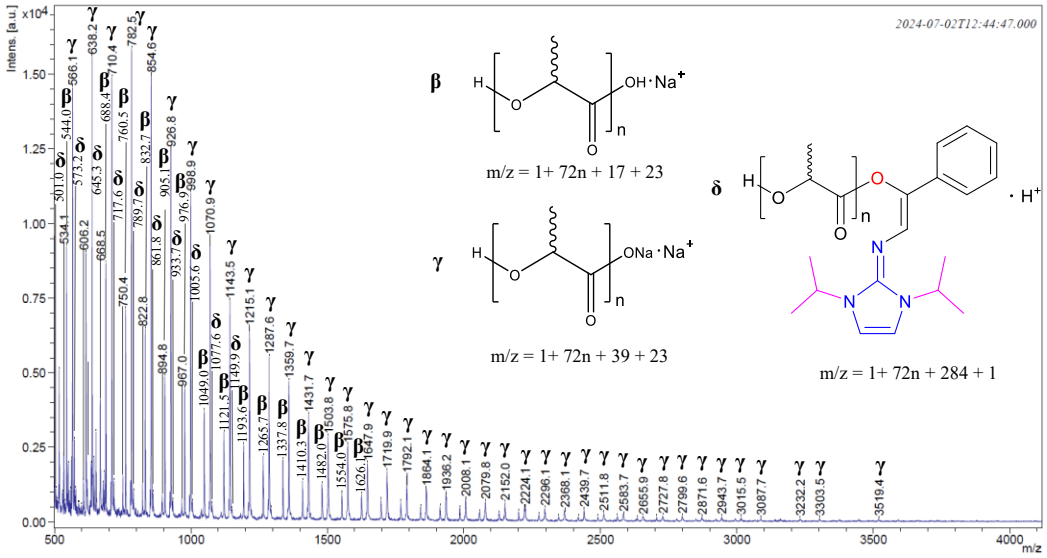

Figure A52**.** MALDI-TOF mass spectrum of PLA generated from Zn(**L1**)Et (Table 4, entry 5) at 130°C in a 100:1:1 stoichiometric ratio of lactide to catalyst to BnOH. All peaks can be found in Table A4.

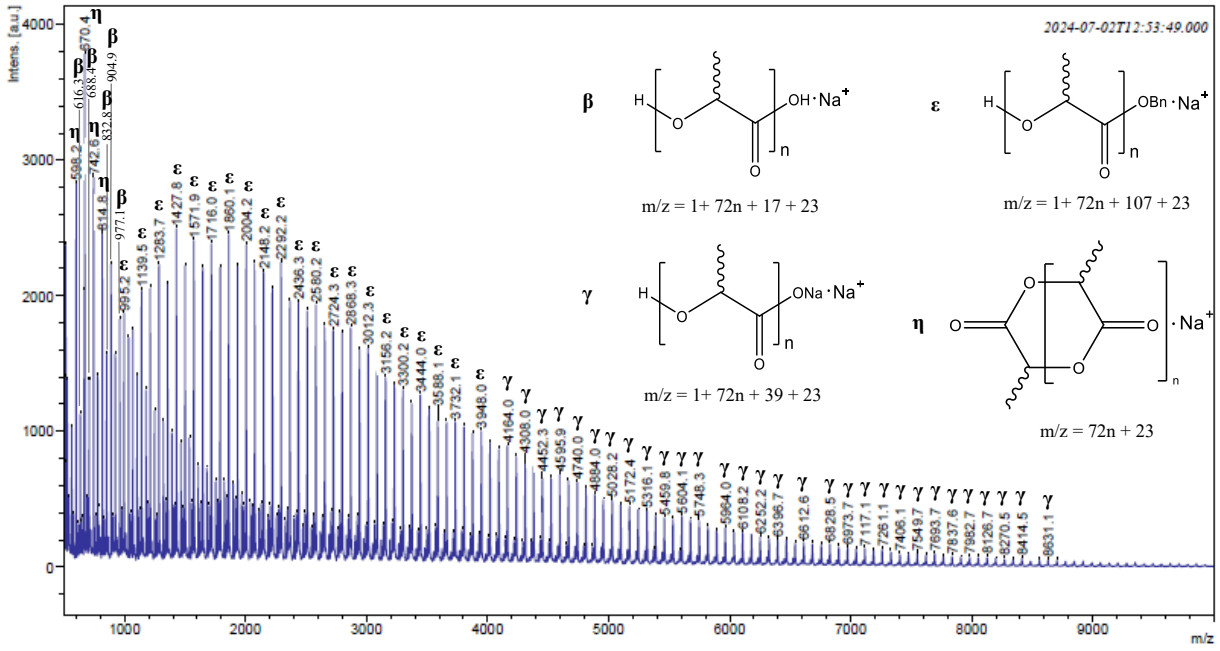

Figure A53. MALDI-TOF mass spectrum of PLA generated from $Zn(OBn)_2$ (Table 4, entry 16) at 130°C in a 100:1:0 stoichiometric ratio of lactide to catalyst to BnOH. All peaks can be found in Table A5.

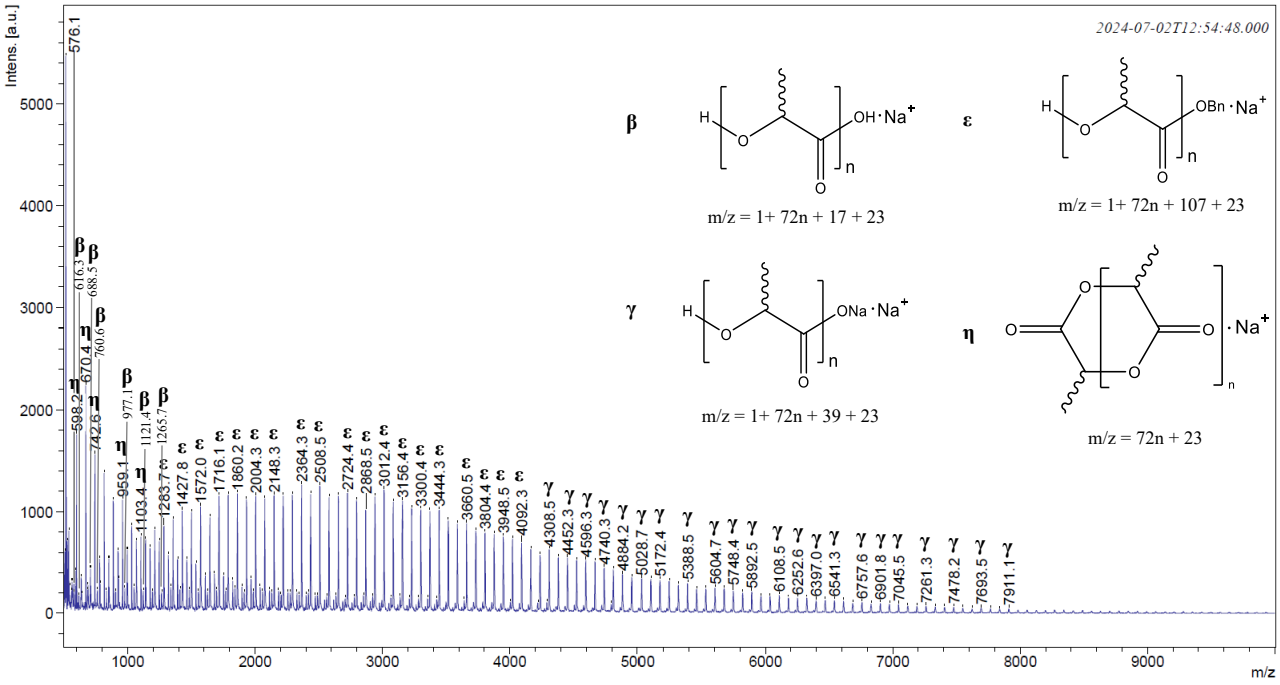

Figure A54**.** MALDI-TOF mass spectrum of PLA generated from $Zn(OBn)_2$ (Table 4, entry 17) at 130°C in a 100:1:1 stoichiometric ratio of lactide to catalyst to BnOH. All peaks can be found in Table A6.

Table A1. MALDI-TOF mass spectrum of PLA generated from **L1**H (Table 4, entry 19) at 130°C in a 100:1:0 stoichiometric ratio of lactide to catalyst to BnOH. Where S/N = signal to noise ratio. Res. = resolution. Intens. = intensity. Refer to Figure A49 for spectrum.

m/z	S/N	Res.	Intens.	Area
501.0	86	1842	11701	5960
506.0	23	419	3253	2735
515.1	16	229	2206	3166
516.1	10	230	1469	3166
517.0	16	227	2212	3166
522.1	13	1703	1842	1170
527.1	16	1626	2200	1076
533.4	9	209	1310	1429
535.0	4	195	610	1429
541.1	4	256	553	303
544.2	8	1413	1133	646
550.2	18	411	2543	3016
555.2	4	2999	568	182
562.2	83	1832	11261	7540
566.2	16	1347	2173	1896
572.4	4	172	668	588
573.2	4	172	593	588
578.3	120	1835	15918	9707
587.3	7	483	1035	663
592.1	4	235	621	760
594.3	4	441	606	334
599.3	10	483	1354	1102
603.3	43	514	5774	4587
610.3	4	2460	659	236
616.2	17	474	2306	2137
619.3	16	145	2160	3453
620.4	10	146	1388	3453
621.4	13	144	1768	3453
622.4	11	144	1473	3453
626.6	5	276	759	668
627.4	4	276	668	668
628.3	5	273	709	668
632.4	5	193	726	1107
633.3	7	193	1012	1107
634.4	6	193	845	1107
638.3	21	1313	2800	2762
646.5	3	354	543	407

647.5	3	354	543	407
651.5	5	150	791	1384
652.5	5	151	759	1384
653.3	5	150	759	1384
666.6	9	552	1273	1384
671.5	9	298	1229	1659
673.3	5	161	779	1659
679.0	8	538	1117	1011
683.6	10	215	1313	3745
684.5	20	215	2624	3745
688.4	10	507	1297	1217
693.5	9	2152	1188	1156
710.4	11	1720	1485	1855
717.8	3	322	521	389
721.5	4	318	599	615
727.5	4	544	646	849
735.6	4	176	571	732
738.6	4	234	619	600
743.7	5	334	695	638
752.5	5	340	647	744
760.5	21	1822	2634	2151
765.9	6	557	857	784
782.8	25	1364	3126	4356
791.0	3	335	488	690
791.5	3	336	488	690
797.3	10	616	1292	1820
815.8	5	734	639	644
833.0	10	1588	1268	1232
837.9	7	2000	886	967
854.7	13	412	1655	3286
862.2	3	388	488	484
888.0	4	680	558	796
901.6	6	822	741	1190
904.9	20	1781	2455	2521
910.6	5	720	648	907
926.8	24	1243	2852	4369
977.3	10	720	1190	1623
982.4	4	718	542	608
999.3	16	784	1848	2904
1006.5	4	1250	504	467
1049.5	24	1775	2652	3364
1054.4	4	732	516	864
1071.4	31	1446	3279	5187

1104.2	4	2526	438	495
1121.7	12	765	1293	2045
1126.6	4	924	433	691
1143.5	14	682	1457	3585
1150.6	3	965	403	812
1176.7	3	907	372	526
1193.8	23	792	2302	3614
1198.6	5	1625	550	821
1215.6	34	790	3282	6057
1265.8	14	1512	1343	1834
1287.8	18	654	1738	3963
1320.9	4	3105	401	476
1338.0	24	915	2211	4026
1343.0	3	1000	353	734
1359.8	29	791	2627	6271
1409.9	17	1086	1480	2229
1431.8	17	605	1484	3875
1482.0	26	957	2208	4307
1503.9	31	719	2525	6731
1554.1	15	1053	1192	2343
1576.1	16	817	1263	3927
1626.3	21	917	1551	4071
1647.8	24	664	1822	5920
1698.2	11	762	820	2217
1720.1	18	608	1278	4288
1770.3	20	705	1397	4250
1792.1	24	687	1649	5207
1842.2	10	720	672	2514
1864.1	16	724	1101	3661
1914.4	17	731	1071	3491
1936.0	21	728	1325	4538
1986.3	11	937	695	2136
2008.1	13	729	780	2966
2058.4	14	782	803	2777
2080.1	17	652	984	3710
2130.2	11	794	612	1989
2152.3	10	516	549	2280
2202.4	10	747	545	2225
2224.1	13	666	677	2775
2274.6	9	883	463	1382
2296.0	10	769	509	2025
2346.4	10	927	504	1819
2368.1	12	842	617	2271

2418.3	6	807	316	1377
2440.4	8	592	365	1749
2490.4	8	706	366	1542
2512.0	8	687	378	1732
2562.4	7	970	319	1198
2584.2	8	588	379	1519
2634.5	5	813	211	1222
2656.2	7	589	294	1371
2706.7	5	650	211	1041
2728.4	6	678	267	1370
2778.4	3	834	142	962
2800.5	5	728	194	1199
2850.4	5	720	197	762
2872.0	5	651	213	1012
2922.2	4	924	151	877
2944.0	6	593	204	1013
2994.2	5	751	189	720
3016.0	6	664	222	967
3066.1	4	407	153	728
3088.0	5	983	174	821
3138.4	3	490	112	689
3210.2	4	1008	142	626
3231.4	4	437	140	702
3282.3	4	532	120	507
3304.1	4	536	141	634
3354.6	3	739	109	520
3426.5	4	736	119	478
3448.4	3	842	107	457
3498.9	3	683	97	422
3520.1	3	699	93	456
3663.6	4	500	105	430
3714.3	3	557	82	311
3735.3	3	450	86	467
3807.8	3	637	82	379

Table A2. MALDI-TOF mass spectrum of PLA generated from Zn(**L1**)$_2$ (Table 4, entry 2) at 130°C in a 100:1:0 stoichiometric ratio of lactide to catalyst to BnOH. Where S/N = signal to noise ratio. Res. = resolution. Intens. = intensity. Refer to Figure A50 for spectrum.

m/z	S/N	Res.	Intens.	Area
704.2	13	680	1229	718
718.3	42	7458	3631	1462
726.5	50	2969	4226	2100
735.3	8	143	837	889
736.7	16	241	1455	889
742.8	3	203	426	962
757.3	9	622	862	1262
776.6	10	906	944	539
798.4	36	3102	2981	1667
814.4	4	222	449	634
823.3	10	194	950	569
823.4	10	401	950	569
829.6	7	513	681	871
833.6	91	70.1	7166	1380
843.1	3	253	396	419
862.2	17	722	1425	674
870.5	25	1779	2049	1126
886.2	8	819	744	648
895.6	5	2063	467	259
901.9	4	609	381	595
920.7	5	2438	457	335
934.5	13	455	1057	522
977.7	58	232	4269	929
991.9	3	373	336	233
1078.3	9	914	650	308
1086.3	10	443	754	469
1101.9	3	155	249	357
1150.4	5	524	387	298
1288	18	1222	1058	361
1294.5	4	257	252	239
1338.1	16	1251	908	313
1365.4	4	283	244	229
1431.4	8	444	435	314
1481.5	7	1398	339	203
1554	5	1372	223	159

Table A3. MALDI-TOF mass spectrum of PLA generated from Zn(**L1**)$_2$ (Table 4, entry 3) at 130°C in a 100:1:1 stoichiometric ratio of lactide to catalyst to BnOH. Where S/N = signal to noise ratio. Res. = resolution. Intens. = intensity. Refer to Figure A51 for spectrum.

m/z	S/N	Res.	Intens.	Area
501.0	110	1879	10836	4893
510.6	4	233	460	367
511.0	4	233	409	367
517.0	20	433	2009	2033
526.2	4	229	423	325
534.0	8	240	884	1184
539.1	4	2128	434	192
544.0	47	1795	4549	2564
550.2	9	1543	880	710
557.1	5	168	517	662
562.2	6	432	602	473
566.0	89	1408	8634	6839
573.2	29	1941	2839	2417
578.2	5	2448	546	313
590.3	4	464	411	243
606.2	11	1393	1065	1392
616.2	41	1756	3884	2172
619.3	9	464	923	900
624.4	3	613	355	169
628.3	4	290	441	325
634.3	7	496	702	529
638.2	88	1402	8264	7655
645.4	18	1910	1747	1664
652.5	9	538	914	704
657.4	3	287	340	286
661.6	3	291	362	300
662.4	3	291	362	300
668.7	4	162	436	694
669.4	3	162	355	694
670.5	4	161	410	694
678.3	9	1107	884	1310
684.5	5	223	559	617
688.4	42	2234	3797	2419
710.4	94	1605	8456	8187
717.5	11	510	1027	1328
750.6	13	1509	1201	1540
760.5	30	1780	2723	2121
782.5	96	1647	8332	8160
789.6	8	624	785	1279

822.6	13	1650	1111	1726
832.6	23	1710	1995	1941
854.6	80	1552	6776	8210
861.7	6	390	567	910
895.0	8	1281	751	1255
905.1	17	716	1436	1654
926.8	75	1594	6107	7229
934.1	5	429	444	836
954.7	3	313	296	375
966.9	7	1489	606	1087
977.3	18	1858	1462	1490
998.9	53	1519	4152	6274
1006.0	5	460	428	751
1038.7	6	2222	485	907
1049.3	15	1962	1182	1274
1070.9	43	1404	3143	5598
1078.1	4	480	330	542
1121.5	10	927	761	1158
1143.5	38	778	2664	4613
1149.8	3	438	262	549
1193.5	11	816	794	1257
1215.5	31	784	2022	4017
1265.8	5	897	341	1011
1287.6	28	825	1744	3367
1337.8	3	820	217	740
1359.7	21	752	1238	2840
1410.2	4	865	264	714
1431.7	16	858	898	2371
1481.9	4	1428	252	555
1503.7	14	836	757	2035
1554.4	3	653	170	533
1575.9	14	966	726	1612
1626.2	3	670	169	428
1648.0	12	1026	563	1369
1698.3	5	1301	219	422
1719.9	9	673	426	1376
1792.1	6	780	263	1079
1863.8	6	1181	269	886
1936.1	3	576	133	584
2007.3	6	779	223	721
2080.2	4	925	155	442
2152.1	4	341	131	483

Table A4. MALDI-TOF mass spectrum of PLA generated from Zn(**L1**)Et (Table 4, entry 5) at 130°C in a 100:1:1 stoichiometric ratio of lactide to catalyst to BnOH. Where S/N = signal to noise ratio. Res. = resolution. Intens. = intensity. Refer to Figure A52 for spectrum.

m/z	S/N	Res.	Intens.	Area
501.0	61	1679	9494	5092
505.0	6	154	1025	1366
511.0	4	399	739	608
517.0	33	1757	5087	4789
529.5	6	239	989	889
534.1	14	239	2191	2548
539.2	4	240	677	598
544.0	61	1586	9220	4792
550.2	12	480	1951	1495
557.1	7	496	1083	687
562.2	13	1465	2052	1375
566.1	96	1220	14541	13540
573.2	18	1930	2745	2282
578.5	7	498	1114	780
588.3	3	498	613	319
589.2	3	498	589	319
598.6	3	274	556	504
599.0	3	274	556	504
606.2	9	1175	1367	2085
616.2	61	1667	9011	5498
634.4	12	515	1887	1499
638.2	107	1450	15581	13545
645.3	14	2094	2115	2138
652.5	19	548	2898	2572
668.5	28	1790	4117	3948
678.3	8	1199	1259	1853
684.5	11	305	1638	1802
688.4	61	1812	8675	6747
710.4	106	1400	14896	15099
717.6	9	502	1382	1945
750.4	10	1694	1543	1781
760.5	51	1695	7119	5653
782.5	117	1550	15861	16939
789.7	6	354	941	1825
822.8	9	1182	1270	1824
832.7	47	1765	6334	5613
854.6	112	1455	14929	18531

861.8	7	620	963	1384
894.8	6	684	908	1549
905.1	37	1704	4862	5410
926.8	97	1444	12437	17619
933.7	5	417	722	1464
967.0	5	1330	738	1313
976.9	36	1823	4456	4897
998.9	89	1396	11010	16255
1005.6	5	450	677	1357
1049.0	30	1708	3707	4700
1070.9	81	797	9210	15082
1077.6	4	456	580	1114
1121.5	27	838	2998	4790
1143.5	68	747	7400	13918
1149.9	4	481	443	1263
1193.6	24	844	2578	3997
1215.1	63	823	6361	12740
1265.7	23	883	2203	3858
1287.6	57	849	5531	11079
1293.7	4	573	445	1018
1337.8	22	1000	2079	3544
1359.7	52	812	4718	10299
1410.3	11	782	1019	3075
1431.7	43	784	3578	8922
1482.0	15	681	1258	3068
1503.8	36	864	2854	8300
1554.0	13	797	1022	2552
1575.8	34	866	2552	7212
1626.1	12	878	912	2376
1647.9	27	678	1962	6268
1698.3	8	827	584	1821
1719.9	25	653	1700	5628
1770.1	8	1038	563	1580
1792.1	18	944	1199	4567
1842.4	8	688	491	1478
1864.1	17	753	1042	4215
1914.1	9	1050	523	1466
1936.2	15	725	868	3568
1986.1	8	723	464	1144
2008.1	13	697	721	3137
2058.2	6	709	330	1110
2079.8	13	680	678	2703
2130.4	5	789	285	1073

2152.0	13	884	640	2349
2202.2	5	1300	242	742
2224.1	10	652	491	1997
2274.0	5	827	241	825
2296.1	10	643	450	1883
2346.4	4	780	172	551
2368.1	7	658	311	1501
2418.5	3	637	156	549
2439.7	9	986	386	1431
2490.3	4	780	158	493
2511.8	7	712	290	1181
2562.3	5	942	188	475
2583.7	5	647	204	1052
2634.1	3	1031	128	442
2655.9	5	541	185	876
2706.0	4	2352	157	361
2727.8	6	625	205	841
2799.6	6	729	192	806
2871.6	4	918	136	669
2943.7	5	716	169	508
3015.5	5	700	145	447
3087.7	3	1043	103	424
3232.2	3	363	96	457
3303.5	3	671	95	405
3519.4	3	933	79	332
6892.6	3	19210	33	32

Table A5. MALDI-TOF mass spectrum of PLA generated from $Zn(OBn)_2$ (Table 4, entry 16) at 130°C in a 100:1:0 stoichiometric ratio of lactide to catalyst to BnOH. Where S/N = signal to noise ratio. Res. = resolution. Intens. = intensity. Refer to Figure A53 for spectrum.

m/z	S/N	Res.	Intens.	Area
505.9	8	185	773	1731
513.9	27	671	2373	4256
518.0	14	700	1271	1534
526.0	15	645	1376	1499
535.8	5	217	512	932
538.0	4	206	431	792
562.1	11	698	1029	1062
576.1	4	550	385	713
598.2	33	661	2825	2984
616.3	3	681	315	331
634.3	13	685	1127	1247
638.3	3	534	330	491
648.3	3	451	364	882
665.6	23	629	2035	2859
670.4	44	680	3781	4921
688.4	5	645	509	1104
691.6	5	388	509	1152
706.5	16	682	1373	1835
710.3	4	604	374	638
742.6	34	682	2871	3878
760.7	4	636	381	706
778.7	16	686	1409	1962
782.6	3	556	331	523
814.8	29	259	2458	6363
832.8	3	614	349	886
850.9	18	696	1566	2444
854.6	4	622	406	683
886.9	27	709	2232	3494
904.9	4	702	372	960
923.0	19	708	1570	2883
959.1	22	705	1825	3232
977.1	4	458	419	1383
995.2	22	714	1868	4180
1031.2	20	712	1690	3106
1049.2	4	433	387	1212
1067.3	21	685	1750	4226
1103.4	17	677	1409	2910
1121.4	5	541	418	1364
1139.5	25	565	2039	5165

1175.4	16	694	1303	2689
1193.5	5	546	467	1728
1211.6	26	623	2061	5758
1247.5	14	675	1151	2607
1265.6	4	494	377	1298
1283.7	28	613	2229	6157
1319.6	13	650	1071	2379
1337.7	6	565	484	1443
1355.7	27	650	2085	5869
1391.8	12	669	990	2292
1409.6	5	549	458	1491
1427.8	32	658	2495	7174
1463.8	11	760	913	2128
1481.8	5	522	432	1632
1499.9	29	651	2219	6545
1535.9	12	698	951	2375
1553.8	5	614	472	1433
1571.9	31	683	2406	7307
1607.9	9	661	742	1962
1626.1	5	623	465	1668
1644.0	28	680	2205	7074
1680.0	9	688	729	2068
1698.0	5	571	449	1833
1716.0	31	679	2380	7734
1752.0	8	706	631	1819
1769.8	6	589	478	1801
1788.0	28	715	2206	7440
1824.1	8	708	628	1842
1842.1	6	682	508	1786
1860.1	32	760	2451	8702
1896.1	7	733	613	1745
1914.1	6	741	500	1824
1932.2	29	742	2221	8203
1968.1	6	767	534	1514
1986.1	5	649	450	1769
2004.2	31	715	2373	9055
2040.1	6	735	475	1475
2057.9	5	689	445	1773
2076.1	29	726	2237	8342
2112.1	5	674	413	1347
2130.1	6	709	466	1764
2148.2	28	733	2172	8515
2184.2	4	661	365	1376

2201.8	5	731	449	1762
2220.2	27	683	2048	8980
2256.2	4	677	382	1236
2274.0	5	803	427	1677
2292.2	30	763	2243	9275
2328.2	4	644	332	1275
2346.2	5	782	424	1772
2364.3	26	732	1958	8418
2400.0	4	773	357	1163
2418.2	5	554	394	1827
2436.3	26	739	1947	8813
2472.1	3	817	299	1060
2490.1	5	637	393	1758
2508.2	25	783	1888	7934
2544.3	3	668	290	1019
2562.2	5	707	380	1652
2580.2	26	765	1931	8509
2634.2	4	663	369	1938
2652.3	24	767	1778	7842
2706.2	5	746	402	1835
2724.3	24	753	1746	7651
2760.0	3	892	276	1043
2777.9	5	748	400	1737
2796.2	24	776	1727	7797
2850.4	5	773	360	1634
2868.3	25	816	1764	8184
2922.6	5	842	375	1652
2940.2	23	803	1599	7377
2994.3	4	650	306	1630
3012.3	23	846	1613	7277
3066.0	4	789	314	1516
3084.2	21	835	1447	6819
3138.3	4	810	310	1390
3156.2	20	767	1396	7015
3210.4	4	825	326	1566
3228.2	20	773	1342	6825
3282.6	3	630	265	1428
3300.2	20	773	1306	6737
3354.3	4	763	281	1500
3372.0	19	781	1204	6146
3426.2	4	736	268	1525
3444.0	20	839	1268	6323
3497.9	4	713	273	1334

3516.2	19	810	1165	6057
3570.3	4	868	291	1366
3588.1	18	845	1073	5683
3642.0	4	829	255	1281
3660.1	18	878	1066	5802
3714.1	4	850	255	1529
3732.1	19	858	1068	5397
3785.7	4	947	272	1372
3804.1	18	951	1034	5247
3858.1	4	828	228	1422
3876.1	18	895	988	5186
3930.4	4	764	245	1301
3948.0	18	990	1000	5126
4002.2	3	880	212	1033
4020.2	17	925	914	4950
4073.9	4	906	231	1128
4091.9	16	937	867	4386
4146.2	3	798	200	1133
4164.0	17	958	890	4573
4218.2	3	992	196	1040
4236.1	16	917	812	4442
4289.8	3	805	186	959
4308.0	15	860	761	4335
4362.0	3	937	186	950
4379.9	15	961	738	3964
4434.2	4	1197	203	930
4452.3	14	896	650	3858
4506.0	3	1022	182	1001
4523.9	14	913	654	3792
4595.9	15	938	682	3923
4649.9	3	1067	157	877
4667.8	15	940	635	3658
4740.0	15	1013	622	3538
4794.4	3	862	153	889
4811.9	14	956	578	3368
4865.7	3	1028	147	769
4884.0	13	894	535	3192
4956.0	13	910	496	3007
5028.2	13	962	493	3066
5099.9	12	972	454	2629
5172.4	12	1014	449	2707
5244.0	12	954	421	2545
5316.1	12	1031	409	2412

5370.3	3	1258	125	690
5388.0	11	1085	378	2149
5459.8	11	992	360	2267
5531.9	11	983	351	2207
5586.6	3	1497	118	668
5604.1	12	1077	371	2209
5676.4	12	1069	350	2087
5748.3	11	1120	340	2031
5820.3	10	1048	296	1817
5892.0	10	1005	267	1694
5964.0	10	1086	283	1722
6036.1	9	1145	253	1578
6108.2	9	1100	252	1601
6180.3	9	1206	240	1450
6252.2	9	1072	219	1340
6324.7	8	1009	203	1445
6396.7	8	1151	198	1235
6468.6	8	1138	198	1343
6540.9	7	1072	175	1201
6612.6	8	1182	180	1175
6684.5	8	1181	168	1072
6756.8	7	1101	163	1049
6828.5	8	1202	168	1034
6901.3	7	1231	146	920
6973.7	7	1094	138	981
7045.3	6	1001	125	940
7117.1	7	1202	137	904
7189.3	6	1076	121	845
7261.1	7	1245	130	801
7332.9	6	1284	121	795
7406.1	5	1084	91.9	702
7477.6	5	1101	92.1	788
7549.7	6	1226	98.3	754
7622.0	5	1259	87.1	707
7693.7	6	1449	94.6	648
7765.9	4	1114	74	606
7837.6	5	1160	78.7	610
7909.8	4	1111	71.3	589
7982.7	4	1211	70.9	583
8054.4	4	1311	67.9	527
8126.7	4	1302	69.4	553
8198.9	4	1422	63.5	490
8270.5	4	1315	56.3	420

8342.7	3	1089	53.6	443
8414.5	4	1298	60	431
8559.2	3	1371	47.6	362
8631.1	3	1372	51.1	374
8704.1	3	1574	49.1	333

Table A6. MALDI-TOF mass spectrum of PLA generated from $Zn(OBn)_2$ (Table 4, entry 17) at 130°C in a 100:1:1 stoichiometric ratio of lactide to catalyst to BnOH. Where S/N = signal to noise ratio. Res. = resolution. Intens. = intensity. Refer to Figure A54 for spectrum.

m/z	S/N	Res.	Intens.	Area
506	12	313	608	1197
514	112	639	5468	10597
526	14	636	704	931
536	16	568	809	1728
544	3	812	179	232
558	4	656	216	235
562	6	256	308	543
566	4	683	240	327
576	5	241	292	810
580	3	552	181	277
592	8	343	416	583
598	36	675	1756	1801
616	3	649	175	194
634	7	722	353	538
638	3	560	185	343
670	47	689	2239	2730
685	4	737	228	294
689	5	599	275	745
707	9	735	436	567
711	5	681	273	504
743	33	673	1563	2297
761	4	733	224	378
779	11	725	534	703
783	6	607	288	584
815	29	705	1378	2023
833	4	641	222	464
851	11	674	538	832
855	5	676	254	477
887	24	680	1108	1829
905	4	791	214	433
923	13	730	612	969
927	7	689	336	729
959	24	755	1114	1845
977	5	723	244	605
995	13	701	623	1153
999	6	519	297	741
1031	19	704	859	1574
1049	5	725	254	520
1067	16	766	711	1504

1103	17	717	751	1502
1121	5	451	219	675
1140	16	679	725	2118
1176	14	540	642	1479
1194	4	436	214	715
1212	19	624	816	2470
1248	16	631	706	1517
1266	4	478	206	799
1284	20	675	858	2614
1320	13	649	571	1265
1338	6	796	256	676
1356	22	660	921	2915
1392	12	603	531	1286
1410	5	551	233	738
1428	24	655	1007	3169
1464	12	681	523	1235
1482	5	685	227	689
1500	24	666	993	3212
1536	11	773	486	1074
1554	5	539	211	720
1572	25	712	1049	3423
1608	8	598	370	1021
1626	5	534	210	844
1644	23	668	943	3346
1680	9	704	387	1057
1698	5	640	226	749
1716	28	765	1151	3852
1752	8	818	369	900
1770	5	651	221	771
1788	28	778	1163	3869
1824	7	768	318	918
1842	5	729	246	801
1860	28	713	1174	4260
1896	6	582	260	820
1914	4	638	206	831
1932	27	679	1117	4000
1968	8	900	335	900
1986	5	666	214	879
2004	28	746	1147	4230
2040	6	771	254	796
2059	5	602	213	833
2076	27	768	1127	4395
2113	5	697	226	657

2130	4	620	206	886
2148	28	725	1157	4508
2184	5	847	222	681
2203	4	550	183	791
2220	28	739	1151	4444
2257	4	733	205	738
2274	4	708	203	742
2293	28	778	1163	4875
2328	4	960	203	616
2346	4	670	184	703
2364	30	785	1261	4983
2401	4	780	180	610
2418	4	752	202	881
2436	28	757	1168	4783
2472	4	923	172	622
2490	4	618	175	883
2509	30	826	1255	5098
2562	4	725	168	761
2580	28	755	1138	5123
2635	4	753	174	866
2652	28	771	1152	5135
2706	3	624	146	704
2724	29	827	1179	5396
2778	3	722	154	695
2797	28	761	1112	4959
2850	4	922	175	806
2869	26	751	1014	5015
2923	4	758	167	813
2941	29	887	1146	5034
3012	32	896	1213	5334
3066	3	808	153	674
3084	28	840	1094	4908
3138	4	946	162	784
3156	29	888	1103	5030
3210	3	660	143	767
3228	28	821	1033	4765
3283	3	873	145	765
3300	28	830	1019	5187
3355	3	1043	145	612
3372	28	888	1004	4828
3427	3	760	138	714
3444	28	863	1014	4954
3516	26	826	911	4649

3588	26	879	880	4380
3643	3	1050	127	487
3661	26	891	885	4424
3732	25	911	812	3942
3804	24	814	790	4311
3876	24	921	776	4014
3949	24	932	752	3781
4004	3	842	110	553
4020	24	993	733	3564
4092	23	913	691	3547
4164	21	962	631	3261
4219	3	876	100	501
4237	20	865	571	3278
4290	3	1263	105	497
4309	22	1039	626	3259
4380	20	910	550	2967
4452	21	992	545	2891
4525	19	972	516	2753
4596	20	1023	520	2863
4668	20	1095	509	2768
4740	18	1055	445	2441
4795	3	1328	88.3	374
4812	18	1051	428	2486
4884	16	1034	376	2159
4957	16	966	355	2055
5029	15	913	340	2019
5101	15	932	335	2063
5172	15	1028	326	1921
5244	15	1105	313	1831
5317	14	959	280	1796
5389	14	1184	293	1658
5460	12	1018	237	1436
5533	12	978	241	1520
5605	13	1125	247	1481
5676	12	1188	242	1443
5748	11	1170	221	1313
5821	11	1209	204	1196
5893	11	1212	214	1247
5965	9	1001	166	1132
6036	9	940	166	1065
6109	10	1322	179	1071
6181	9	1165	153	954
6253	9	1362	153	956

6324	9	1070	150	1010
6397	7	960	121	933
6469	8	1143	128	871
6541	8	1207	130	858
6613	8	1329	122	757
6686	6	1064	97.1	636
6758	7	1195	106	688
6829	6	1041	91.6	697
6902	7	1234	96.5	635
6973	6	1211	90.9	651
7046	6	1394	85.3	503
7118	5	1106	72.1	531
7190	5	1160	68.8	505
7261	5	1371	70.4	482
7334	4	1196	63.4	426
7406	4	1060	58.1	434
7478	4	1261	60.7	412
7550	4	1193	51.1	400
7622	3	1163	42.9	369
7694	4	999	48.2	432
7767	3	1513	45.3	335
7839	3	1192	41.5	365
7911	3	1274	45.2	352

Table A7. Crystal data for Zn(**L1**)$_2$

Empirical formula	$C_{70}H_{92}Cl_4N_{12}O_4Zn_2$
Formula weight	1438.09
Temperature/K	173
Crystal system	monoclinic
Space group	C2/c
a/Å	24.1720(9)
b/Å	24.1263(10)
c/Å	26.0170(11)
α/°	90
β/°	100.809(2)
γ/°	90
Volume/Å^3	14903.4(10)
Z	8
ρ_{calc}g/cm^3	1.282
μ/mm^{-1}	0.841
F(000)	6048
Crystal size/mm^3	0.2 × 0.2 × 0.2
Radiation	MoKα (λ = 0.71073)
2Θ range for data collection/°	3.376 to 55.164
Index ranges	$-29 \leq h \leq 31$, $-31 \leq k \leq 31$, $-33 \leq l \leq 33$
Reflections collected	151609
Independent reflections	17215 [R_{int} = 0.0472, R_{sigma} = 0.0278]
Data/restraints/parameters	17215/0/856
Goodness-of-fit on F^2	1.159
Final R indexes [I>=2σ (I)]	R_1 = 0.0797, wR_2 = 0.1925
Final R indexes [all data]	R_1 = 0.0952, wR_2 = 0.1997
Largest diff. peak/hole / e Å^{-3}	1.43/-1.94

Table A8. Crystal data for Zn(**L3**)$_2$

Empirical formula	C35H44N6O2Zn
Formula weight	646.13
Temperature/K	173
Crystal system	monoclinic
Space group	C2
a/Å	16.6284(13)
b/Å	7.7825(5)
c/Å	13.3721(10)
α/°	90
β/°	119.519(3)
γ/°	90
Volume/Å3	1505.86(19)
Z	2
ρcalcg/cm3	1.425
μ/mm-1	0.86
F(000)	684
Crystal size/mm3	0.25 × 0.1 × 0.05
Radiation	MoKα (λ = 0.71073)
2Θ range for data collection/°	4.952 to 56.544
Index ranges	-22 ≤ h ≤ 22, -10 ≤ k ≤ 10, -17 ≤ l ≤ 17
Reflections collected	22980
Independent reflections	3746 [Rint = 0.1014, Rsigma = 0.0805]
Data/restraints/parameters	3746/1/170
Goodness-of-fit on F2	1.031
Final R indexes [I>=2σ (I)]	R1 = 0.0505, wR2 = 0.1102
Final R indexes [all data]	R1 = 0.0728, wR2 = 0.1188
Largest diff. peak/hole / e Å-3	0.30/-0.38
Flack parameter	0.052(10)

Table A9. Crystal data for Zn(**L4**)$_2$

Empirical formula	$C_{27}H_{34}Cl_2N_6O_2Zn$
Formula weight	610.87
Temperature/K	173
Crystal system	monoclinic
Space group	$P2_1/n$
a/Å	9.0603(2)
b/Å	13.3422(4)
c/Å	23.8357(7)
α/°	90
β/°	99.9990(10)
γ/°	90
Volume/Å^3	2837.60(13)
Z	4
ρ_{calc}g/cm^3	1.43
μ/mm^{-1}	1.09
F(000)	1272
Crystal size/mm^3	0.25 × 0.15 × 0.15
Radiation	MoKα (λ = 0.71073)
2Θ range for data collection/°	4.594 to 61.014
Index ranges	$-12 \leq h \leq 12$, $-19 \leq k \leq 19$, $-34 \leq l \leq 32$
Reflections collected	86692
Independent reflections	8633 [R_{int} = 0.0547, R_{sigma} = 0.0302]
Data/restraints/parameters	8633/0/356
Goodness-of-fit on F^2	1.021
Final R indexes [I>=2σ (I)]	R_1 = 0.0375, wR_2 = 0.0889
Final R indexes [all data]	R_1 = 0.0549, wR_2 = 0.0961
Largest diff. peak/hole / e Å^{-3}	0.94/-0.38

Table A10. Crystal data for Al(**L1**)$_2$OBn

Empirical formula	$C_{82}H_{102}Al_2N_{12}O_6$
Formula weight	1405.7
Temperature/K	173
Crystal system	monoclinic
Space group	$P2_1/n$
a/Å	20.780(2)
b/Å	13.3302(16)
c/Å	28.744(3)
α/°	90
β/°	99.897(3)
γ/°	90
Volume/Å^3	7843.8(16)
Z	4
ρ_{calc}g/cm^3	1.19
μ/mm^{-1}	0.097
F(000)	3008
Crystal size/mm^3	0.1 × 0.1 × 0.1
Radiation	MoKα (λ = 0.71073)
2Θ range for data collection/°	4.044 to 55.034
Index ranges	$-26 \leq h \leq 26$, $-17 \leq k \leq 17$, $-35 \leq l \leq 37$
Reflections collected	128551
Independent reflections	18006 [R_{int} = 0.4320, R_{sigma} = 0.2863]
Data/restraints/parameters	18006/0/935
Goodness-of-fit on F^2	0.993
Final R indexes [I>=2σ (I)]	R_1 = 0.1272, wR_2 = 0.2634
Final R indexes [all data]	R_1 = 0.3193, wR_2 = 0.3487
Largest diff. peak/hole / e Å^{-3}	0.27/-0.47